NASA Technical Paper 1330

Effect of Winglets on a First-Generation Jet Transport Wing

VI - Stability Characteristics for a Full-Span Model at Subsonic Speeds

Stuart G. Flechner

OCTOBER 1979

NASA

NASA Technical Paper 1330

Effect of Winglets on a First-Generation Jet Transport Wing

VI - Stability Characteristics for a Full-Span Model at Subsonic Speeds

Stuart G. Flechner
Langley Research Center
Hampton, Virginia

National Aeronautics
and Space Administration

**Scientific and Technical
Information Branch**

1979

SUMMARY

A wind-tunnel investigation was conducted for a 0.035-scale full-span model of the KC-135A to identify changes in stability and control characteristics due to the addition of winglets. Low-speed data (Mach number of 0.30) were obtained at angles of attack from approximately -8° to 16° and at angles of sideslip up to approximately $\pm 12^{\circ}$. High-subsonic-speed data were obtained at Mach numbers from 0.50 to 0.82, at angles of attack from approximately -6° to 16°, and at angles of sideslip of 0°, 5°, and -5°.

The results indicate that winglets produce favorable effects on the lift-curve slope and longitudinal stability, require only small changes in horizontal-tail deflection for trim, delay pitch-up, and increase the lateral-directional stability. A tabular summary of the papers in the series of investigations of winglets on the KC-135A is included.

INTRODUCTION

Winglets, described in reference 1, are intended to provide reductions in drag due to lift at subsonic speeds. To fully explore the applicability of winglets, the National Aeronautics and Space Administration (NASA) has been conducting extensive experimental investigations of the use of winglets on various jet transports. (See refs. 2 to 5.) The results of one of these investigations indicated that winglets reduced induced drag on a U.S. Air Force KC-135A first-generation jet-transport model by approximately 20 percent with a resulting increase in wing lift-to-drag ratio of about 8 percent (refs. 5 to 7). As a result of that investigation, NASA and the U.S. Air Force have initiated a joint flight research and demonstration program to determine the effectiveness of winglets on the KC-135A. In support of the flight program, wind-tunnel investigations have been conducted in the Langley 8-foot transonic pressure tunnel (refs. 8 to 9).

The investigation reported herein has been conducted to identify any changes in stability and control characteristics due to the addition of winglets. Therefore, the results have been analyzed with emphasis on the differences between the basic KC-135A and the KC-135A with winglets as well as variations in stability characteristics at critical design-load conditions identified in reference 10.

The current paper presents force and moment data obtained on a 0.035-scale full-span model of the KC-135A. Low-speed data (Mach number at 0.30) are presented at angles of attack from approximately -8° to 16° and at angles of sideslip up to approximately $\pm 12^{\circ}$. The data at sideslip angles greater than 5° were obtained in the Langley high-speed 7- by 10-foot tunnel. High-subsonic-speed data are presented at Mach numbers from 0.50 to 0.82, at angles of attack from approximately -6° to 16°, and at angles of sideslip of 0°, 5°, and -5°.

This paper is one of a series of papers to report the results of a number of investigations of NASA designed winglets on KC-135A models. Table I lists these papers along with a short model description, the Mach number range, and a brief description of the more important data presented and discussed.

SYMBOLS

The results presented in this report are referred to the stability-axis system for the longitudinal aerodynamic characteristics and to the body-axis system for the lateral-directional aerodynamic characteristics. Force and moment data have been reduced to conventional coefficient form based on the geometry of the basic wing planform. Moments are referenced to the quarter-chord point of the mean aerodynamic chord of the basic wing (fig. 1). All dimensional values are given in both the International System of Units (SI) and U.S. Customary Units; however, all measurements and calculations were made in U.S. Customary Units. (See ref. 11.)

Coefficients and symbols used herein are defined as follows:

b	wing span, 138.7 cm (54.6 in.)
C_D	drag coefficient, Drag/$q_\infty S$
C_L	lift coefficient, Lift/$q_\infty S$
$C_{L,trim}$	lift coefficient at $C_m = 0$
C_{L_α}	lift-curve slope, $\Delta C_L/\Delta\alpha$, per degree
C_l	rolling-moment coefficient, Rolling moment/$q_\infty Sb$
C_{l_β}	effective-dihedral parameter, $\Delta C_l/\Delta\beta$, per degree
C_m	pitching-moment coefficient, Pitching moment/$q_\infty S\bar{c}$
$C_{m_{C_L}}$	longitudinal-stability derivative (static margin), $\Delta C_m/\Delta C_L$
$C_{m,o}$	pitching-moment coefficient at zero lift
C_n	yawing-moment coefficient, Yawing moment/$q_\infty Sb$
C_{n_β}	directional-stability parameter, $\Delta C_n/\Delta\beta$, per degree
C_Y	side-force coefficient, Side force/$q_\infty S$
C_{Y_β}	side-force parameter, $\Delta C_Y/\Delta\beta$, per degree
c	local chord, cm (in.)
$\bar{c}$	mean aerodynamic chord of basic reference wing panel, 21.03 cm (8.28 in.)

c_t	wing-tip chord, cm (in.)
M_∞	free-stream Mach number
q_∞	free-stream dynamic pressure, kPa (psf)
R	Reynolds number per unit length, per m (per ft)
S	basic wing planform reference area, 0.270 m^2 (2.906 ft^2)
α	angle of attack, deg
β	angle of sideslip, deg
Δ	increments obtained by interpolation
$\delta_{a,L}$	left aileron deflection, positive for trailing edge down, deg
$\delta_{a,R}$	right aileron deflection, positive for trailing edge down, deg
δ_f	flap deflection, positive for trailing edge down, deg
δ_h	horizontal tail deflection, positive for trailing edge down, deg

EXPERIMENTAL APPARATUS AND PROCEDURES

Test Facilities

This investigation was conducted in the Langley 8-foot transonic pressure tunnel and the Langley high-speed 7- by 10-foot tunnel. A detailed description of both wind tunnels is given in reference 12.

Model Description

A sting-mounted, full-span, 0.035-scale model of the KC-135A aircraft was used in this investigation. Drawings of the model are shown in figure 1 and photographs of the model are shown in figure 2. Table II presents the several configurations tested during this investigation.

Fuselage.- The model fuselage contours closely simulated those of the full-scale fuselage with the exception of the aft lower-fuselage region. An enlargement of this area was necessary to accommodate the model support sting.

Wing.- The basic wing of the KC-135A model has 7° dihedral, 2° of incidence at the root chord, and no geometric twist. The wing thickness ratio varies nonlinearly from 15 percent at the wing-fuselage juncture to 9 percent at the trailing-edge break station and then remains constant to the wing tip. The trapezoidal planform of the wing has a quarter-chord sweep of 35°, an aspect ratio of 7.12, and a taper ratio of 0.34. For all data analyses, the reference

geometry parameters S, b, and $\bar{c}$ are based on the trapezoidal planform of the basic wing extended to the fuselage centerline.

Two wings were used during the investigation. One had provision for attaching various combinations of flaps and ailerons. This wing, designated wing F in table II, was used for most of the Mach 0.30 tests and for all the tests at large sideslip angles. When the winglets were attached to this wing the left-winglet pressure-orifice tubes were routed along the lower surface of the left-hand panel into the side of the fuselage. A plastic filler material was added over the tubing to produce a "smooth" bump. The other wing, designated wing B, did not have ailerons or flaps but had seven rows of chordwise pressure orifices in the right-hand panel. Winglet pressure-orifice tubes were routed through the left-hand panel. This wing was used for limited tests at a Mach number of 0.30 and for all the tests above a Mach number of 0.30.

Winglet.- The winglet used in this investigation, a detailed drawing of which is given in figure 1(b), was developed during the investigation reported in references 5 to 7. It employs an 8-percent-thick general aviation airfoil, the coordinates for which are presented in reference 1. The winglet has a span equal to the wing-tip chord and a root chord equal to 65 percent of the wing-tip chord. It has an aspect ratio of 2.33, a taper ratio of 0.32, a leading-edge sweep of 38°, and a planform area for both winglets equal to 3.2 percent of the trapezoidal planform area of the basic wing. The winglet is canted outboard 15° from the vertical (75° dihedral) and toed out 4° (leading edge outboard) relative to the fuselage centerline. The winglet trailing edge is located near the wing trailing edge for greatest effectiveness (ref. 1). The winglet is untwisted and the "upper surface" is the inboard surface. To smooth the transition from the wing to the winglet, fillets were added to the inside corners at the junctures and the outside corners were rounded.

Nacelles.- Flow-through nacelles with an inlet diameter of 2.90 cm (1.14 in.) and an exit diameter of 2.07 cm (0.82 in.) were used. The inlet diameter was maintained back to approximately 0.66 of the nacelle length and then tapered linearly to the exit.

Flaps and ailerons.- Fixed flaps and outboard ailerons were attached for part of the tests at a Mach number of 0.30. When attached, the flaps were deflected 30°, the right aileron was undeflected, and the left aileron was deflected to either 0°, 20°, or -20°.

Tail surfaces.- The horizontal tail could be set at fixed deflections of 0°, -4°, and -10°, and was removed to provide tail-off data for the high-speed testing. The vertical tail was fixed at 0°.

Boundary-Layer Transition Strips

Boundary-layer transition strips were applied to all surfaces. The transition strips were comprised of a 0.16-cm (0.06-in.) wide band of carborundum

grains set in a plastic adhesive. The grains were sized according to the techniques discussed in reference 13.

No. 220 carborundum grains were applied to the fuselage 3.81 cm (1.50 in.) aft of the nose. No. 220-grain strips were also applied at 0.05c on the upper and lower surfaces of the wings, horizontal tail, and vertical tail. The pylons and nacelles had No. 240-grain transition strips placed 0.64 cm (0.25 in.) back from the leading edges. Transition strips on the winglets (also 0.16 cm (0.06 in.) wide) were No. 240 grains applied at 0.05c on the upper surface and No. 220 grains applied at 0.35c on the lower surface. Transition strips on the lower surfaces of the winglets were located by the method of reference 14 in an attempt to simulate full-scale boundary-layer displacement at the trailing edge for an ideal Reynolds number of 40×10^6.

Test Conditions

Measurements were taken at Mach numbers of 0.30, 0.50, 0.70, 0.78, and 0.82 with the angle-of-attack range from approximately -8° to 16°. The Reynolds numbers, free-stream dynamic pressures, and the nominal sideslip angles at which data were obtained are shown in table II.

Measurements

Force and moment data were obtained by use of a six-component electrical strain-gage balance. An accelerometer located in the fuselage was used to measure angle of attack. Static pressures were measured in the model sting cavity and at the model base by using differential-pressure transducers referenced to free-stream static pressure.

Corrections

In the 8-foot transonic pressure tunnel the angle of attack was corrected for flow angularity in the test section. The correction was obtained by testing the model upright and inverted. In the high-speed 7- by 10-foot tunnel the angle of attack was measured at the back of the support sting and was corrected for deflections of the balance and sting combination. A correction for test-section flow angularity was assumed to be negligible based on tests with a similar size model. The lift, drag, and pitching-moment coefficients have been adjusted to correspond to a free-stream static-pressure condition at the base of the model and within the sting cavity.

PRESENTATION OF RESULTS

The results of this investigation are presented in the following figures. No performance results are presented for wing F because of interference effects caused by the presence of the winglet pressure tubes on the wing lower surface.

DISCUSSION OF RESULTS

Longitudinal Aerodynamic Characteristics

Performance.- Several models have been utilized to obtain the aerodynamic results for the KC-135A. (See table I.) The models differed both in scale and in wing stiffness. In particular, the semispan model of references 4 to 7 was constructed to obtain the highest possible Reynolds numbers on the winglets and also to achieve a deflected wing shape under load which approximated that of the full-scale airplane in cruise flight. The full-span model of the present investigation, on the other hand, was utilized primarily to obtain stability and control results, particularly in the yawed condition, and employed a steel wing which deflected less than the full-scale wing. As a result, the performance data contained herein should be used with caution, and appropriate adjustments should be made for flexibility effects. Data for the KC-135A semispan model, where available, should be considered as the prime data for use in performance analyses. Results of the present investigation indicate that winglets are effective in reducing drag over the range of Mach numbers tested (figs. 3 to 6).

Low-speed characteristics.- The data indicate that winglets increase the KC-135A longitudinal static stability (slope of the curve of pitching-moment coefficient versus lift coefficient becomes more negative). The winglets also delay the pitch-up characteristics of the basic KC-135A.

The data presented are for an untrimmed configuration without flaps (figs. 3(a) to 3(c)) and for a nearly trimmed take-off configuration, $\delta_f = 30^o$ and $C_L \approx 1.0$ (figs. 4(a) to 4(e)). These data along with data in figure 13 of reference 8 for the take-off condition indicate that the addition of the winglets requires approximately 0.5^o more negative horizontal-tail deflection to

achieve the same nearly trimmed condition. The data obtained in the two wind tunnels (fig. 4(a)) did not differ in lift-curve slope C_{L_α} or longitudinal stability $C_{m_{C_L}}$. Comparison of figure 4(a) with figure 5 of reference 8 shows that the bump on the left-hand panel lower surface (for instrumentation) did not affect the lift-curve slope or the longitudinal stability. The effects due to increasing Reynolds number were, as expected, slight increases in maximum lift coefficient and lift-curve slope at the higher angles of attack, and slight decreases in longitudinal stability. (See fig. 3(b), for example.) Except for small changes in the longitudinal stability at lift coefficients less than 0.6, there was no effect of sideslip angle, up to $\pm 12^\circ$, on the longitudinal characteristics (figs. 4(c) to 4(e)).

High-speed characteristics.- The data in figures 4 and 5 indicate that winglets cause a slight increase in the lift-curve slope. The winglets increase the longitudinal stability slightly and also delay pitch-up in the basic KC-135A. The KC-135A with a horizontal-tail deflection of -4° is trimmed in the range of lift coefficients from 0.30 to 0.40 without winglets and is trimmed in the range of lift coefficients from 0.26 to 0.34 with winglets. (See figs. 6 and 7.) At a lift coefficient of 0.40, the representative cruise condition used in all previous analyses, the addition of the winglets requires between 0.27° and 0.38° more negative horizontal-tail deflection for trim. The associated drag penalty is minimal. Reference 15 indicates that when the flight profile of the KC-135A with winglets is reoptimized for long-range cruise, the average cruise lift coefficient increases from 0.426 to 0.447 and the cruise Mach number increases from 0.770 to 0.774. The data in figure 6(c) ($M_\infty = 0.78$) indicate that this change in average cruise lift coefficient will result in 0.47° more negative tail deflection. The associated drag coefficient penalty would again be minimal, about 0.0001. Reference 5 indicates that this change in average cruise lift coefficient will result in a decrease in drag coefficient of 0.0008.

Summary data at a lift coefficient of 0.40 and horizontal tail deflection of -4° are presented in figure 8. The addition of the winglets has a slight, favorable effect on the lift-curve slope C_{L_α}. This effect decreases with increasing Mach number. Also, the static margin increases by 1.5 to 3.0 percent through the Mach number range.

Lateral-Directional Aerodynamic Characteristics

The addition of the winglets has a significant effect on the lateral-directional stability at all Mach numbers. (See figs. 9 to 13.) Winglets increase the dihedral effect $-C_{l_\beta}$ (lateral stability) at cruise lift coefficients by about 18 percent at low speeds (fig. 11) and by about 20 percent at high subsonic speeds (figs. 13 and 14). Winglets increase the directional stability C_{n_β} for near cruise lift coefficients by about 6 percent at low subsonic speeds (fig. 11) to about 10 percent at high subsonic speeds (figs. 13

and 14). Reference 15 indicates that these large changes in the lateral-directional stability parameters could have a significant effect on the unaugmented Dutch-roll characteristics.

Sideslip angles up to $\pm 12^{\circ}$ have no significant effect on the lateral-directional characteristics of the winglet configuration (figs. 10(b) to 10(e)). Also, variation of Reynolds number does not change the effect of the addition of winglets on the low-speed lateral-directional stability (fig. 11).

SUMMARY OF RESULTS

A wind-tunnel investigation has been conducted to identify variations in stability and control due to the addition of winglets to a model of the KC-135A. Static longitudinal and lateral-directional aerodynamic characteristics have been determined for a 0.035-scale model of the KC-135A with and without winglets at Mach numbers from 0.30 to 0.82, at angles of attack from -8° to 16°, and at angles of sideslip to 12°. The following results were obtained:

1. Winglets produce small favorable effects on the lift-curve slope C_{L_α}. This effect decreases with increasing Mach number.

2. Winglets increase longitudinal static stability.

3. Winglets require less than 0.5° change in the horizontal-tail trim deflection. The associated trim drag coefficient is minimal (about 0.0001 at cruise conditions).

4. Winglets increase the lift coefficient at which pitch-up occurs.

5. Winglets increase the dihedral effect about 18 to 20 percent and the directional stability about 6 to 10 percent. These large changes could have a significant effect on the unaugmented Dutch-roll characteristics.

Langley Research Center
National Aeronautics and Space Administration
Hampton, VA 23665
August 24, 1979

REFERENCES

1. Whitcomb, Richard T.: A Design Approach and Selected Wind-Tunnel Results at High Subsonic Speeds for Wing-Tip Mounted Winglets. NASA TN D-8260, 1976.

2. Flechner, Stuart G.; Jacobs, Peter F.; and Whitcomb, Richard T.: A High Subsonic Speed Wind-Tunnel Investigation of Winglets on a Representative Second-Generation Jet Transport Wing. NASA TN D-8264, 1976.

3. Jacobs, Peter F.; and Flechner, Stuart G.: The Effect of Winglets on the Static Aerodynamic Stability Characteristics of a Representative Second Generation Jet Transport Model. NASA TN D-8267, 1976.

4. Flechner, Stuart G.; and Jacobs, Peter F.: Experimental Results of Winglets on First, Second, and Third Generation Jet Transports. NASA TM-72674, 1978.

5. Jacobs, Peter F.; Flechner, Stuart G.; and Montoya, Lawrence C.: Effect of Winglets on a First-Generation Jet Transport Wing. I - Longitudinal Aerodynamic Characteristics of a Semispan Model at Subsonic Speeds. NASA TN D-8473, 1977.

6. Montoya, Lawrence C.; Flechner, Stuart G.; and Jacobs, Peter F.: Effect of Winglets on a First-Generation Jet Transport Wing. II - Pressure and Spanwise Load Distributions for a Semispan Model at High Subsonic Speeds. NASA TN D-8474, 1977.

7. Montoya, Lawrence C.; Jacobs, Peter F.; and Flechner, Stuart G.: Effect of Winglets on a First-Generation Jet Transport Wing. III - Pressure and Spanwise Load Distributions for a Semispan Model at Mach 0.30. NASA TN D-8478, 1977.

8. Meyer, Robert R., Jr.: Effect of Winglets on a First-Generation Jet Transport Wing. IV - Stability Characteristics for a Full-Span Model at Mach 0.30. NASA TP-1119, 1978.

9. Jacobs, Peter F.: Effect of Winglets on a First-Generation Jet Transport Wing. V - Stability Characteristics of a Full-Span Wing With a Generalized Fuselage at High Subsonic Speeds. NASA TP-1163, 1978.

10. Ishimitsu, K. K.; VanDevender, N.; and Dodson, R.: Design and Analysis of Winglets for Military Aircraft. AFFDL-TR-76-6, U.S. Air Force, Feb. 1976.

11. Mechtly, E. A.: The International System of Units - Physical Constants and Conversion Factors (Second Revision). NASA SP-7012, 1973.

12. Schaefer, William T., Jr.: Characteristics of Major Active Wind Tunnels at the Langley Research Center. NASA TM X-1130, 1965.

13. Braslow, Albert L.; and Knox, Eugene C.: Simplified Method for Determination of Critical Height of Distributed Roughness Particles for Boundary-Layer Transition at Mach Numbers From 0 to 5. NACA TN 4363, 1958.

14. Blackwell, James A., Jr.: Preliminary Study of Effects of Reynolds Number and Boundary-Layer Transition Location on Shock-Induced Separation. NASA TN D-5003, 1969.

15. Ishimitsu, K. K.; and Zanton, D. F.: Design and Analysis of Winglets for Military Aircraft: Phase II. AFFDL-TR-77-23, U.S. Air Force, May 1977. (Available from DDC as AD A046 152.)

TABLE I.- PUBLICATION SERIES ON THE EFFECT OF WINGLETS ON A KC-135A

Part	NASA Pub. No.	Model	M_∞	Data presented (not inclusive)
I	TN D-8473	Semispan; 0.07 scale	0.30 to 0.80	Longitudinal characteristics for basic wing tip and other tip configurations; incremental wing-root bending moments; low-speed longitudinal characteristics for basic wing tip and other tip configurations, with and without high-lift devices.
II	TN D-8474	Semispan; 0.07 scale	0.70 to 0.80	Wing and winglet chordwise pressure and spanwise load distributions for basic and several tip configurations.
III	TN D-8478	Semispan; 0.07 scale	0.30	Wing and winglet chordwise pressure and spanwise load distributions for basic and several tip configurations, with and without high-lift devices.
IV	TP-1119	Full span; 0.035 scale	0.30	Low-speed longitudinal and lateral-directional characteristics for several flap, aileron, and horizontal-tail configurations with and without an upper winglet.
V	TP-1163	Full span; 0.035 scale tailless generalized fuselage	0.50 to 0.95	Longitudinal and lateral-directional characteristics with and without an upper winglet for wide angle-of-attack range; incremental wing bending moments; wing buffet with and without an upper winglet.
VI	TP-1330 (This paper)	Full span; 0.035 scale	0.30 to 0.95	Longitudinal and lateral-directional characteristics with and without an upper winglet; low-speed lateral-directional characteristics up to 12° sideslip for take-off configuration with winglets.

TABLE II.- TEST CONDITIONS AND MODEL CONFIGURATIONS

M_∞	R		q_∞		β, deg	LaRC wind tunnel	Wing	Winglet		δ_h, deg	δ_f, deg	$\delta_{a,R}$, deg	$\delta_{a,L}$, deg
	per m	per ft	kPa	psf				Off	On				
0.30	5.84×10^6 to 6.11×10^6	1.78×10^6 to 1.86×10^6	6.00	125	0, ±5	[a]8' TPT	B	X	X	-10	---	----	------
.30	5.84×10^6 to 6.11×10^6	1.78×10^6 to 1.86×10^6	6.00	125	0	8' TPT	F		X	-10	30	0	0
.30	6.41×10^6 to 7.02×10^6	1.96×10^6 to 2.14×10^6	6.00 to 6.09	125 to 127	0, ±5, ±9, ±12	[b]7 × 10	F		X	-10	30	0	0, +20
.30	11.69×10^6 to 12.22×10^6	3.56×10^6 to 3.72×10^6	12.02	251	0, ±5	8' TPT	B	X	X	-10	---	---	------
.30	11.69×10^6 to 12.22×10^6	3.56×10^6 to 3.72×10^6	12.02	251	0, ±5	8' TPT	F		X	-10	30	0	0, ±20
.50	6.81×10^6	2.08×10^6	11.23	235	0, ±5	8' TPT	B	X	X	Off, 0, -4	---	---	------
.70	8.64×10^6	2.63×10^6	18.83	393	0, ±5	8' TPT	B	X	X	Off, 0, -4	---	---	------
.78	9.18×10^6	2.80×10^6	21.69	453	0, ±5	8' TPT	B	X	X	Off, 0, -4	---	---	------
.82	9.41×10^6	2.87×10^6	23.04	481	0, ±5	8' TPT	B	X	X	Off, 0, -4	---	---	------

[a]Langley 8-foot transonic pressure tunnel.
[b]Langley high-speed 7- by 10-foot tunnel.

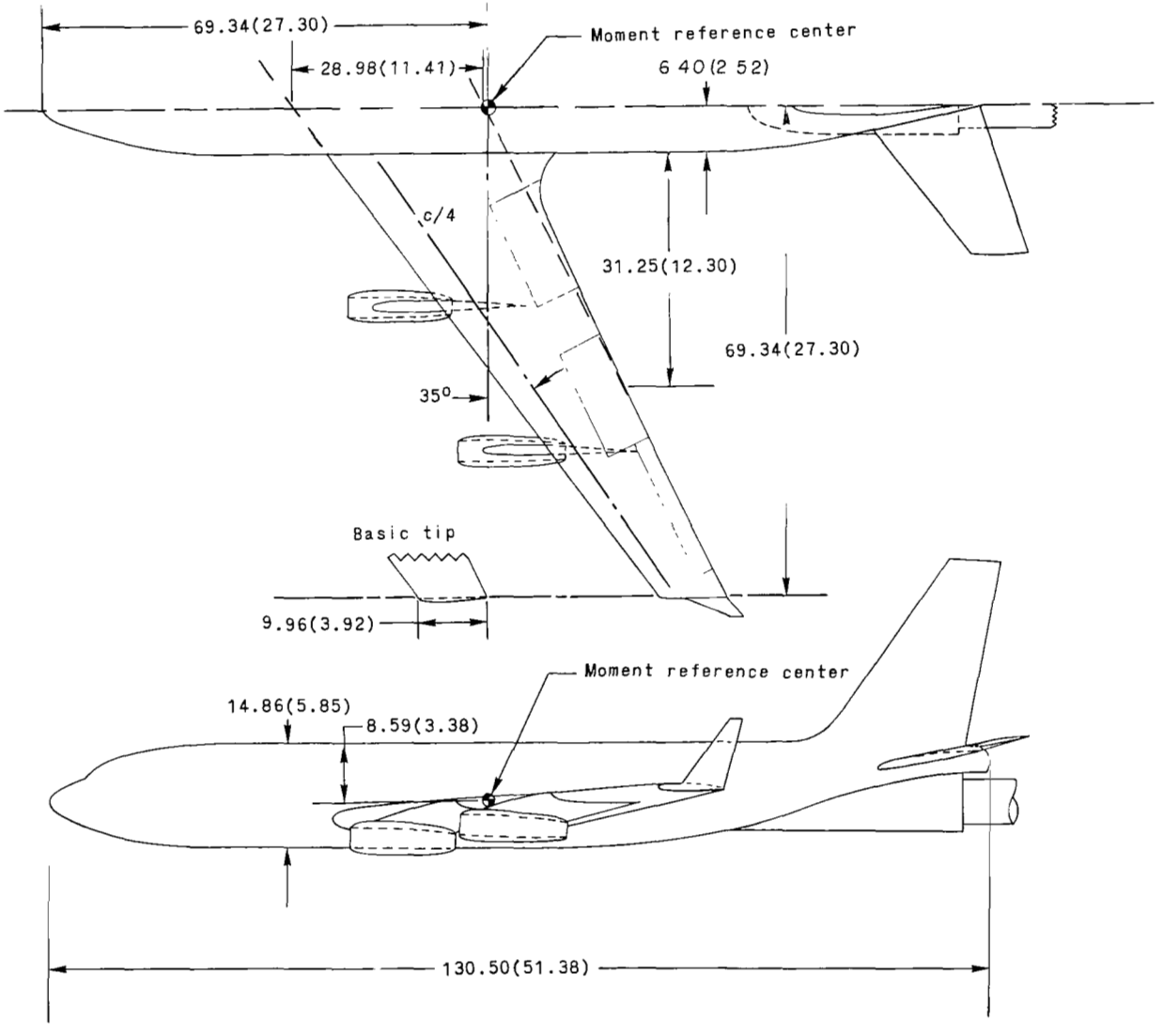

(a) General arrangement.

Figure 1.- Drawing of 0.035-scale, full-span KC-135A model. Dimensions are in centimeters (inches).

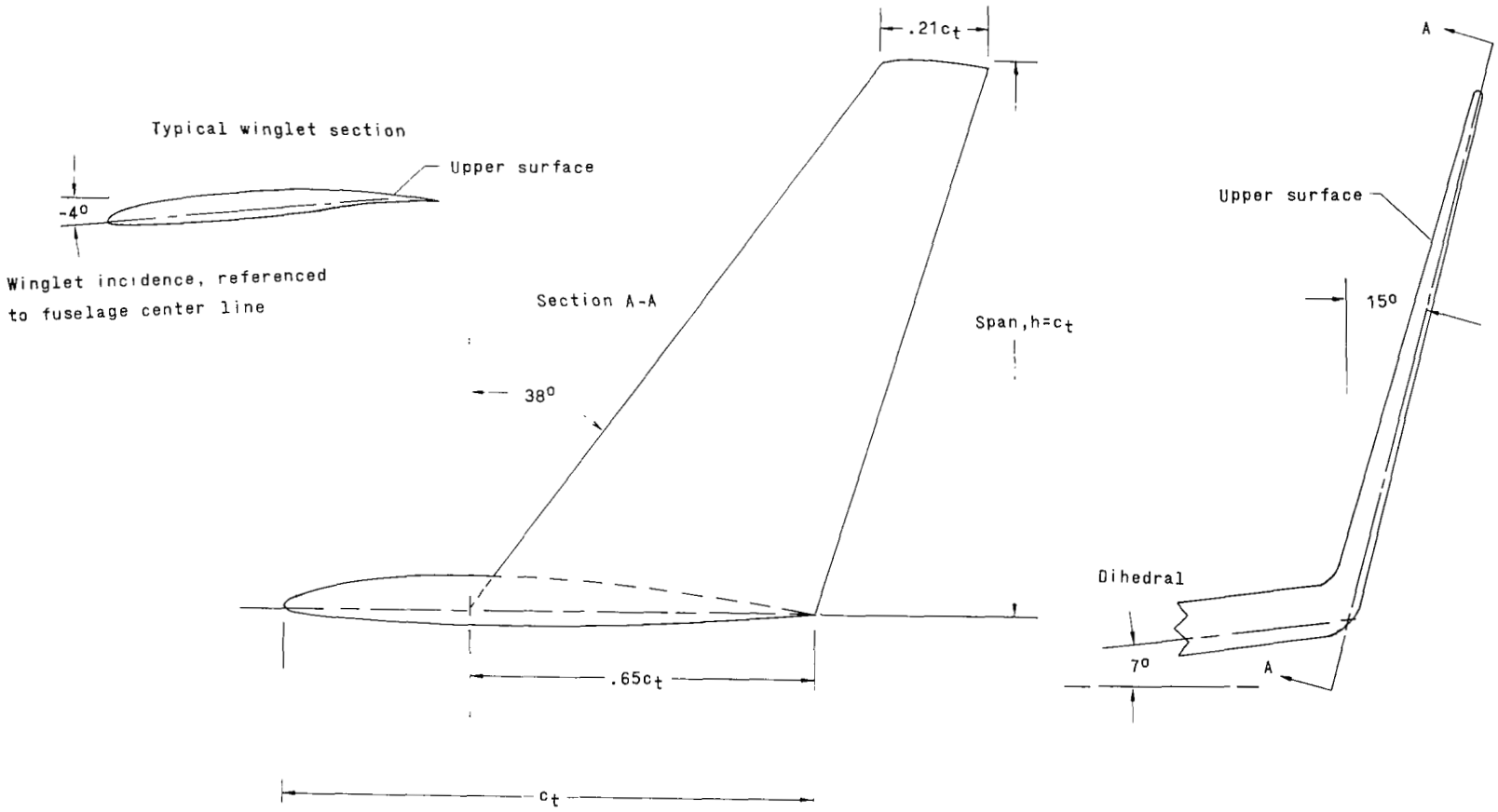

(b) Winglet details.

Figure 1.- Concluded.

L-77-2515

(a) Wing B.

Figure 2.- Photographs of wind-tunnel model with winglets.

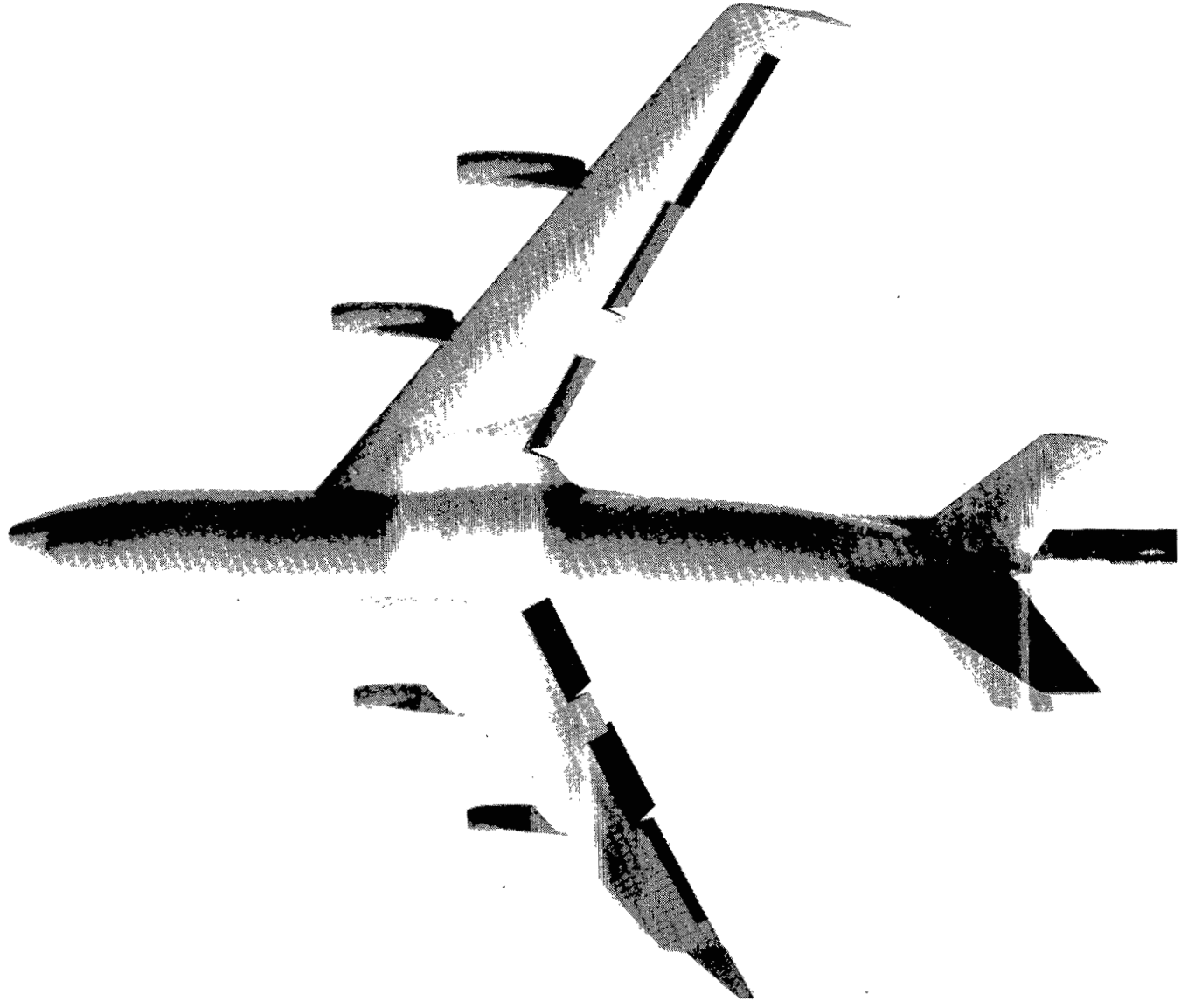

L-76-5691

(b) Wing F.

Figure 2.- Concluded.

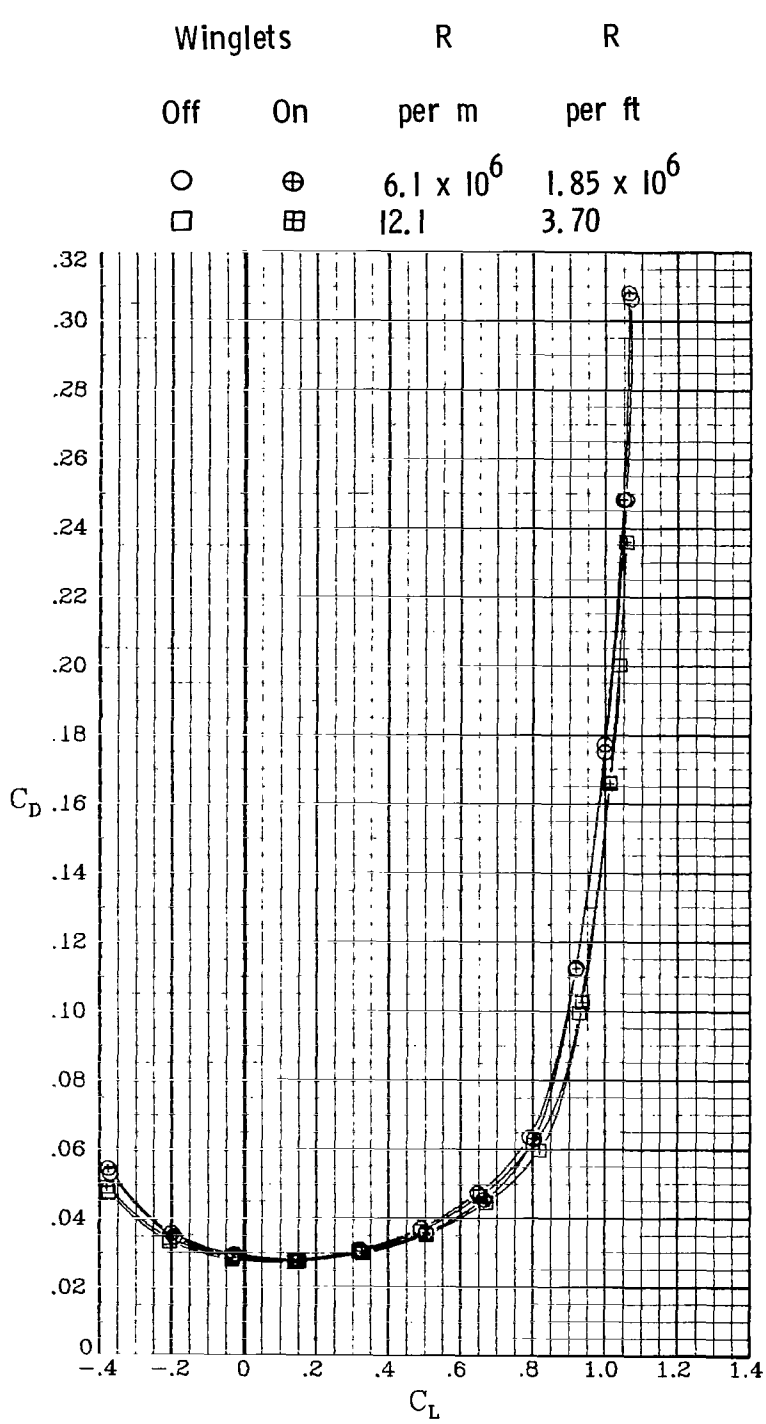

(a) $\beta = 0^{\circ}$.

Figure 3.- Longitudinal aerodynamic characteristics at $M_\infty = 0.30$ for configuration with wing B. $\delta_h = -10^{\circ}$.

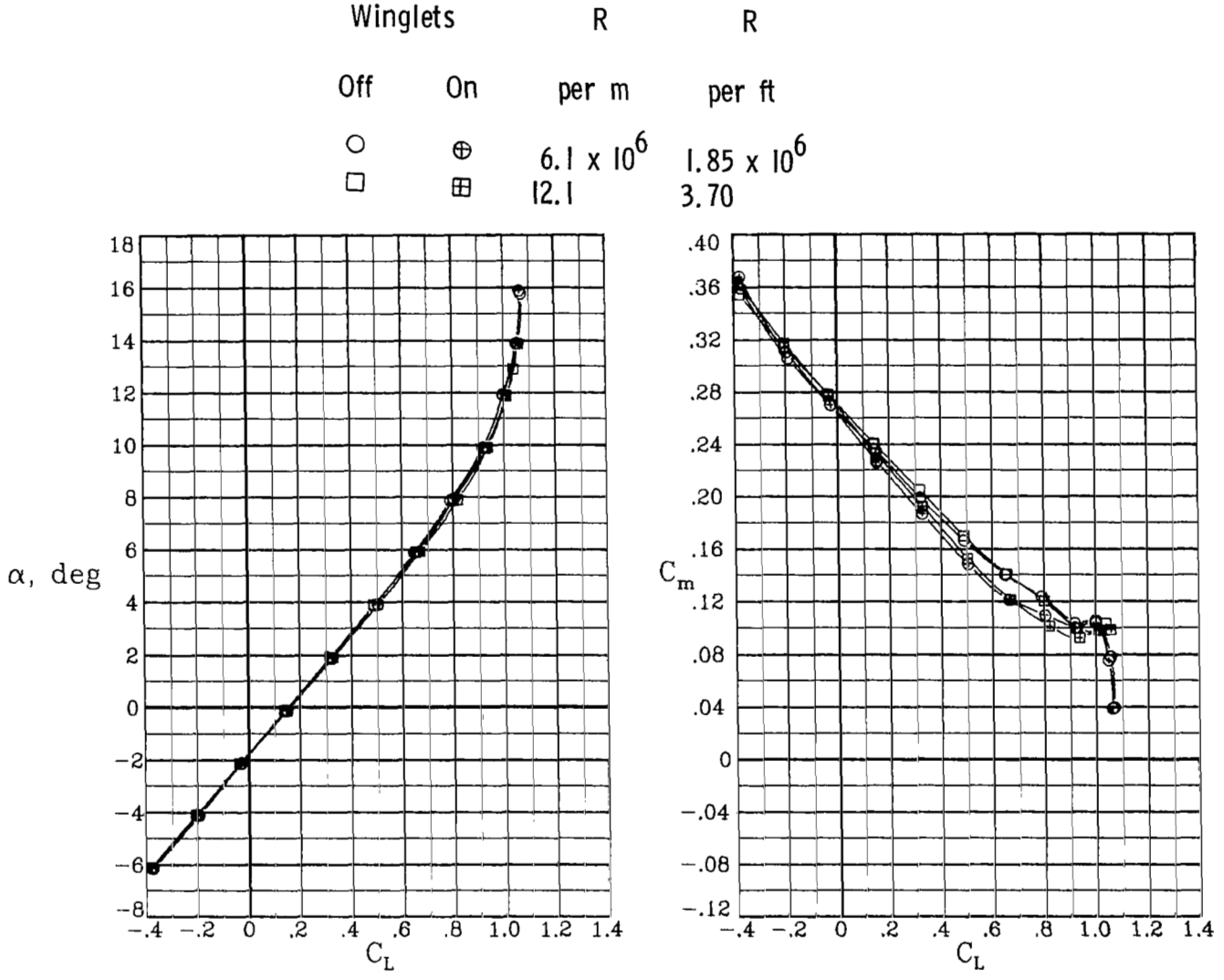

(a) Concluded.

Figure 3.- Continued.

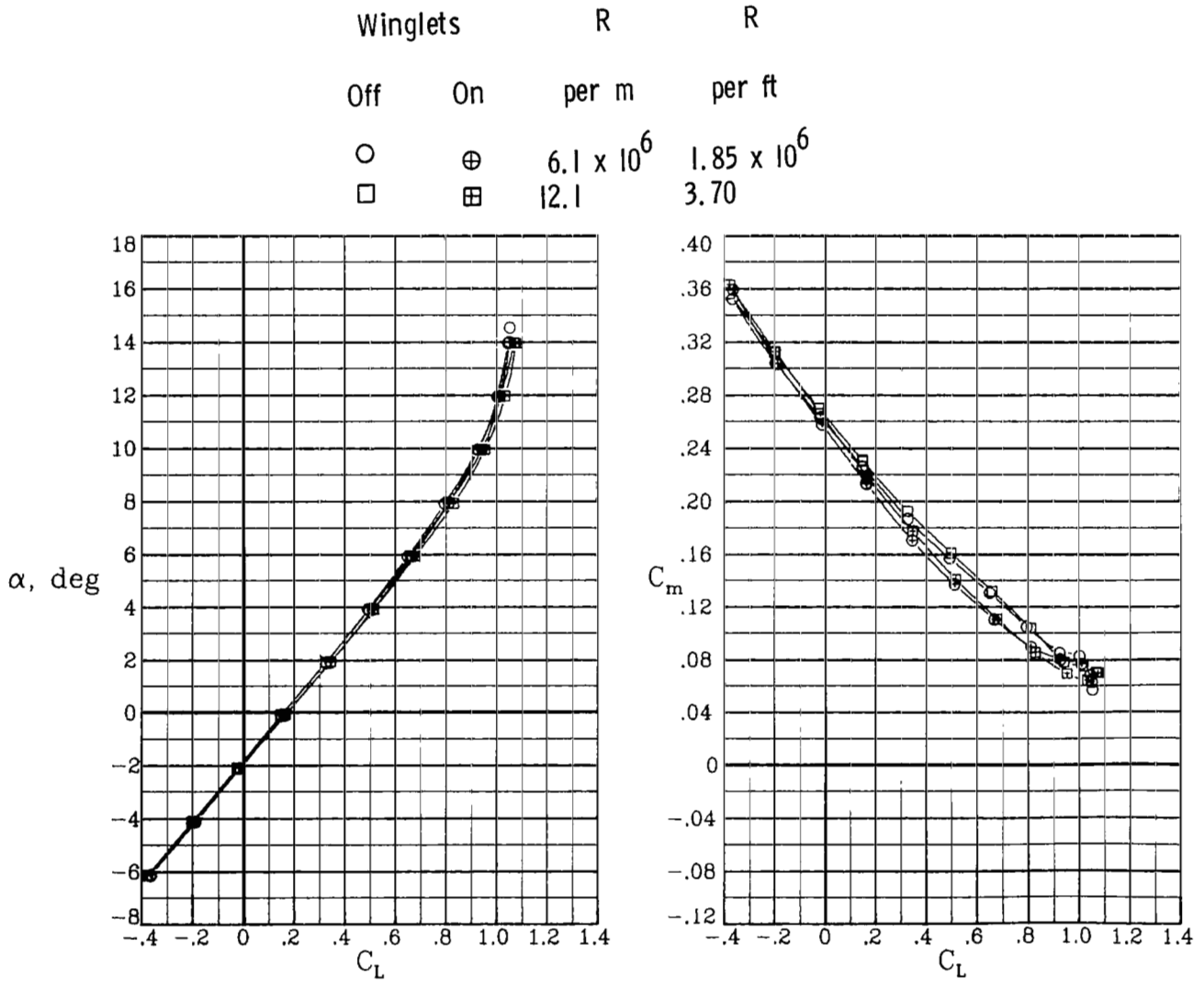

(b) $\beta = 5^{\circ}$.

Figure 3.- Continued.

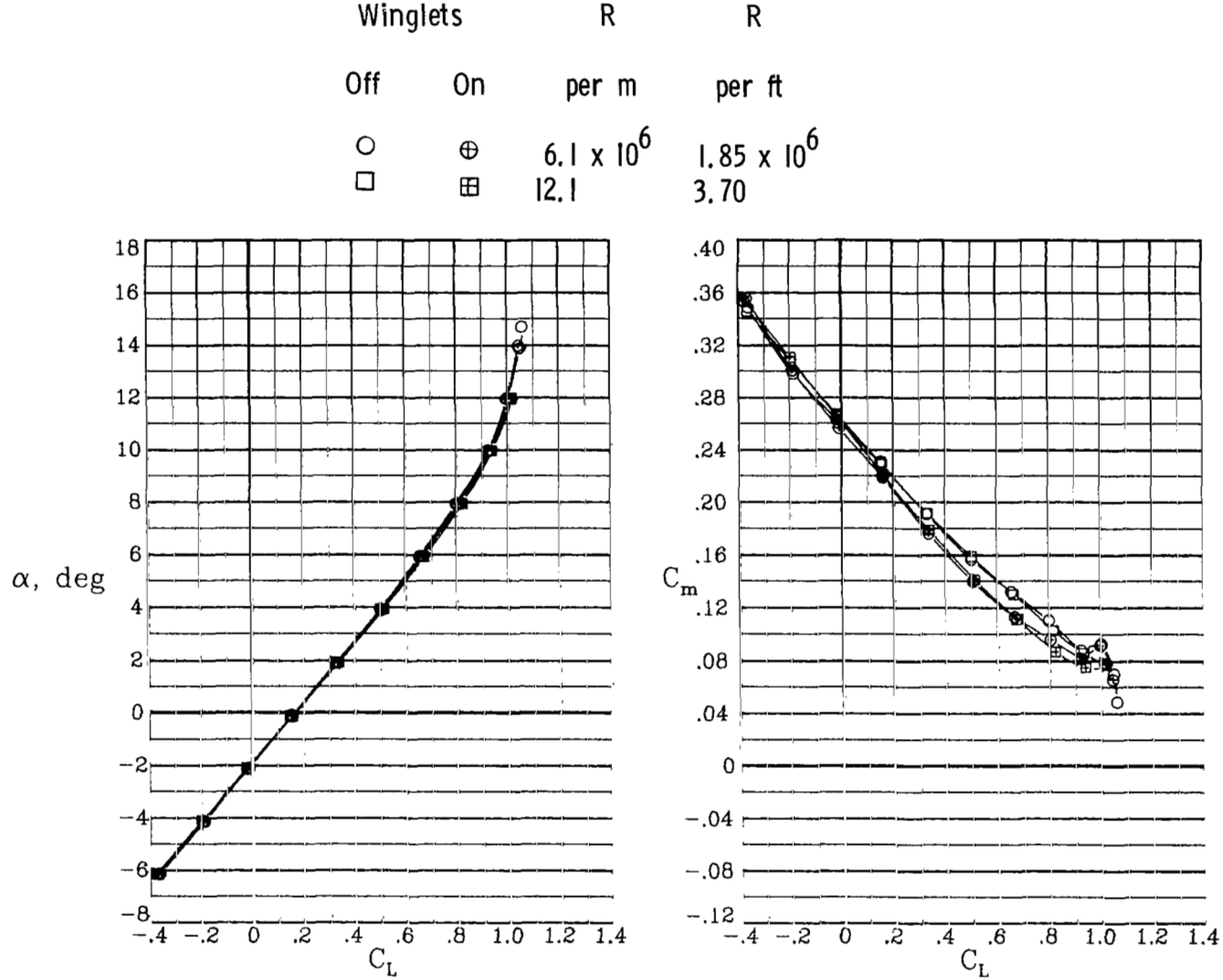

(c) $\beta = -5^{\circ}$.

Figure 3.- Concluded.

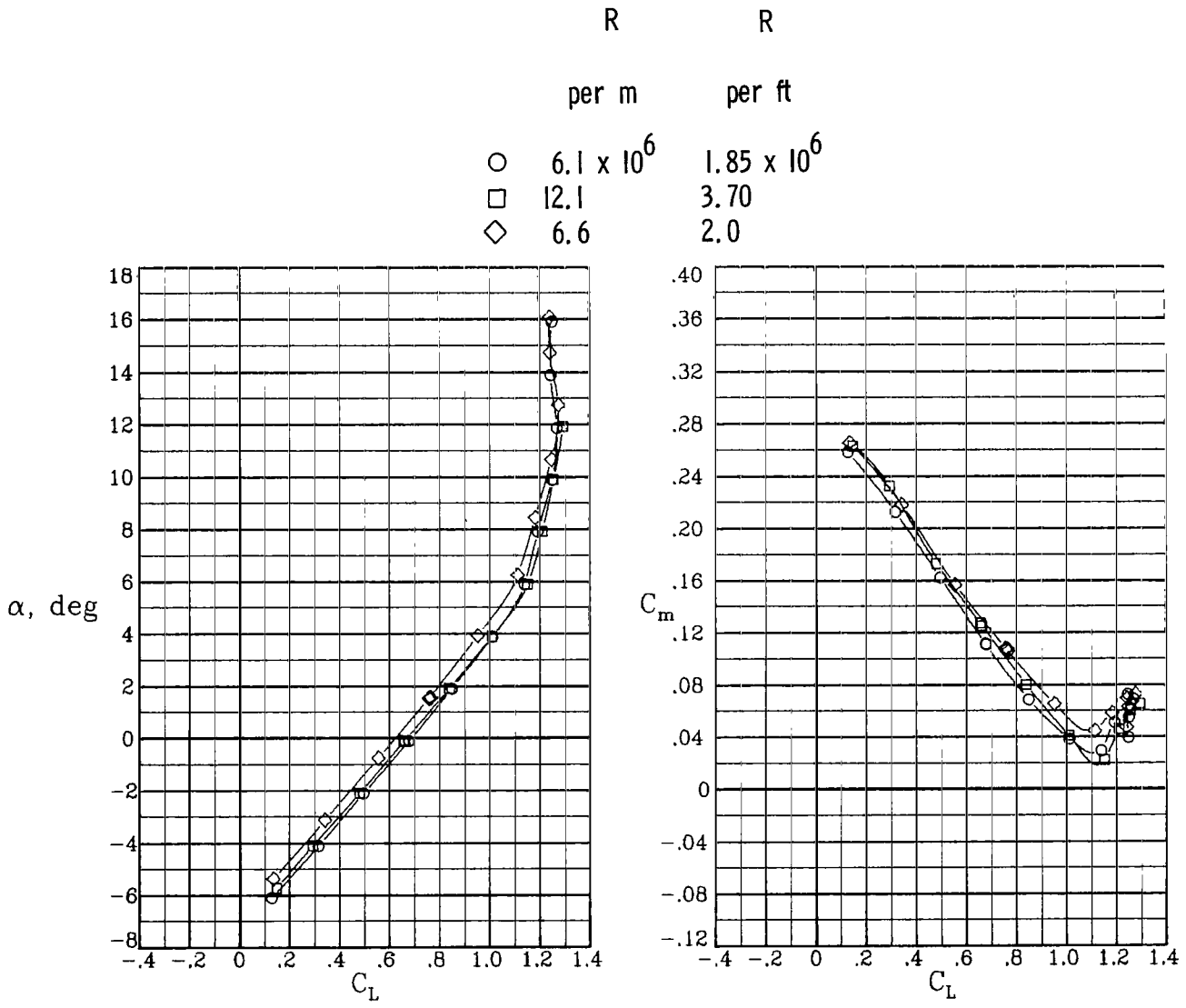

(a) $\beta = 0^{o}$; $\delta_{a,L} = 0^{o}$; $\delta_{a,R} = 0^{o}$; $\delta_{f} = 30^{o}$.

Figure 4.- Longitudinal aerodynamic characteristics at $M_{\infty} = 0.30$ for configuration with wing F. Winglets on; $\delta_{h} = -10^{o}$.

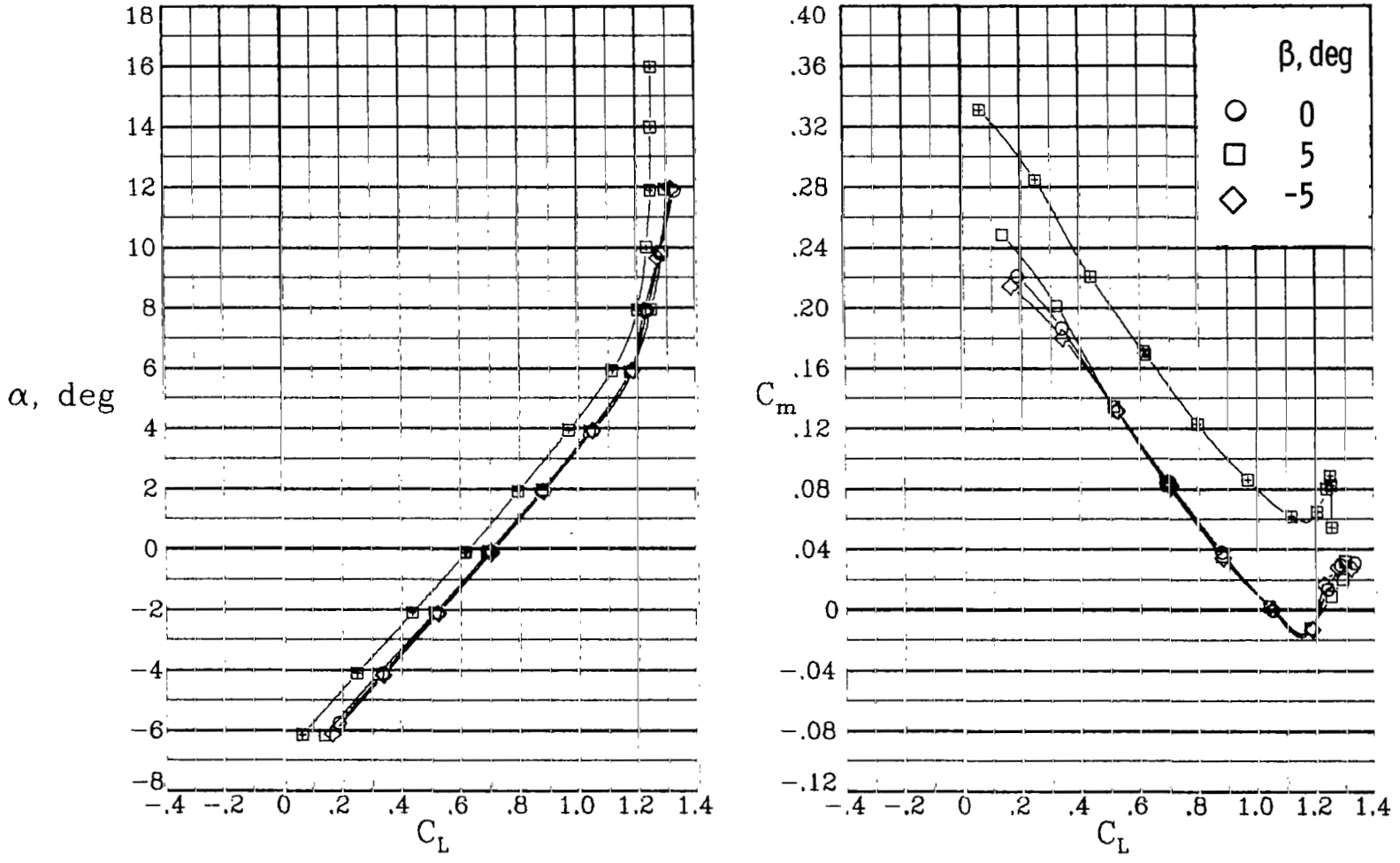

(b) R = 12.1 × 10^6 per m (3.70 × 10^6 per ft); $\delta_{a,L} = 20^o$; $\delta_{a,R} = 0^o$; $\delta_f = 30^o$. ("+" in symbol for $\delta_{a,L} = -20^o$.)

Figure 4.- Continued.

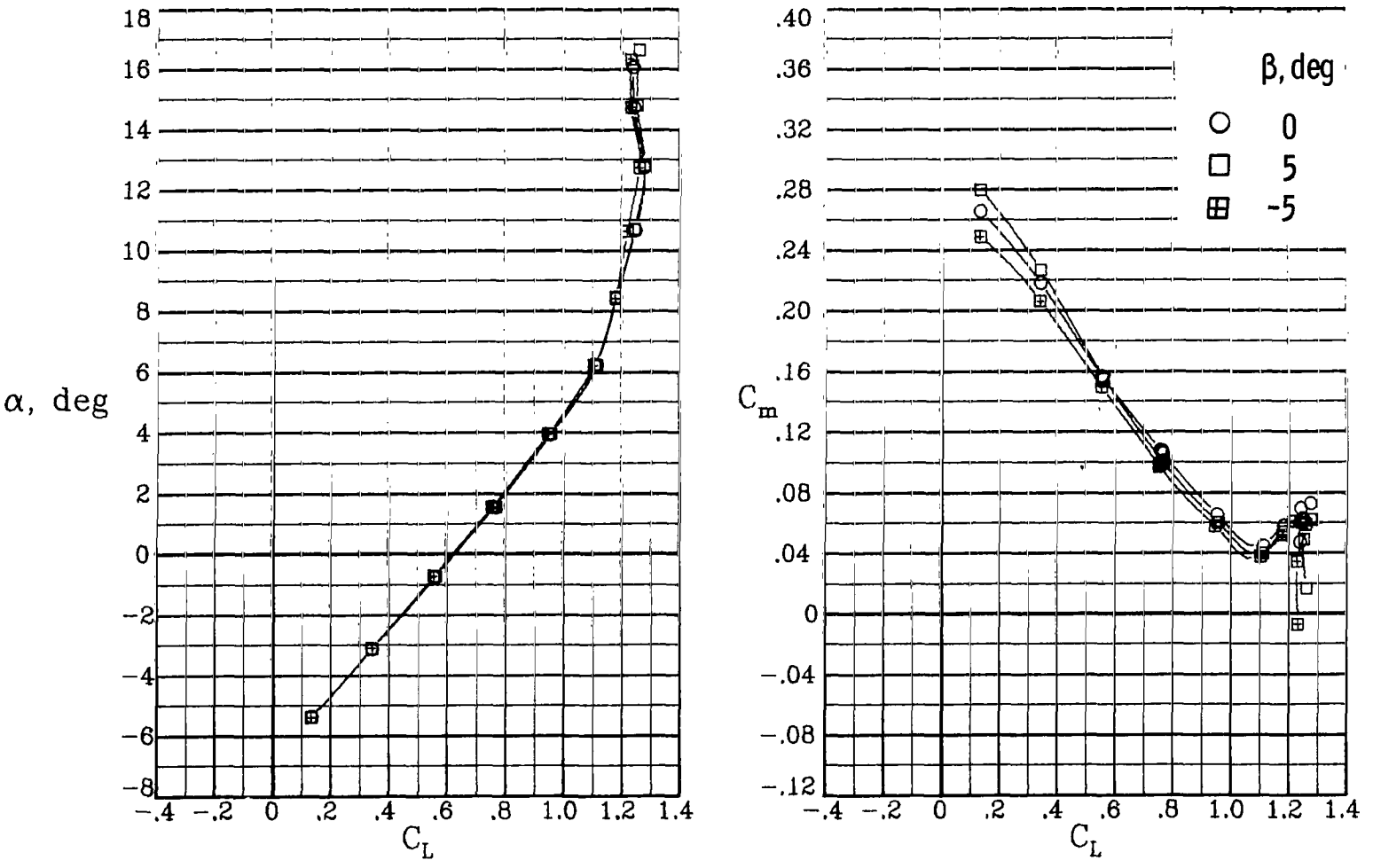

(c) R = 6.6 × 10^6 per m (2.0 × 10^6 per ft); $\delta_{a,L} = 0^o$; $\delta_{a,R} = 0^o$; $\delta_f = 30^o$.

Figure 4.- Continued.

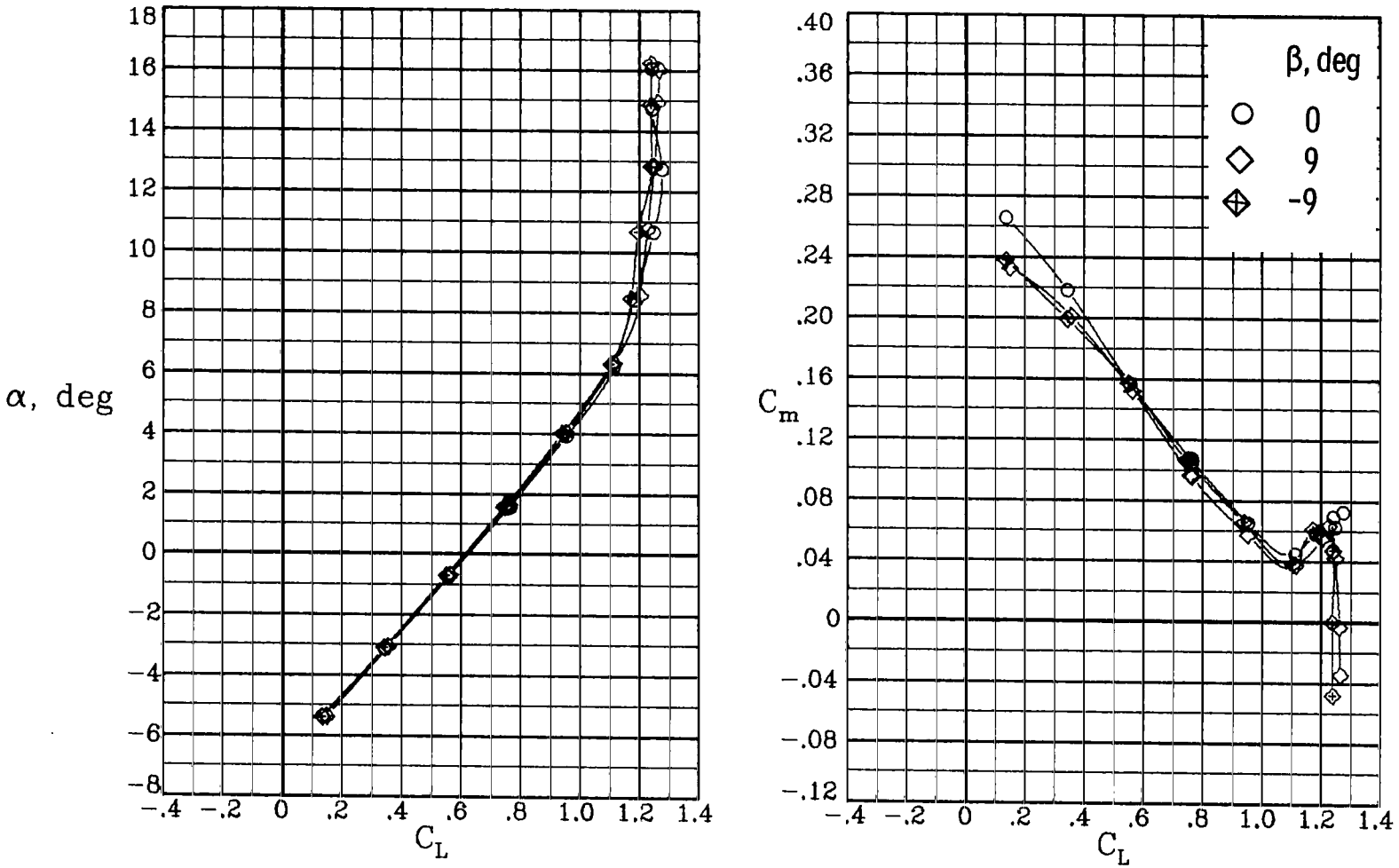

(c) Continued.

Figure 4.- Continued.

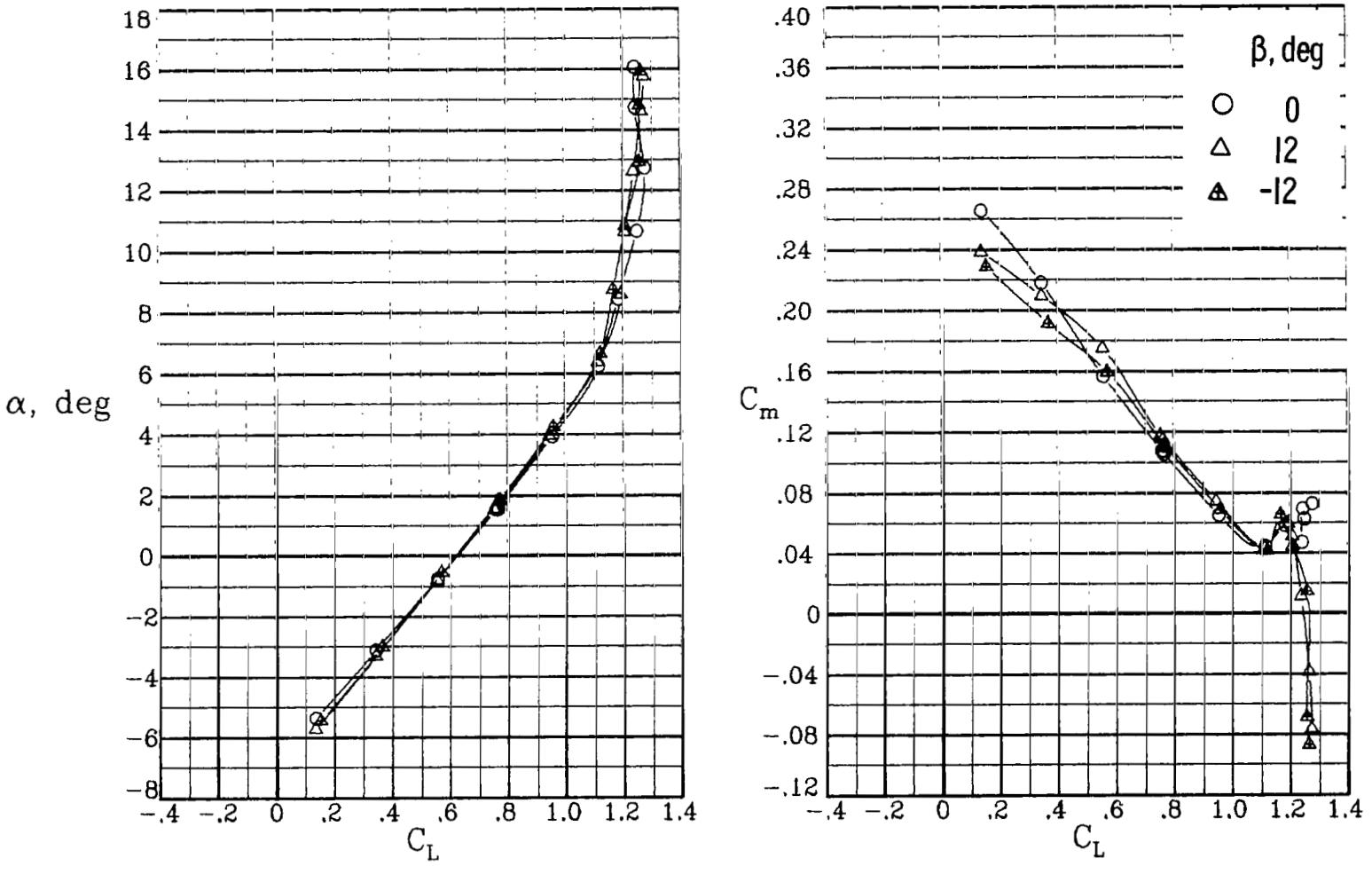

(c) Concluded.

Figure 4.- Continued.

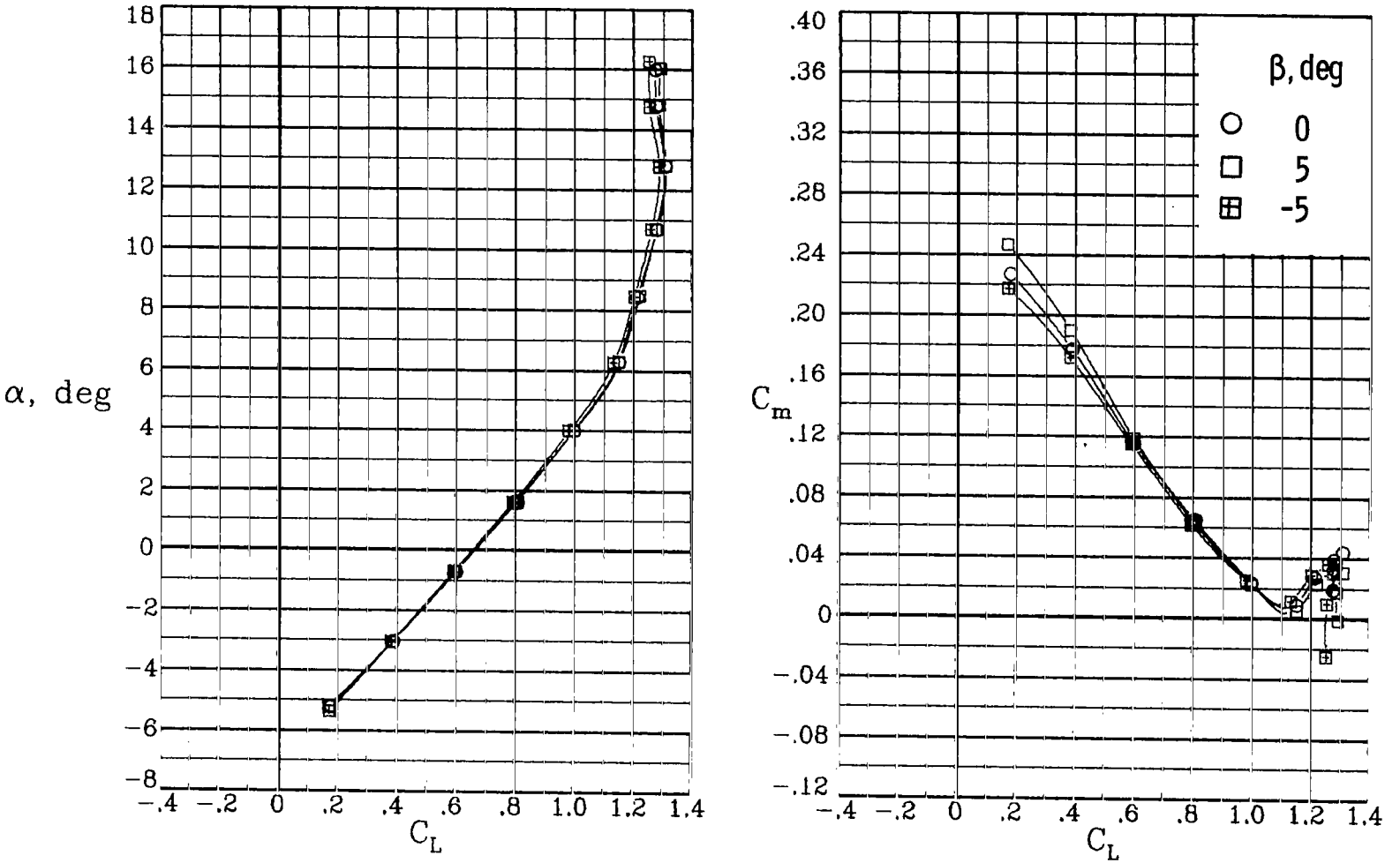

(d) R = 6.6 × 10^6 per m (2.0 × 10^6 per ft); $\delta_{a,L}$ = 20°; $\delta_{a,R}$ = 0°; δ_f = 30°.

Figure 4.- Continued.

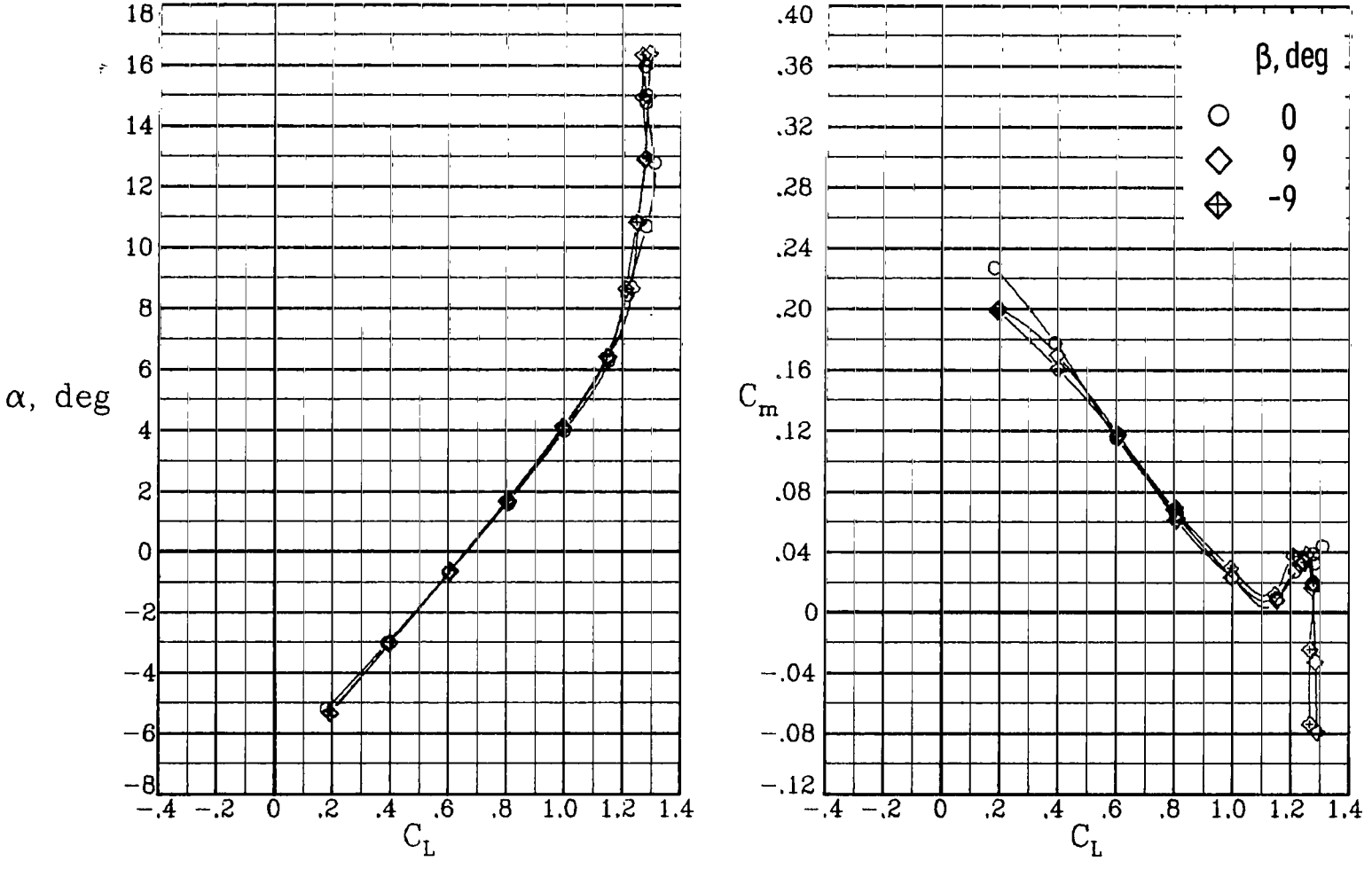

(d) Continued.

Figure 4.- Continued.

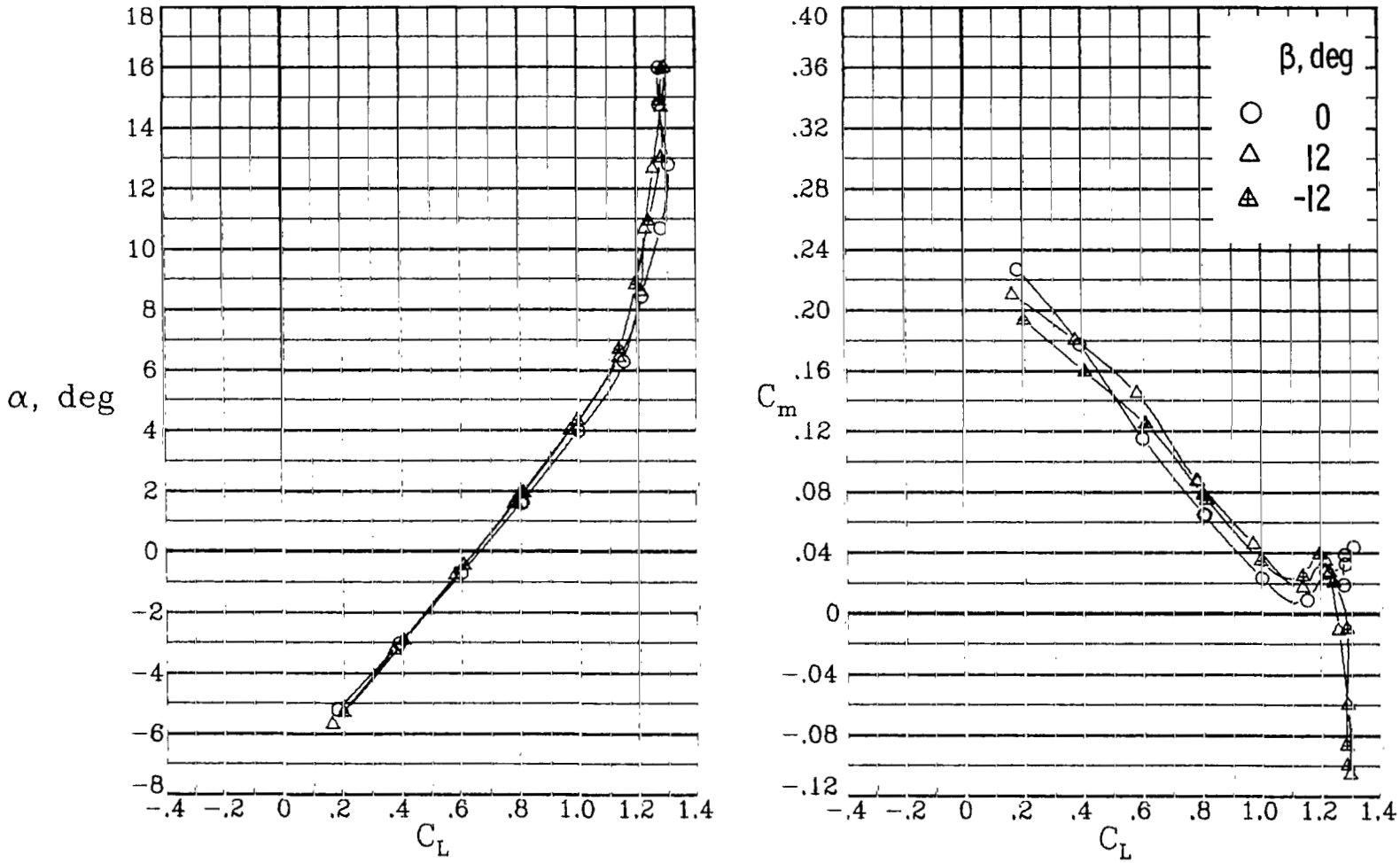

(d) Concluded.

Figure 4.- Continued.

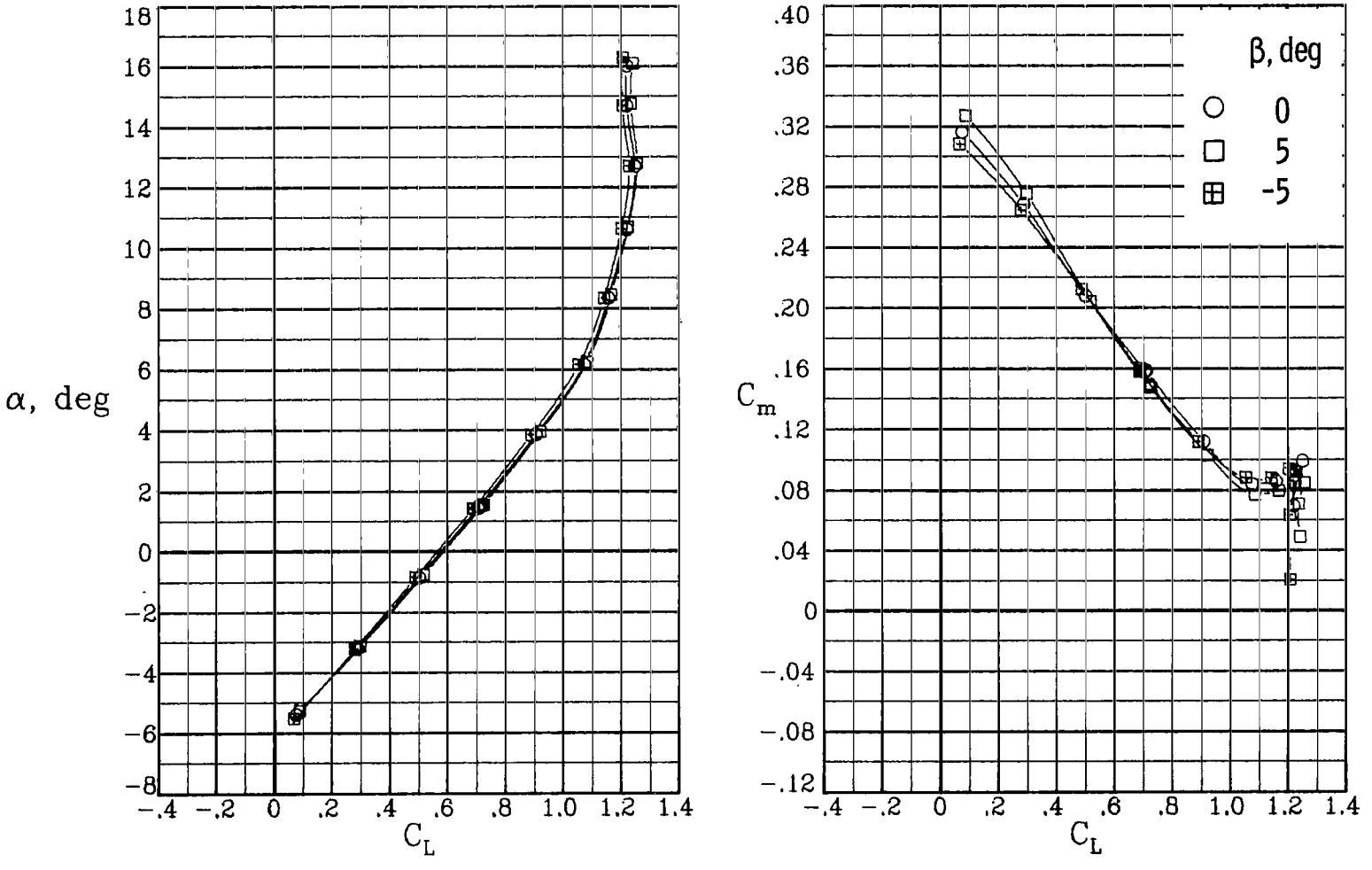

(e) R = 6.6 × 10^6 per m (2.0 × 10^6 per ft); $\delta_{a,L} = -20°$; $\delta_{a,R} = 0°$; $\delta_f = 30°$.

Figure 4.- Continued.

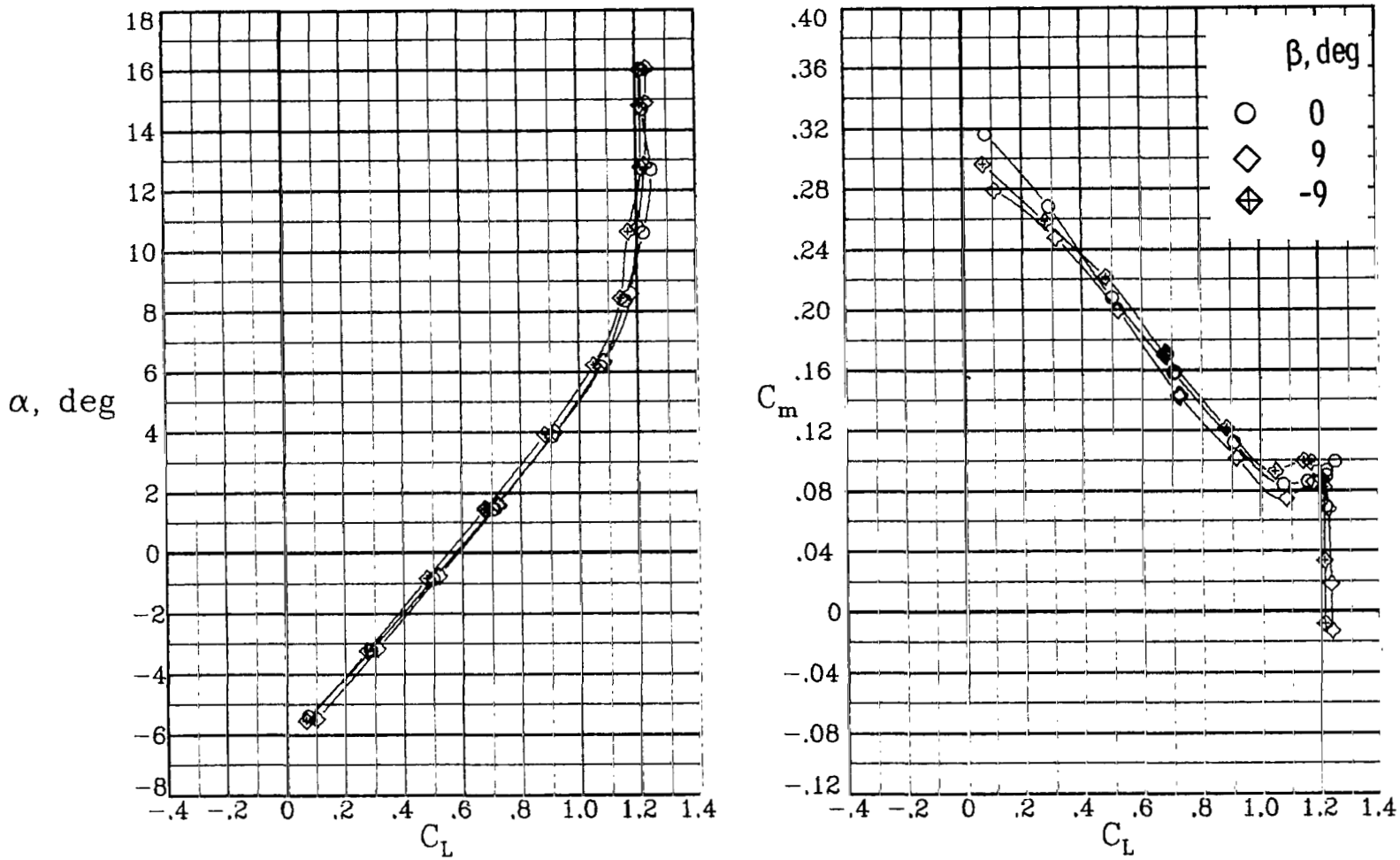

(e) Continued.

Figure 4.- Continued.

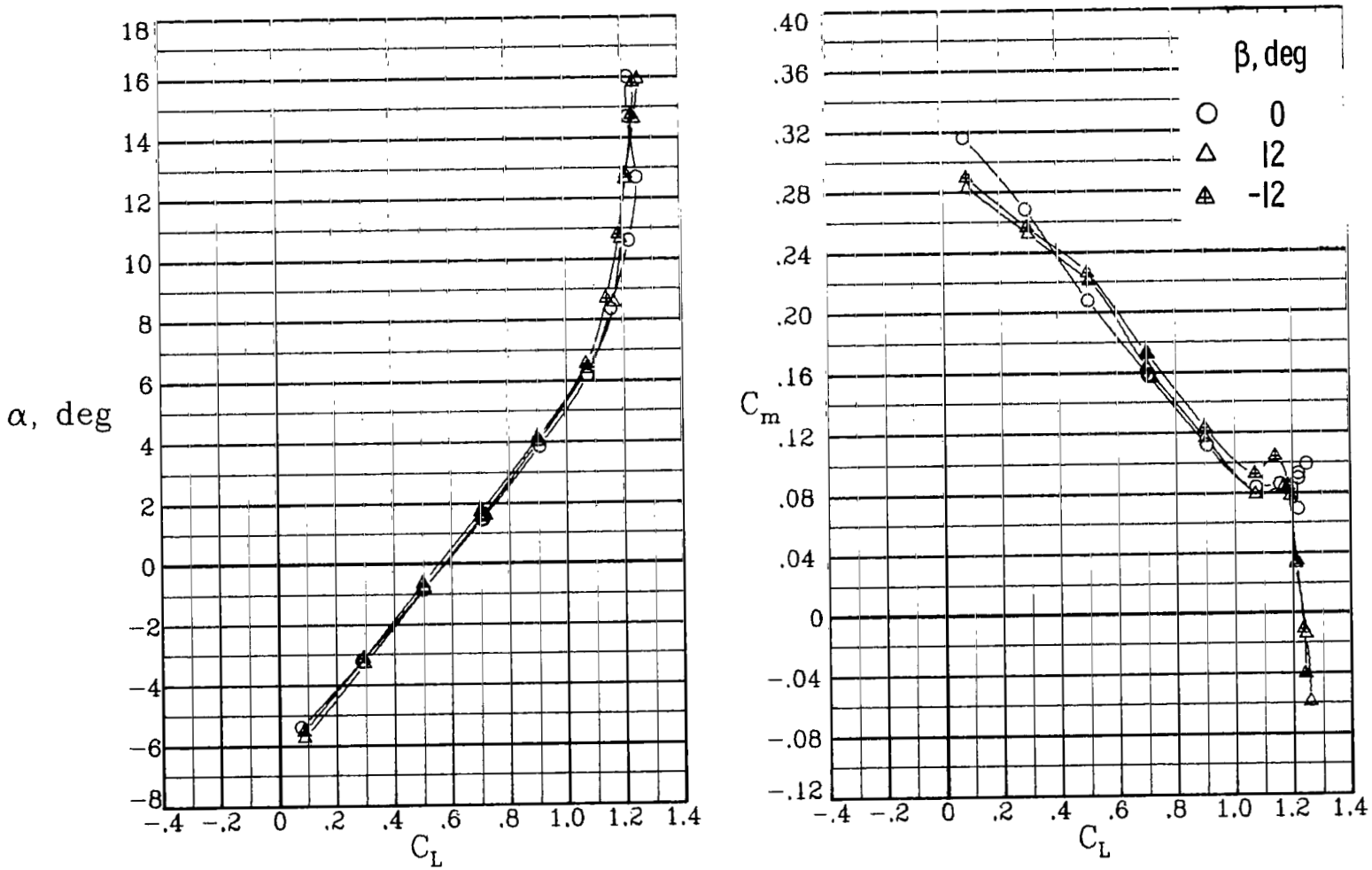

(e) Concluded.

Figure 4.- Concluded.

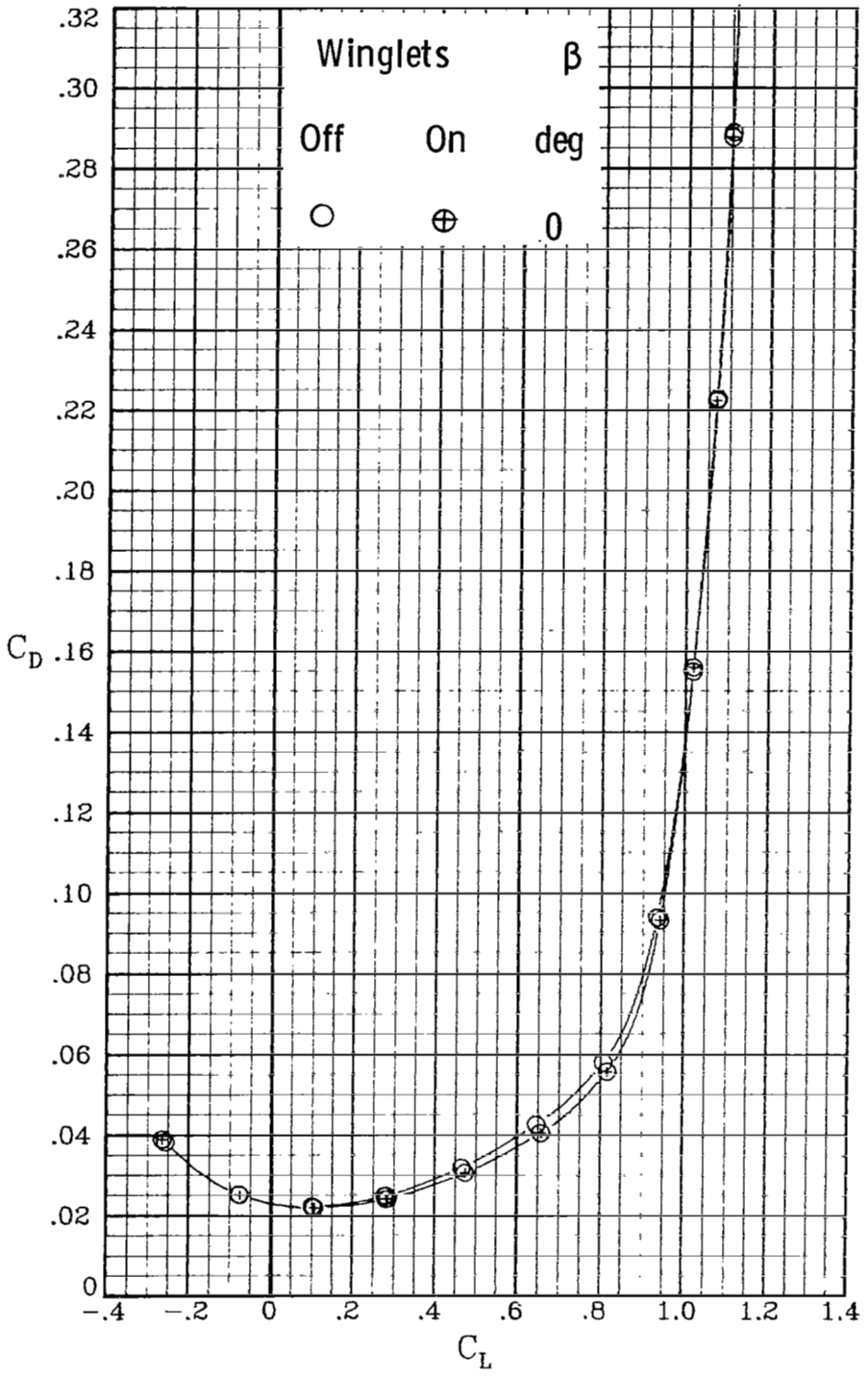

(a) $M_\infty = 0.50$.

Figure 5.- Longitudinal aerodynamic characteristics at high subsonic speeds. $\delta_h = 0^o$.

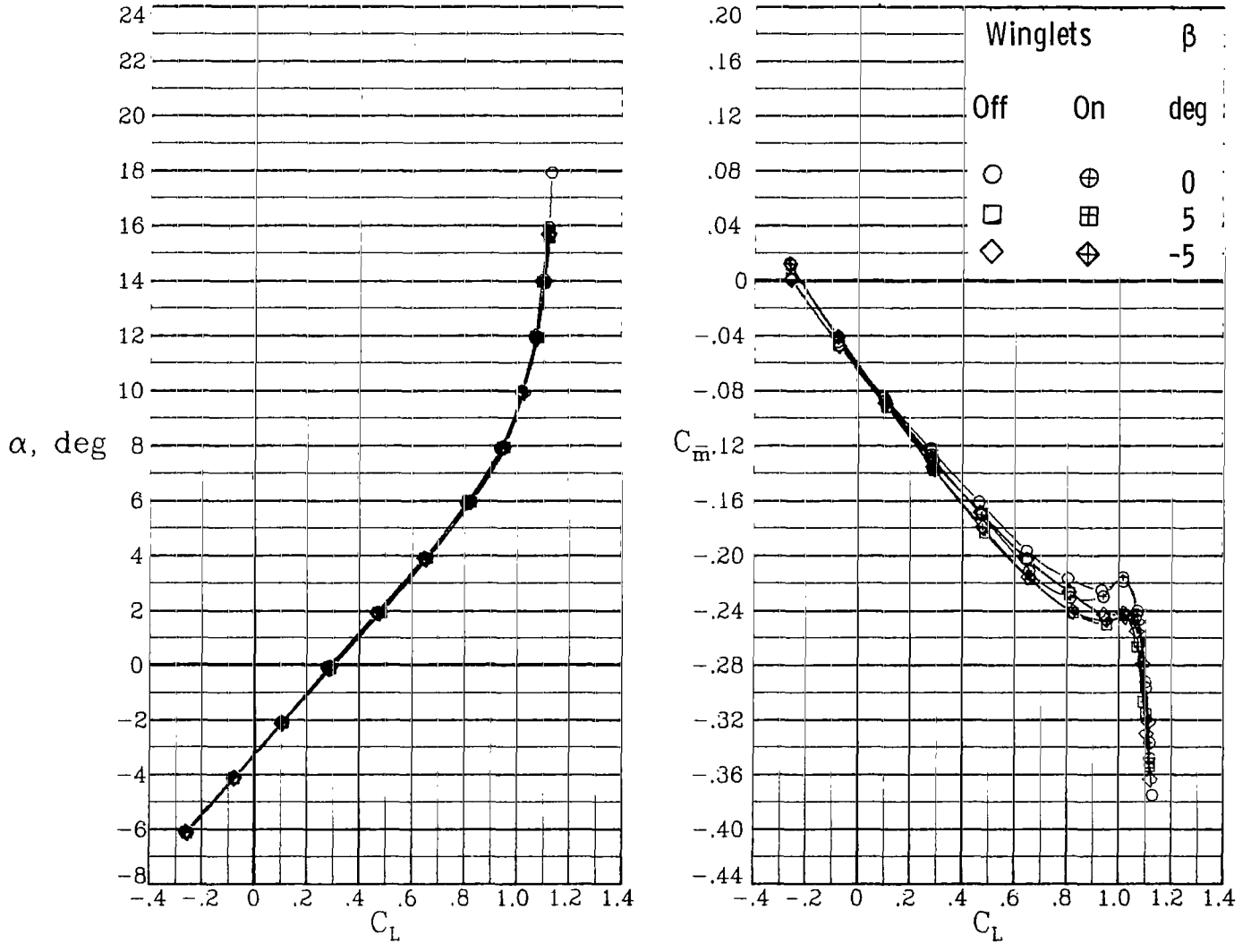

(a) Concluded.

Figure 5.- Continued.

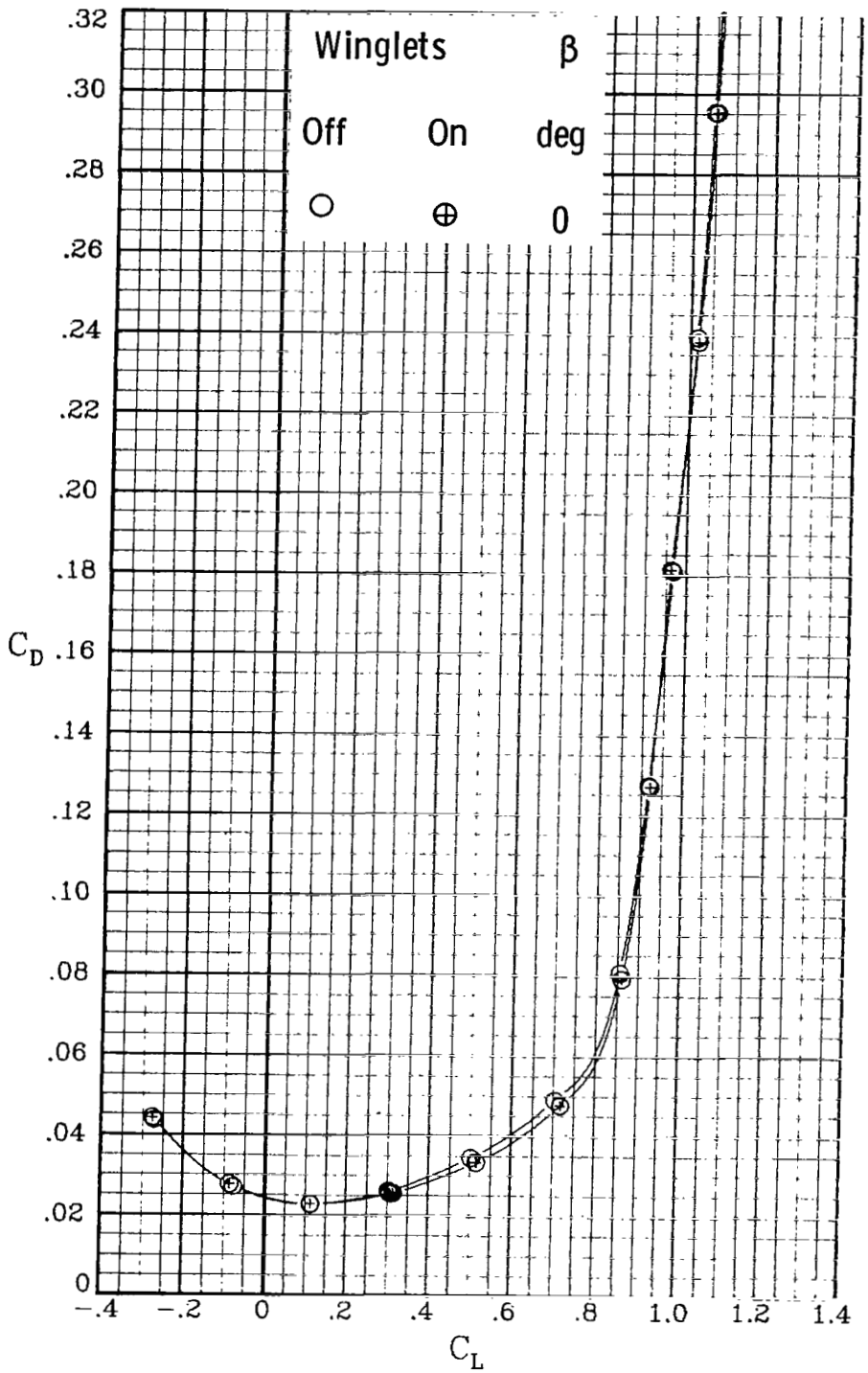

(b) $M_\infty = 0.70$.

Figure 5.- Continued.

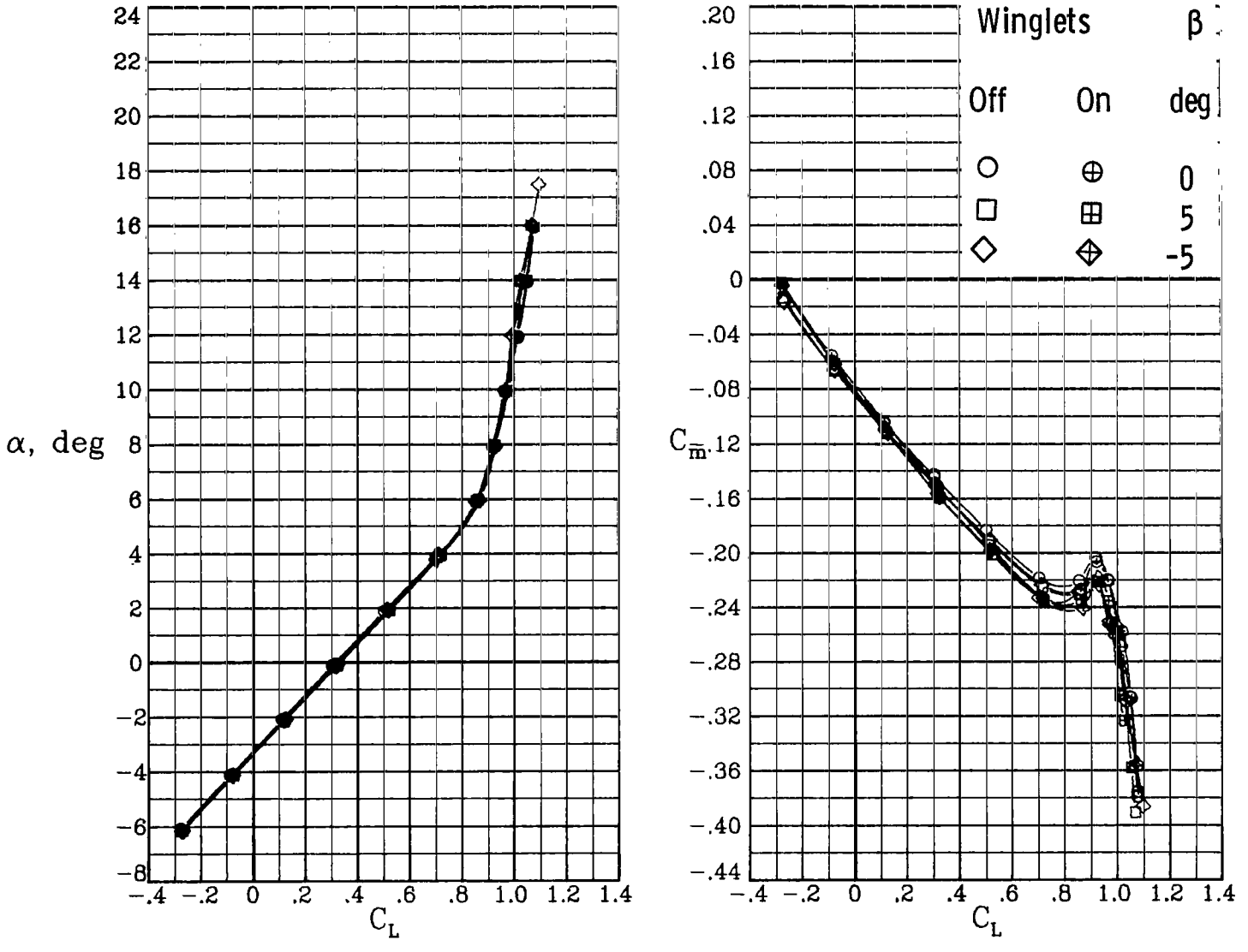

(b) Concluded.

Figure 5.- Continued.

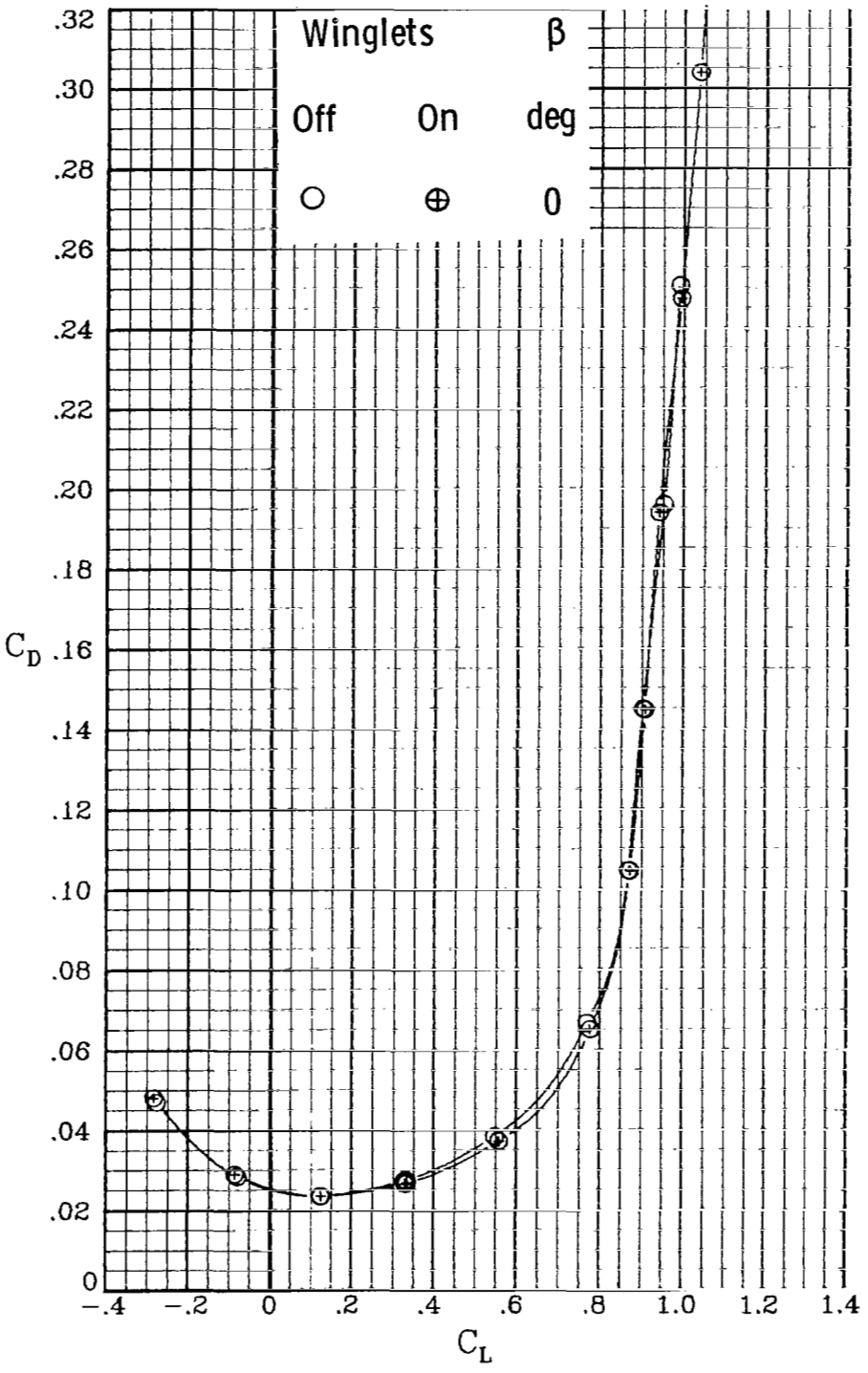

(c) $M_\infty = 0.78$.

Figure 5.- Continued.

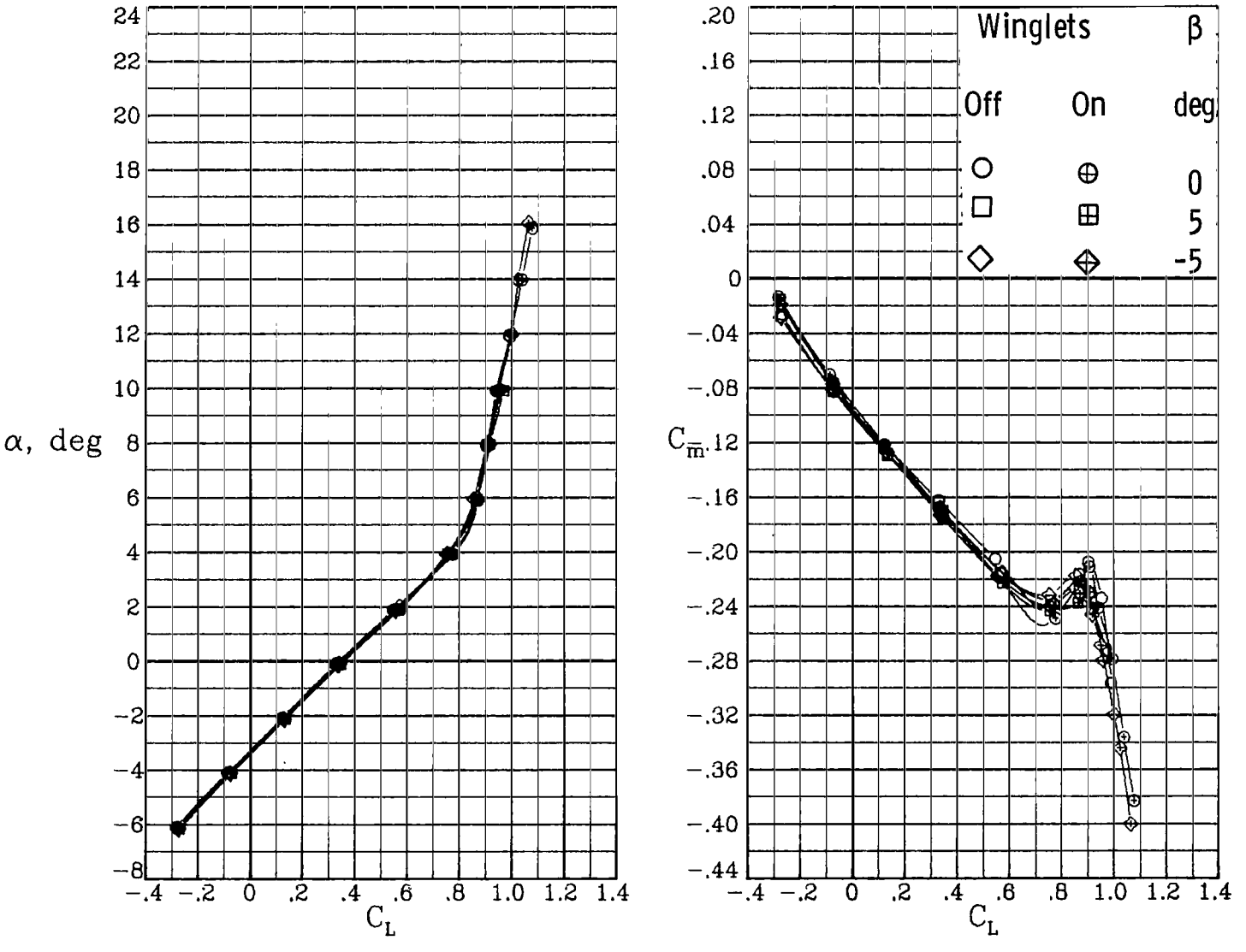

(c) Concluded.

Figure 5.- Continued.

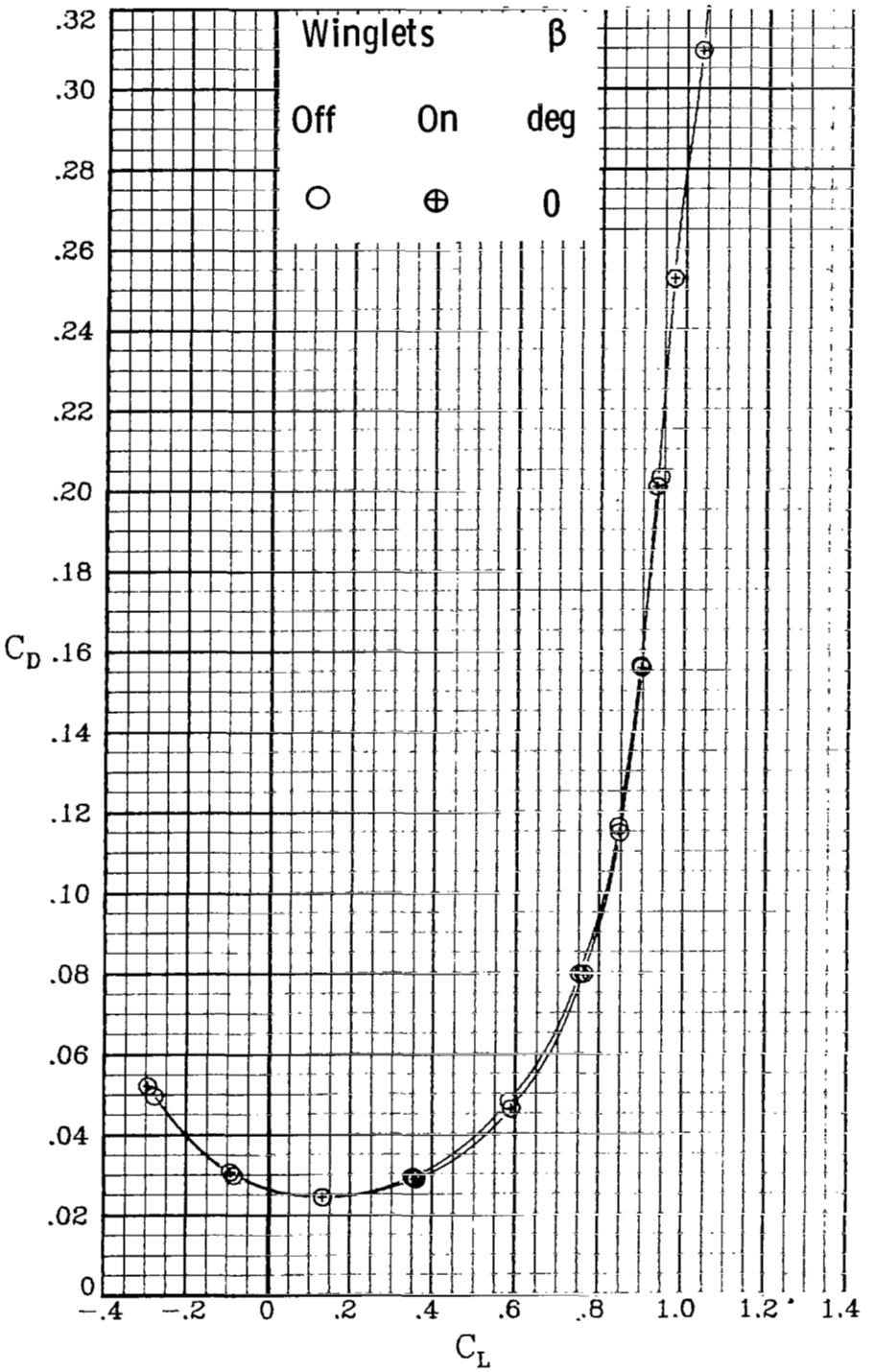

(d) $M_\infty = 0.82$.

Figure 5.- Continued.

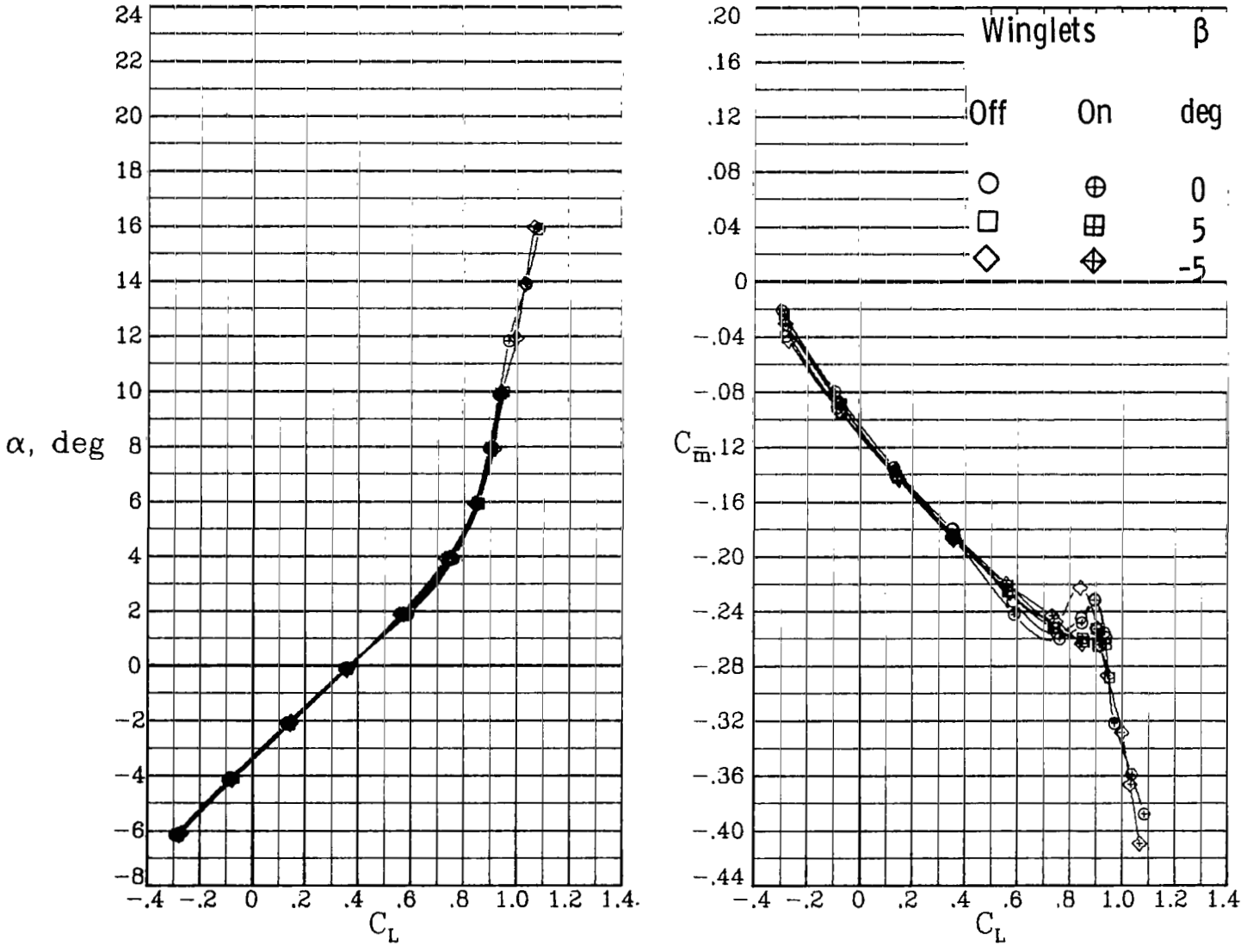

(d) Concluded.

Figure 5.- Concluded.

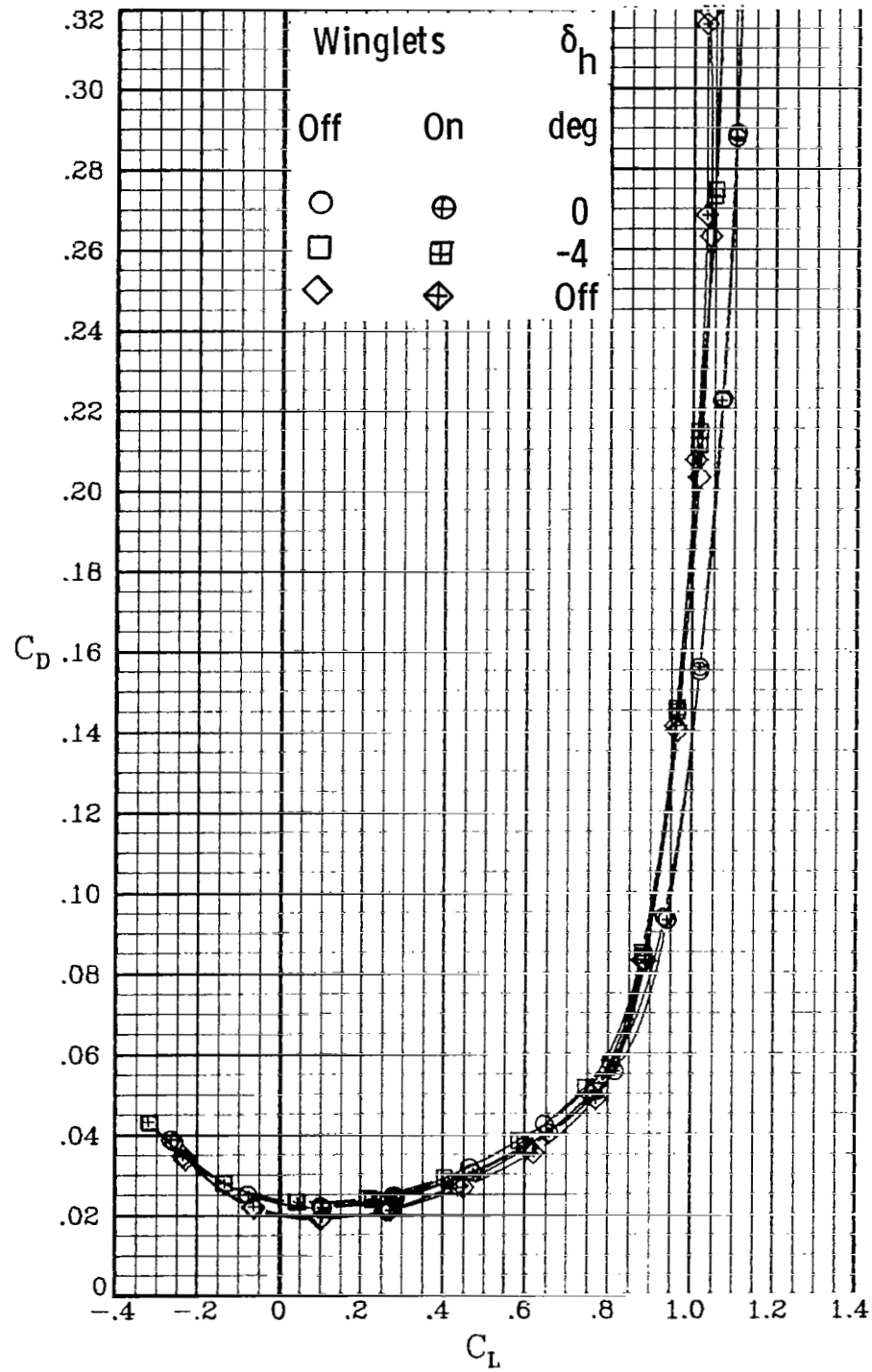

(a) $M_\infty = 0.50$.

Figure 6.- Horizontal-tail effects on longitudinal aerodynamic characteristics at high subsonic speeds. $\beta = 0^\circ$.

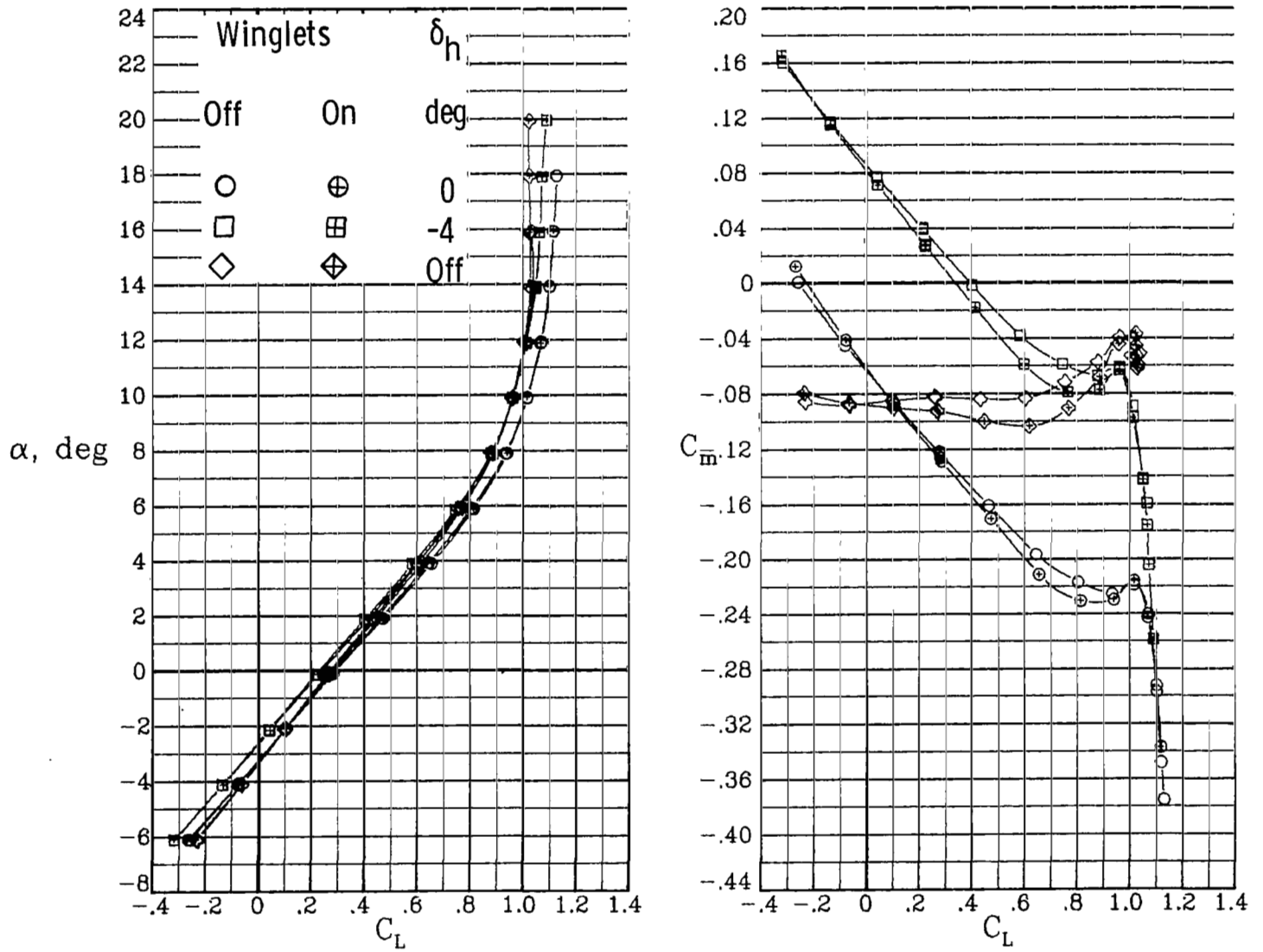

(a) Concluded.

Figure 6.- Continued.

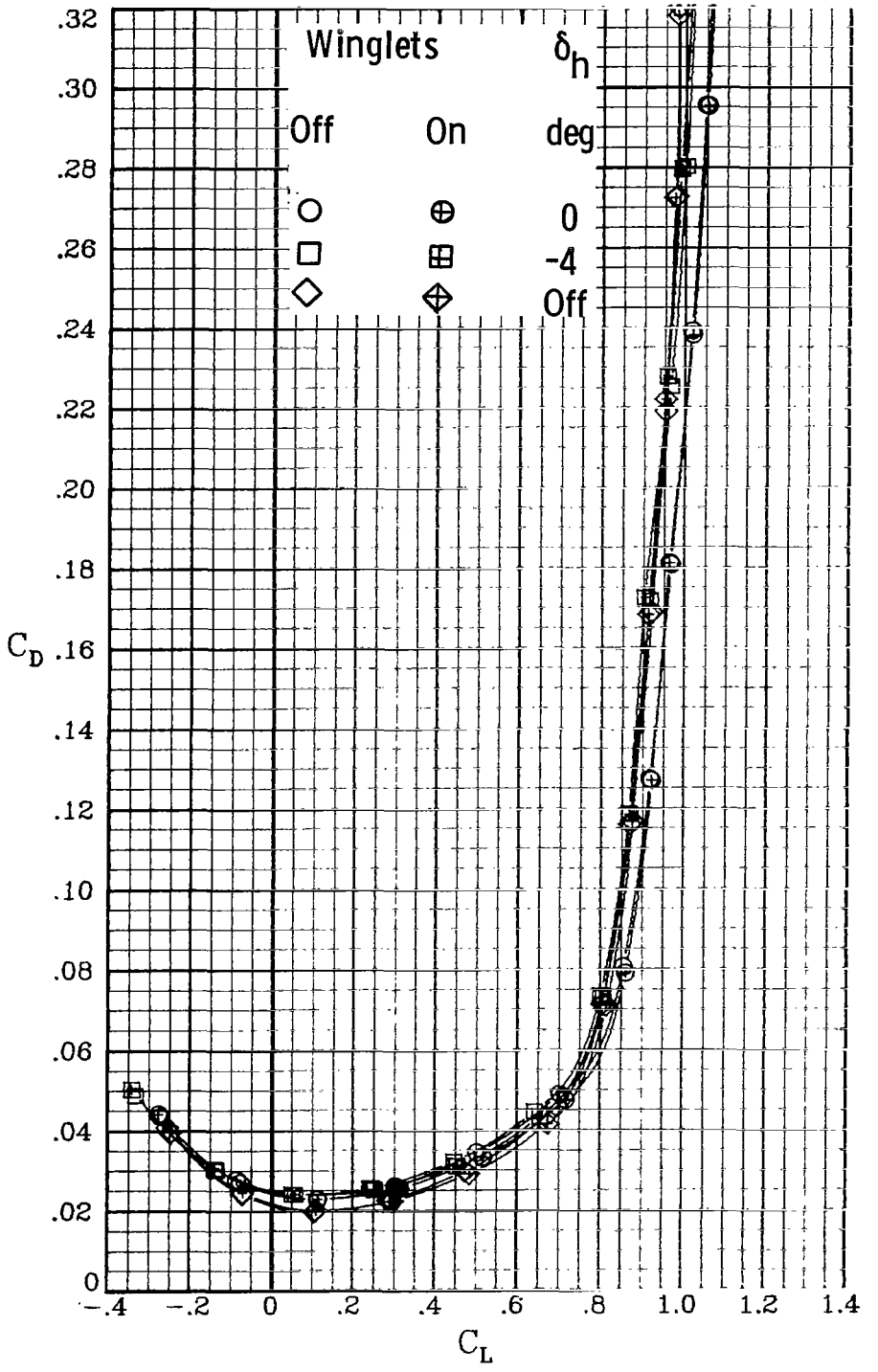

(b) $M_\infty = 0.70$.

Figure 6.- Continued.

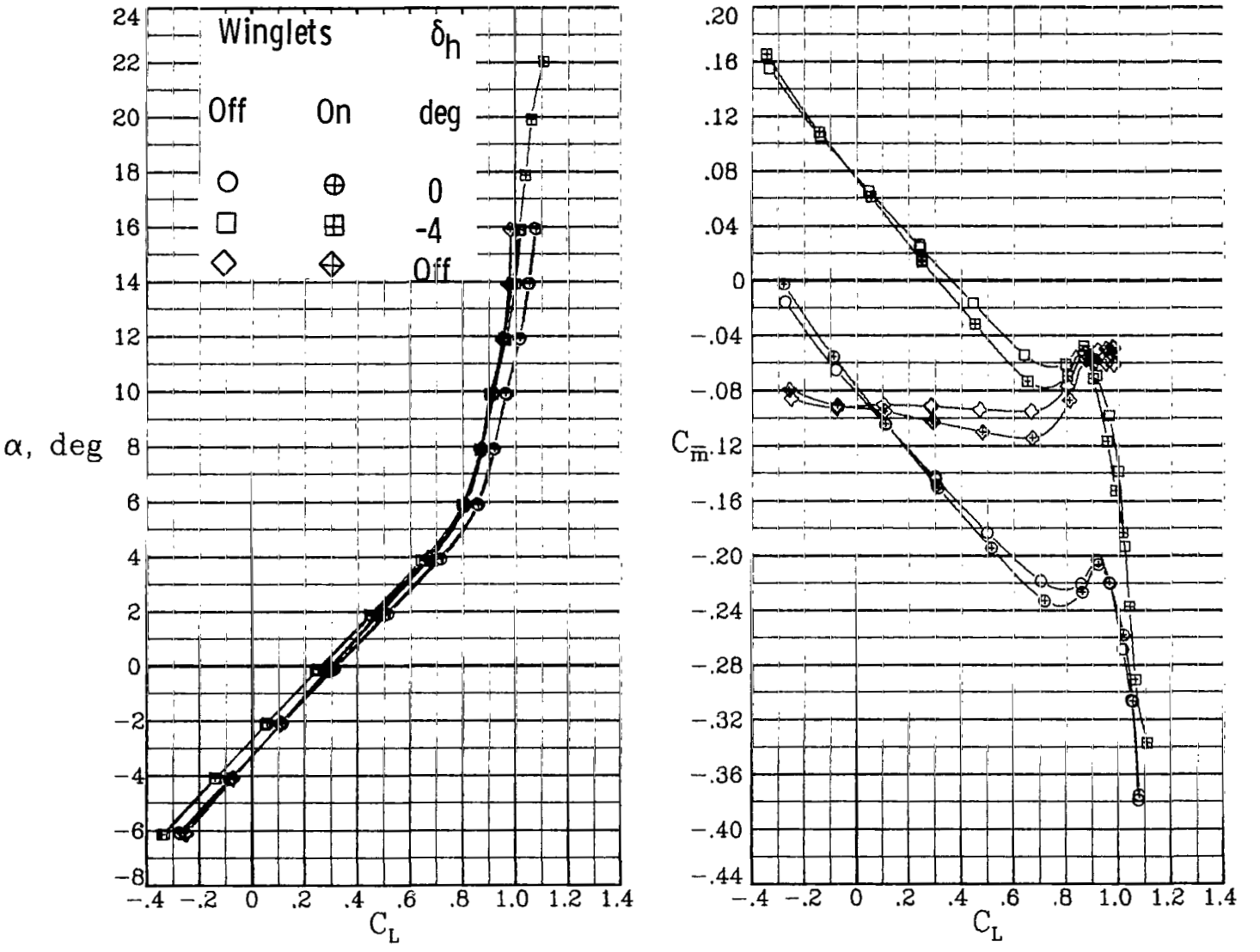

(b) Concluded.

Figure 6.- Continued.

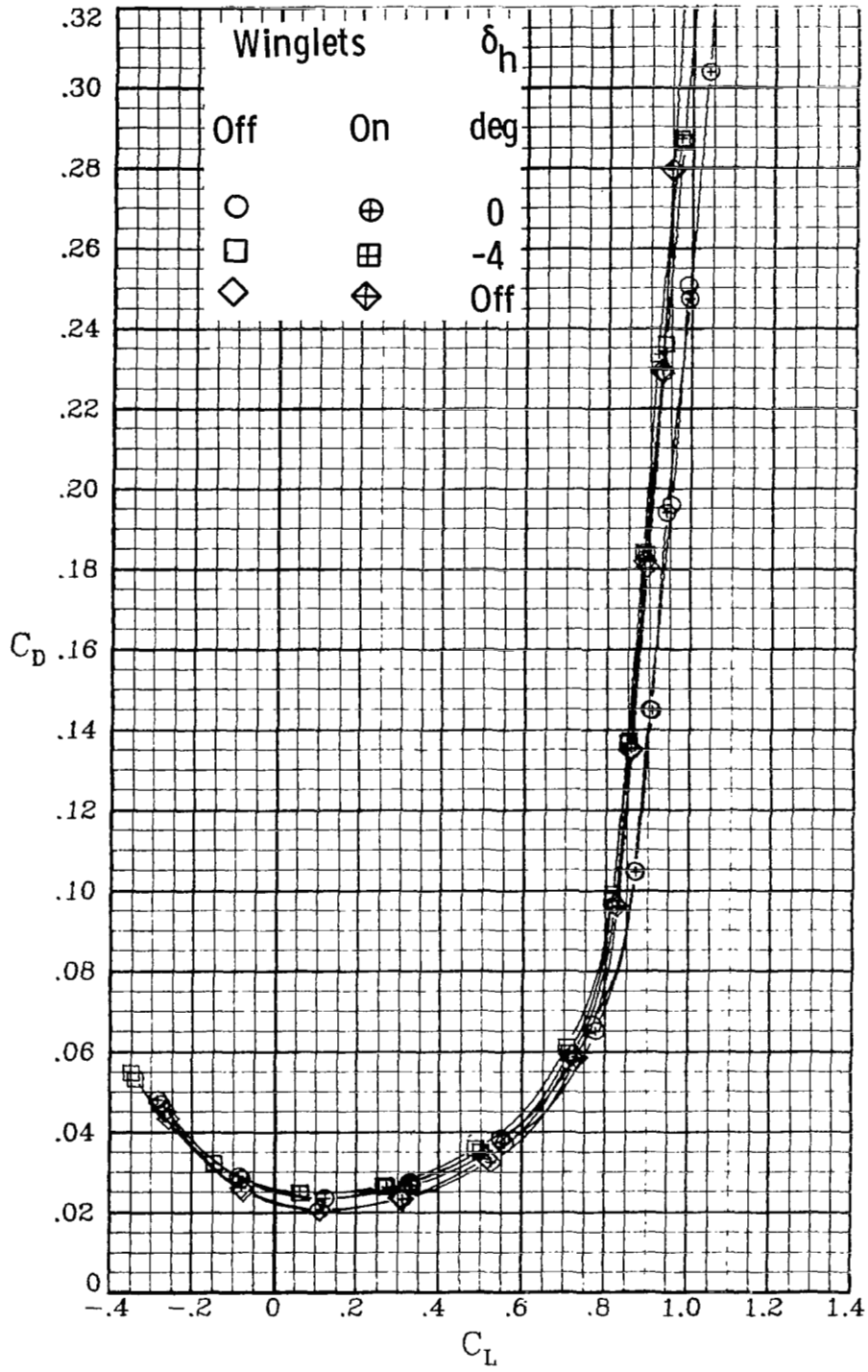

(c) $M_\infty = 0.78$.

Figure 6.- Continued.

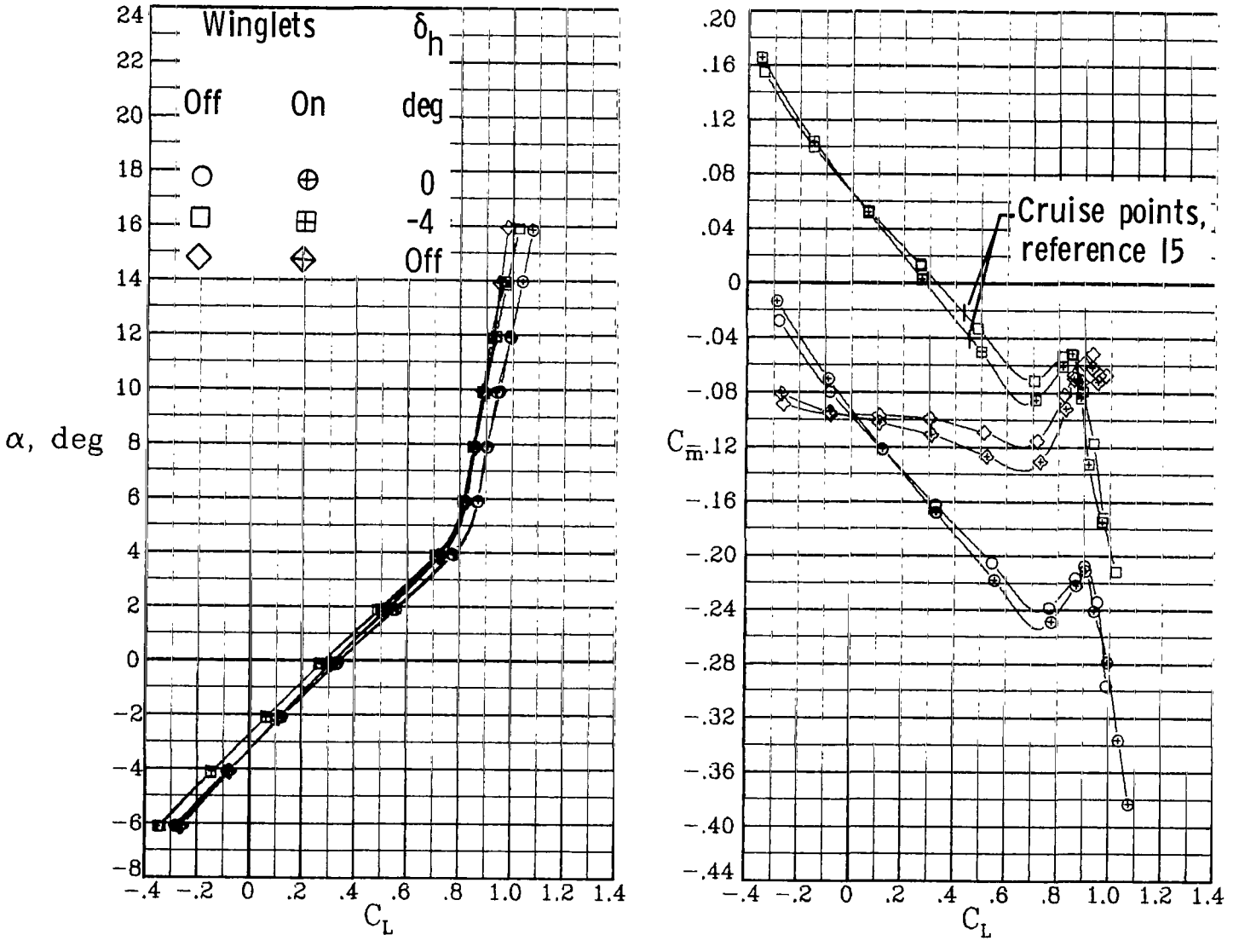

(c) Concluded.

Figure 6.- Continued.

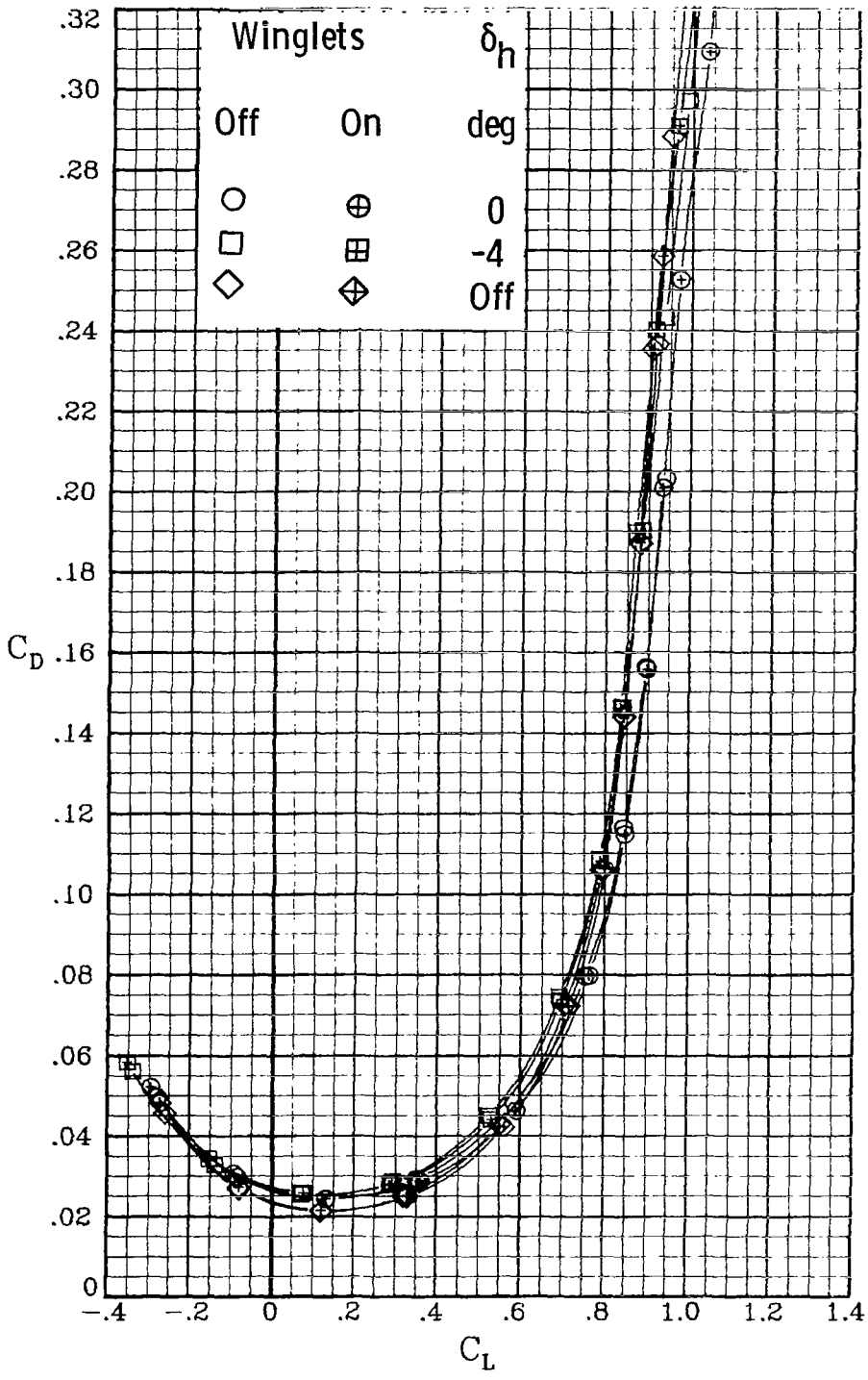

(d) $M_\infty = 0.82$.

Figure 6.- Continued.

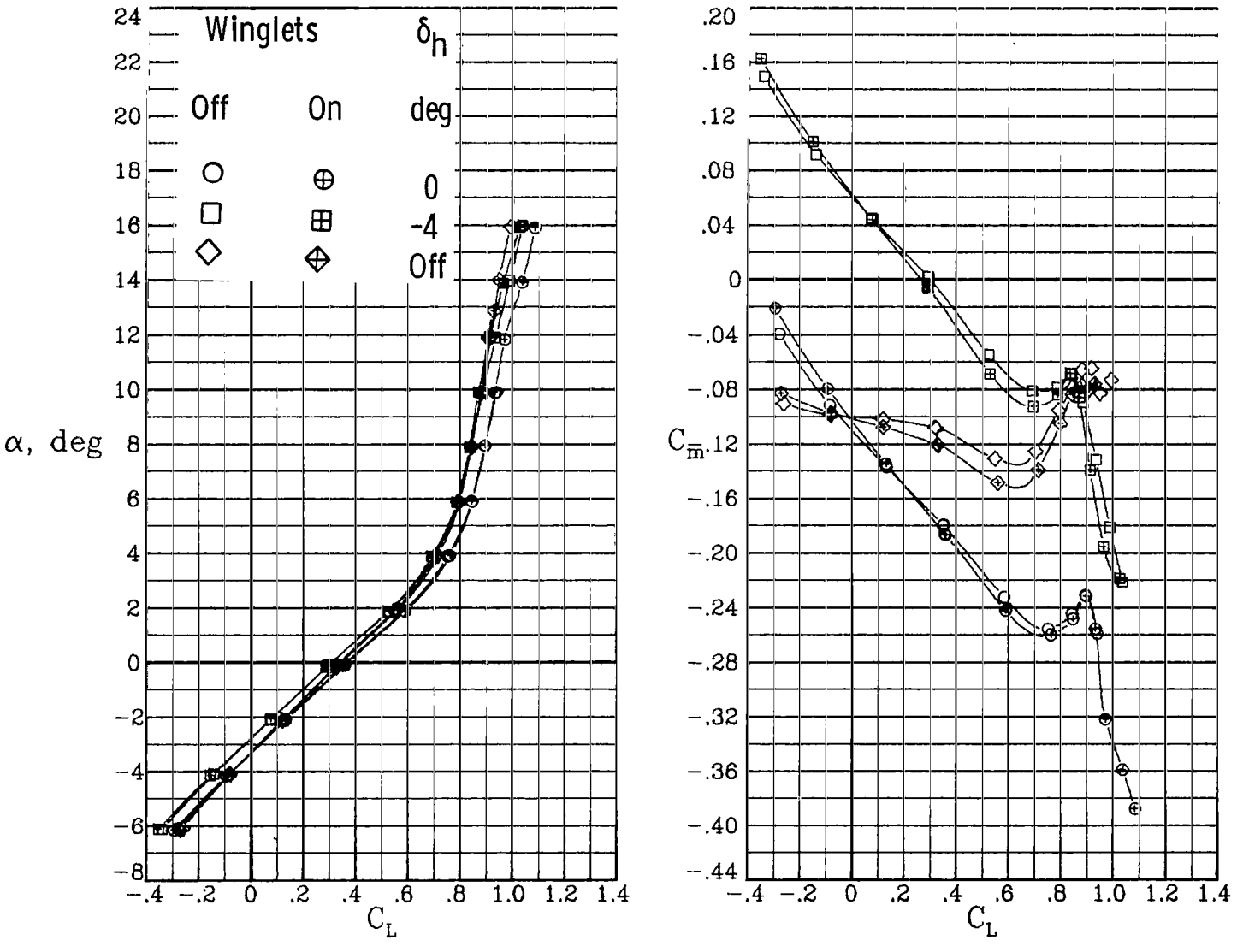

(d) Concluded.

Figure 6.- Concluded.

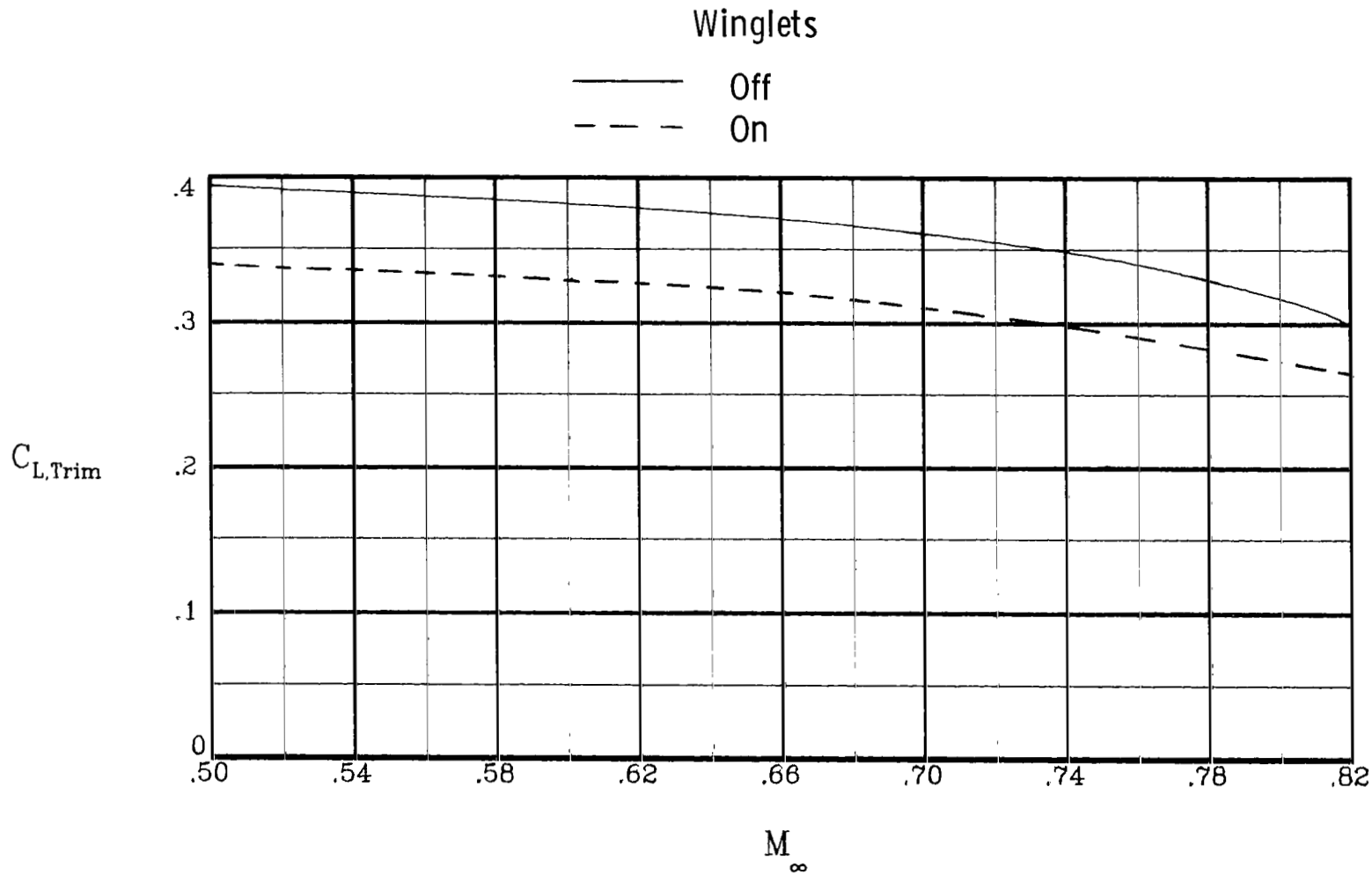

Figure 7.- Trim lift coefficient $C_{L,trim}$ at high subsonic speeds. $\delta_h = -4^o$; $\beta = 0^o$.

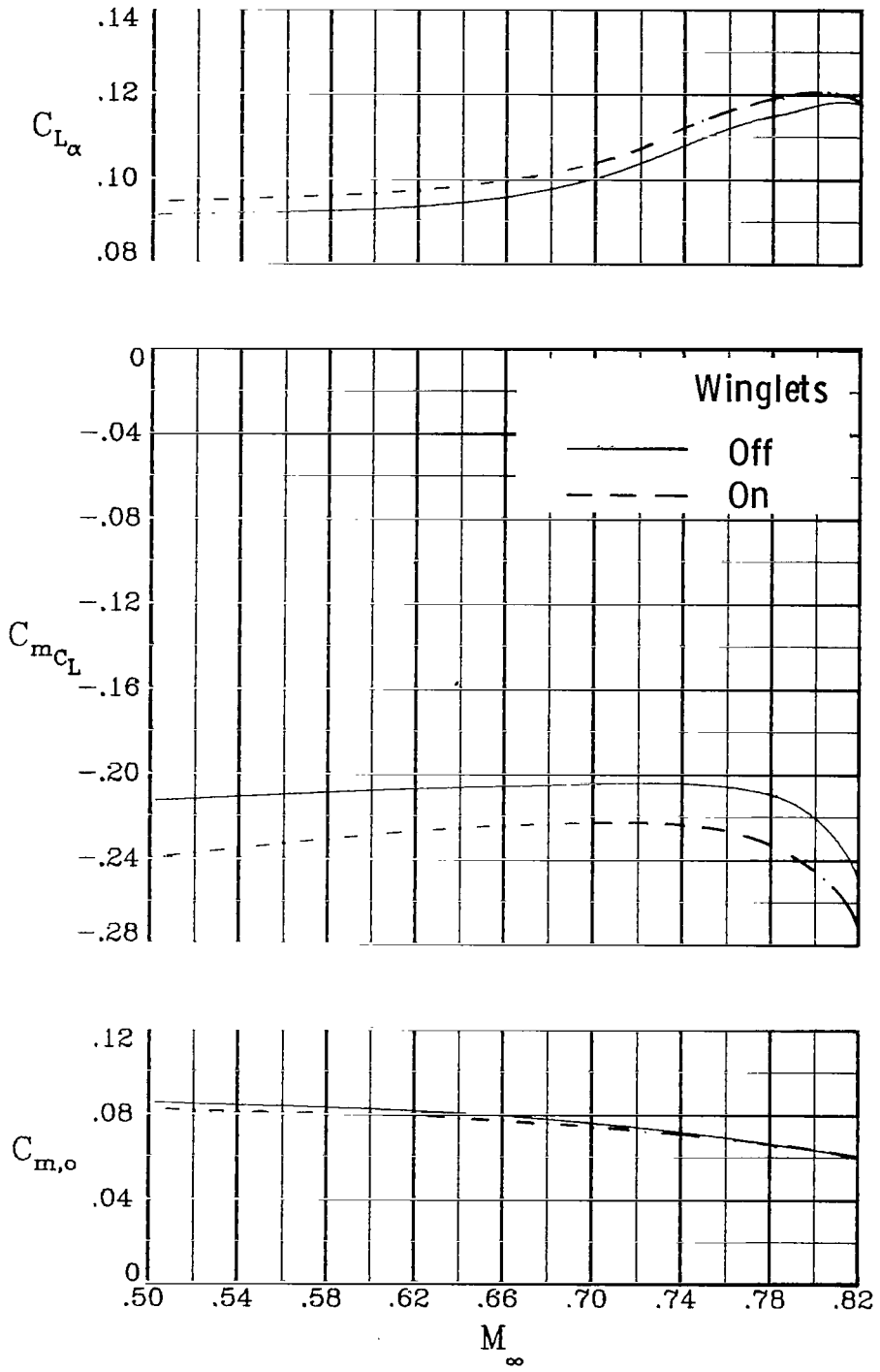

Figure 8.- Summary of longitudinal aerodynamic characteristics at high subsonic speeds. Derivative at $C_L = 0.40$; $\delta_h = -4^o$; $\beta = 0^o$.

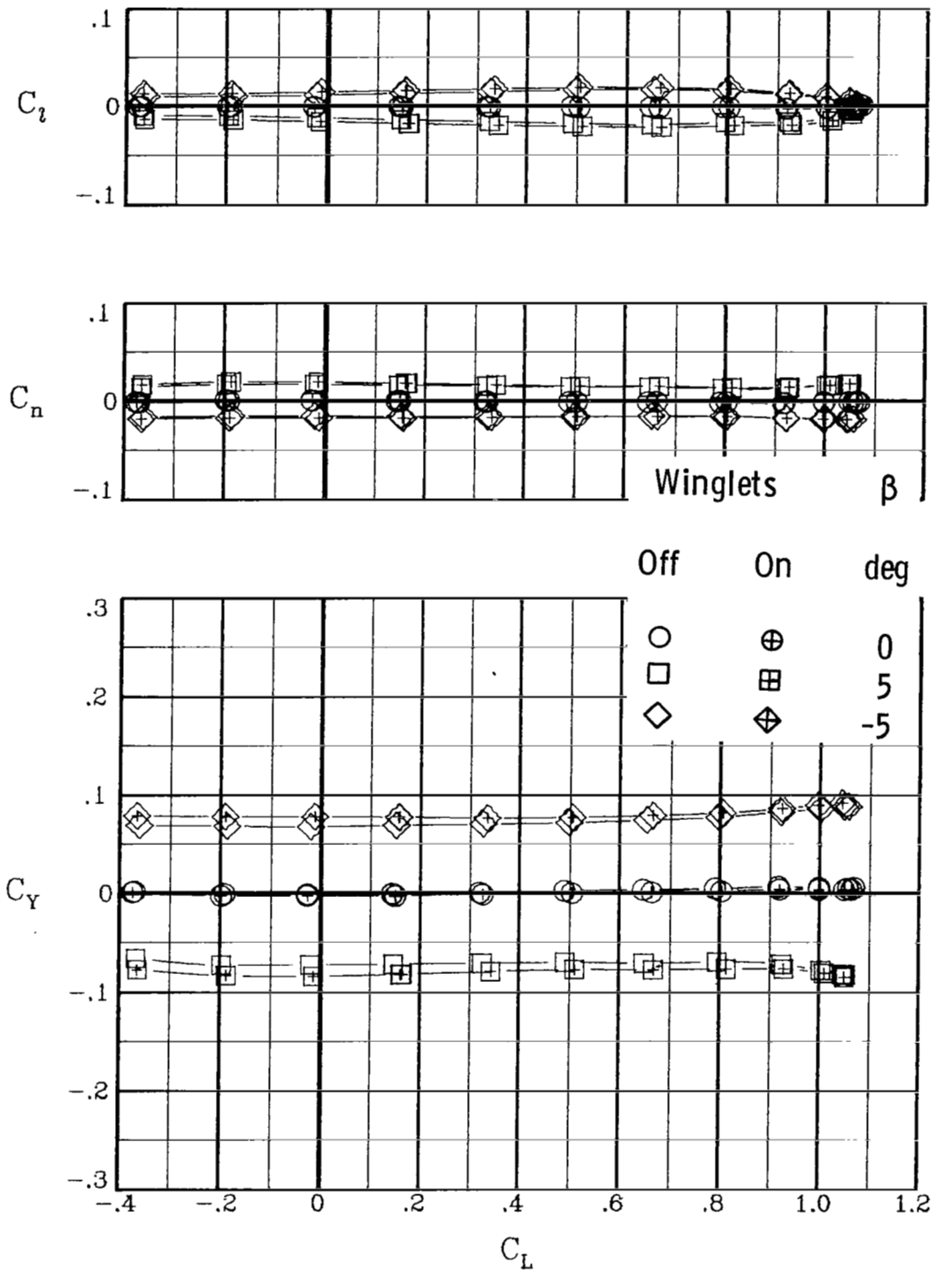

(a) $R = 6.1 \times 10^6$ per m (1.85×10^6 per ft).

Figure 9.- Effect of sideslip on lateral-directional aerodynamic characteristics at $M_\infty = 0.30$ for configuration with wing B. $\delta_h = -10^o$.

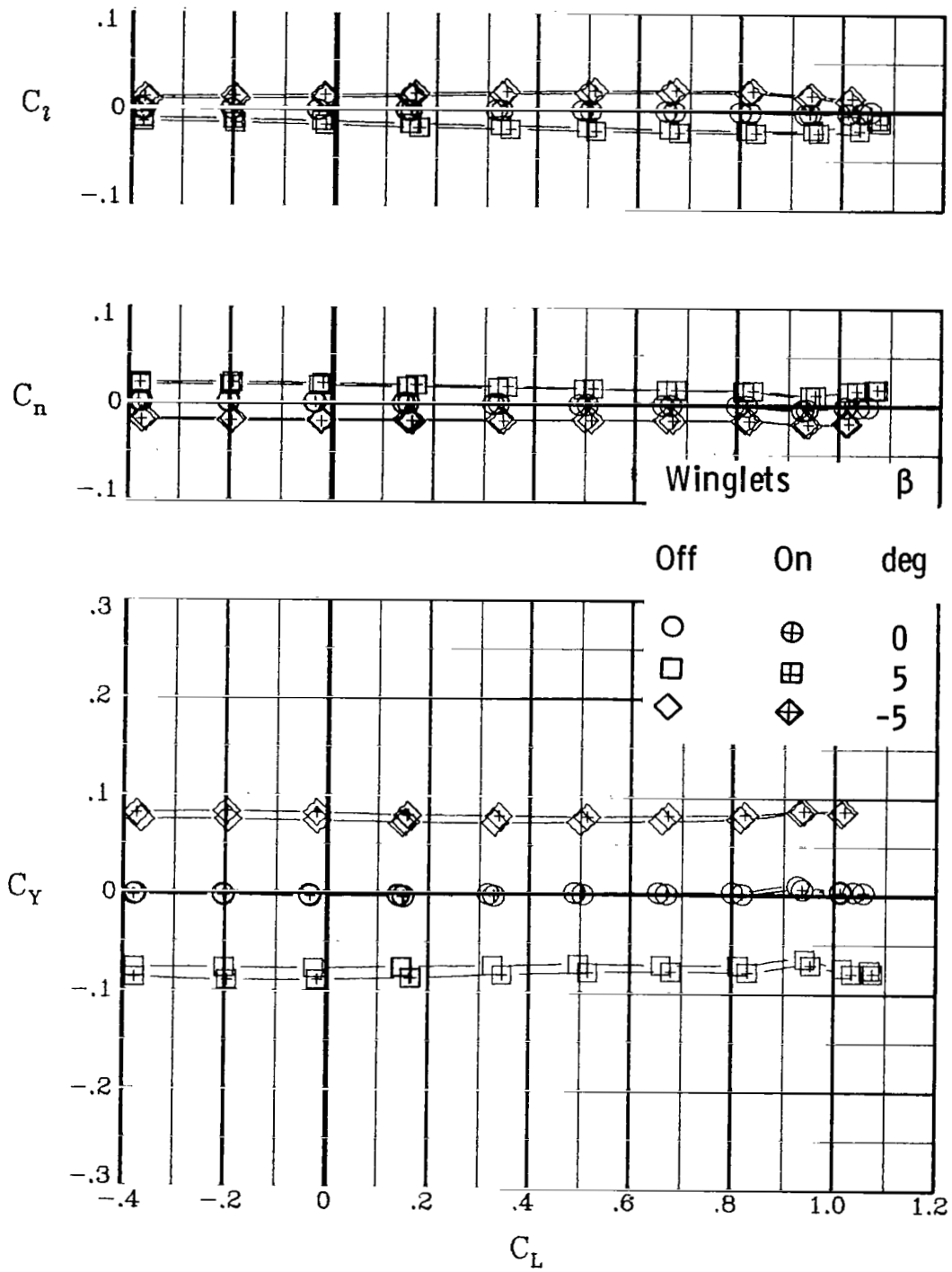

(b) R = 12.1 × 10^6 per m (3.70 × 10^6 per ft).

Figure 9.- Concluded.

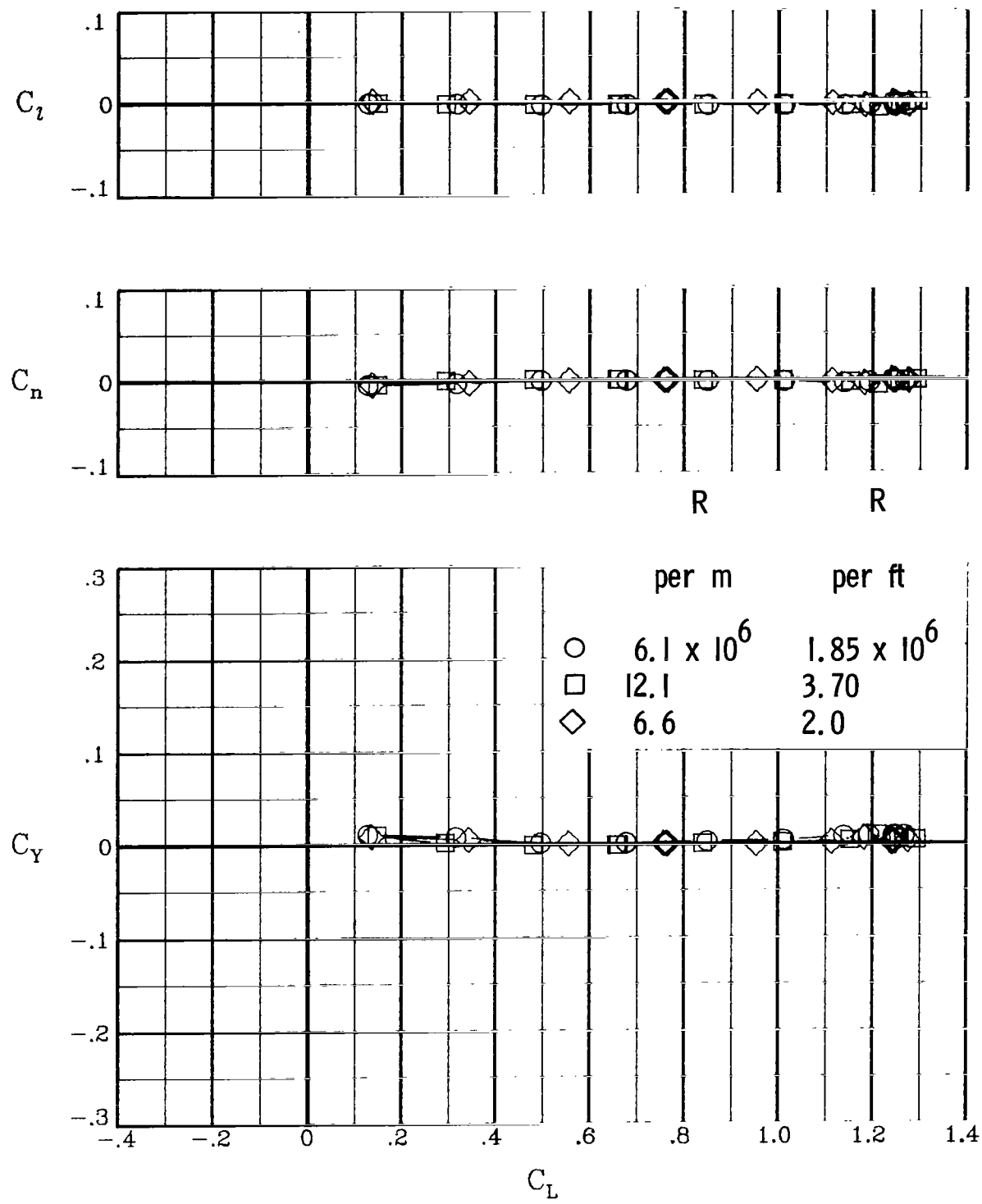

(a) $\beta = 0^o$; $\delta_{a,L} = 0^o$; $\delta_{a,R} = 0^o$; $\delta_f = 30^o$.

Figure 10.- Effect of sideslip on lateral-directional aerodynamic characteristics at $M_\infty = 0.30$ for configuration with wing F. Winglets on; $\delta_h = -10^o$.

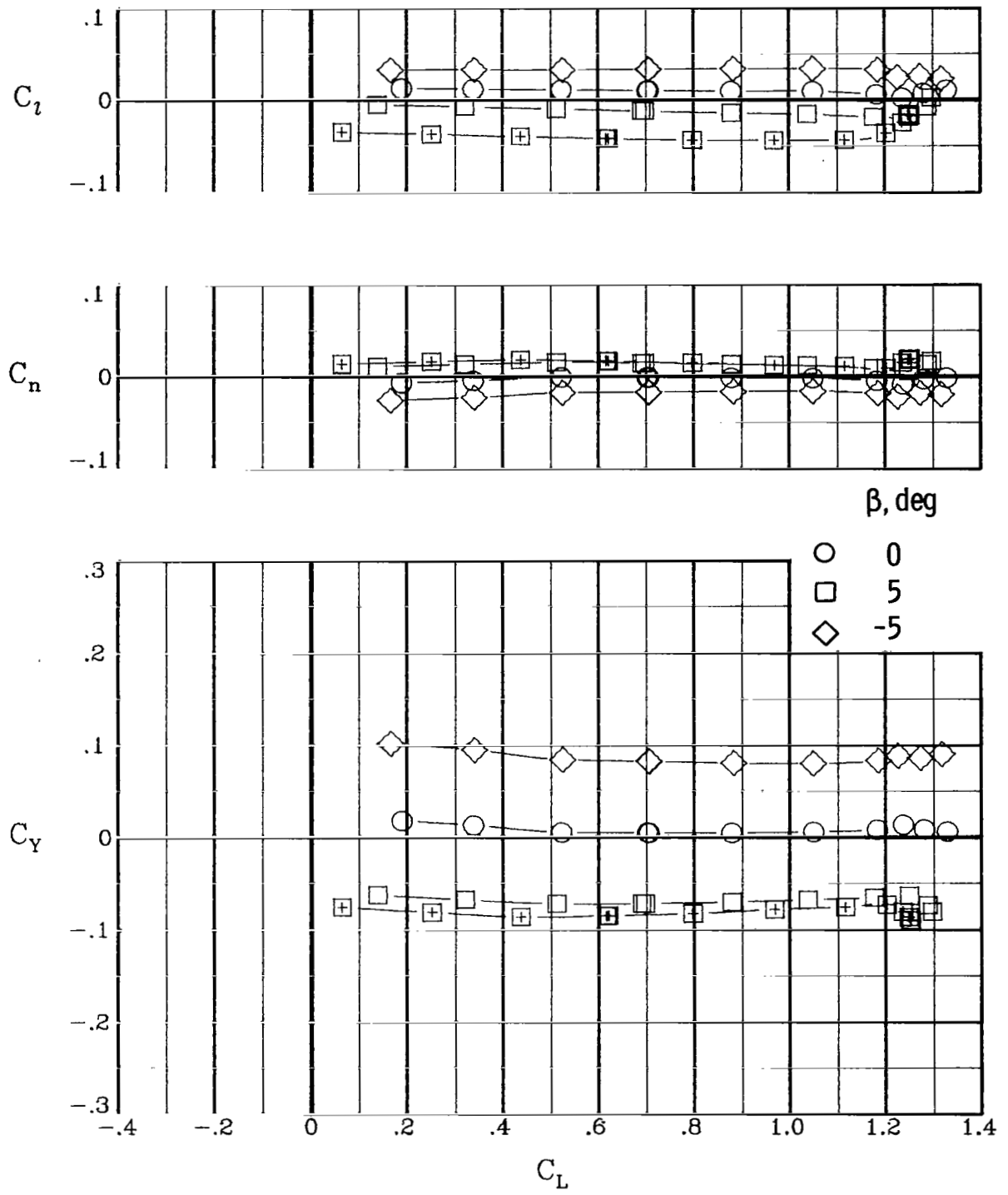

(b) R = 12.1 × 10^6 per m (3.70 × 10^6 per ft); $\delta_{a,L}$ = 20°; $\delta_{a,R}$ = 0°; δ_f = 30°. ("+" in symbol for $\delta_{a,L}$ = -20°.)

Figure 10.- Continued.

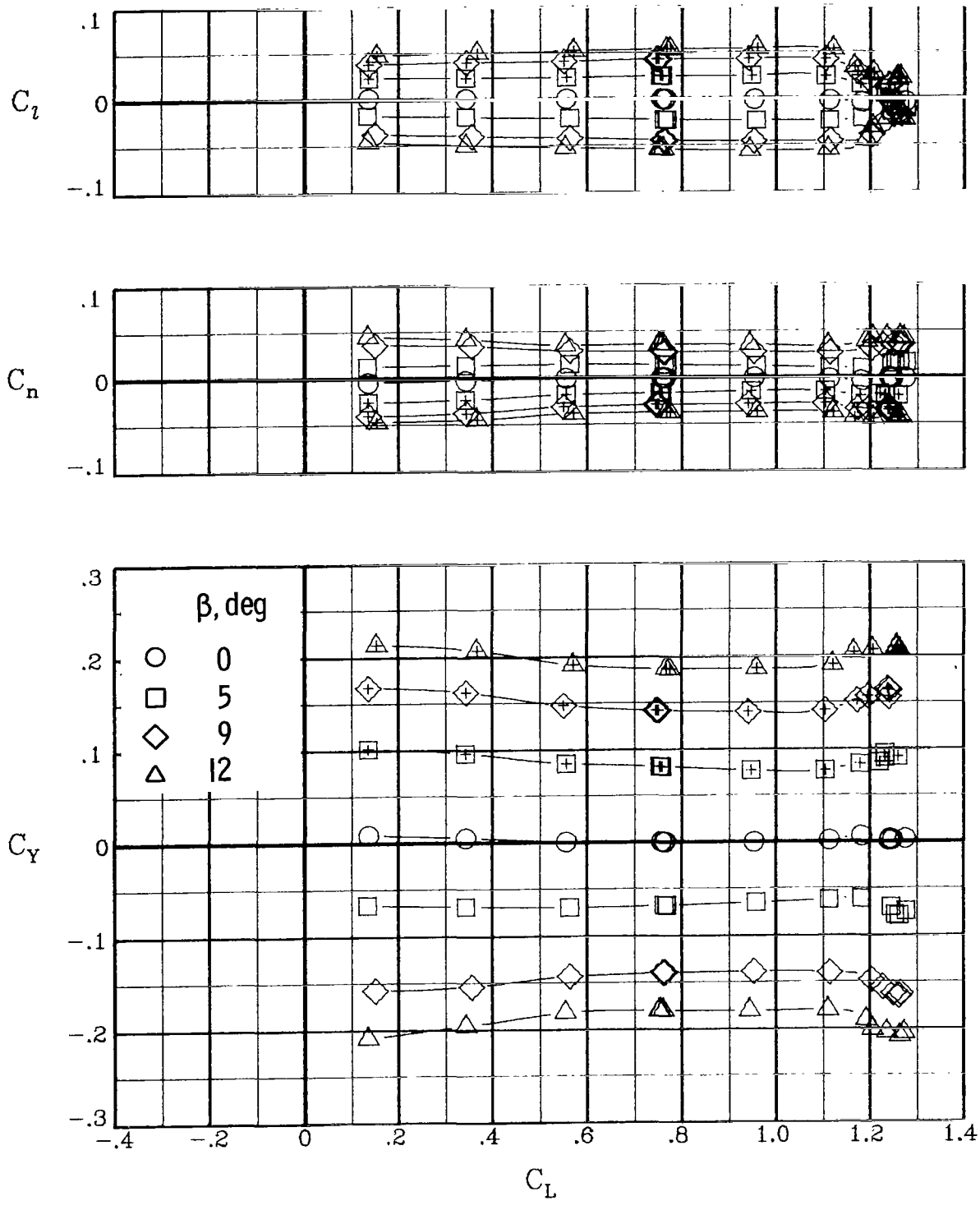

(c) R = 6.6 × 10^6 per m (2.0 × 10^6 per ft); $\delta_{a,L} = 0^o$; $\delta_{a,R} = 0^o$; $\delta_f = 30^o$. ("+" in symbols for negative β.)

Figure 10.- Continued.

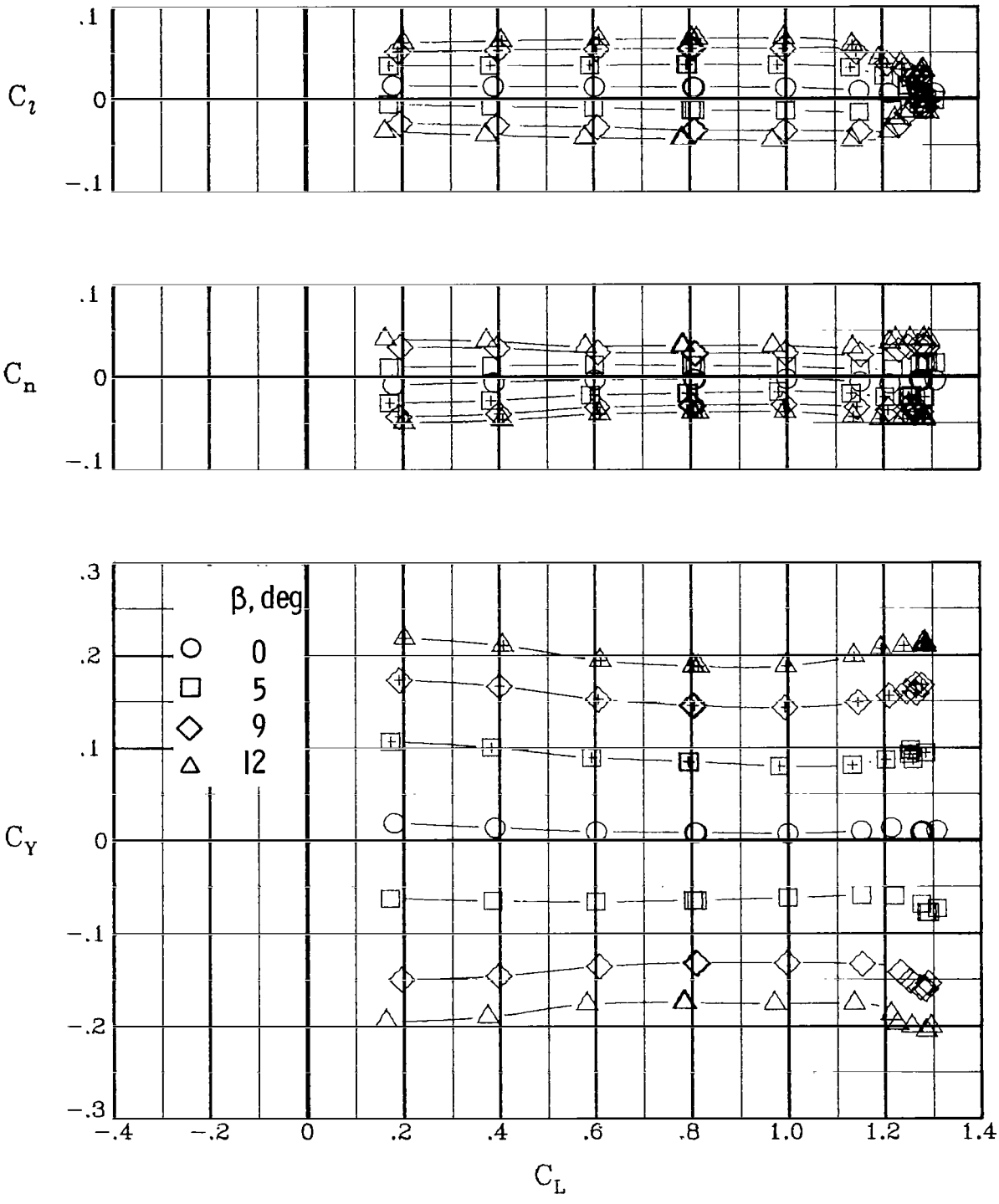

(d) $R = 6.6 \times 10^6$ per m (2.0×10^6 per ft); $\delta_{a,L} = 20^\circ$; $\delta_{a,R} = 0^\circ$; $\delta_f = 30^\circ$. ("+" in symbols for negative β.)

Figure 10.- Continued.

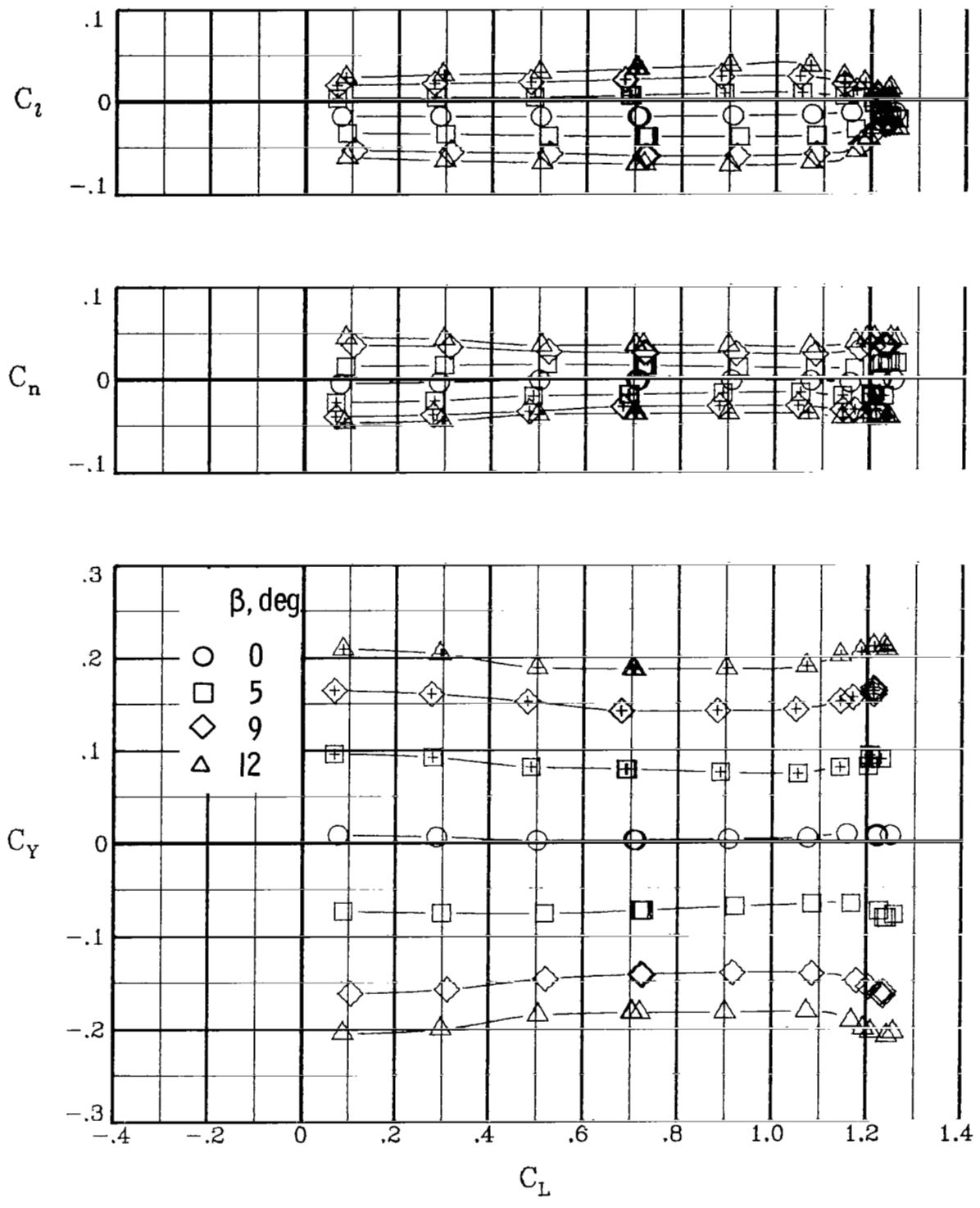

(e) $R = 6.6 \times 10^6$ per m (2.0×10^6 per ft); $\delta_{a,L} = -20^\circ$; $\delta_{a,R} = 0^\circ$; $\delta_f = 30^\circ$. ("+" in symbols for negative β.)

Figure 10.- Concluded.

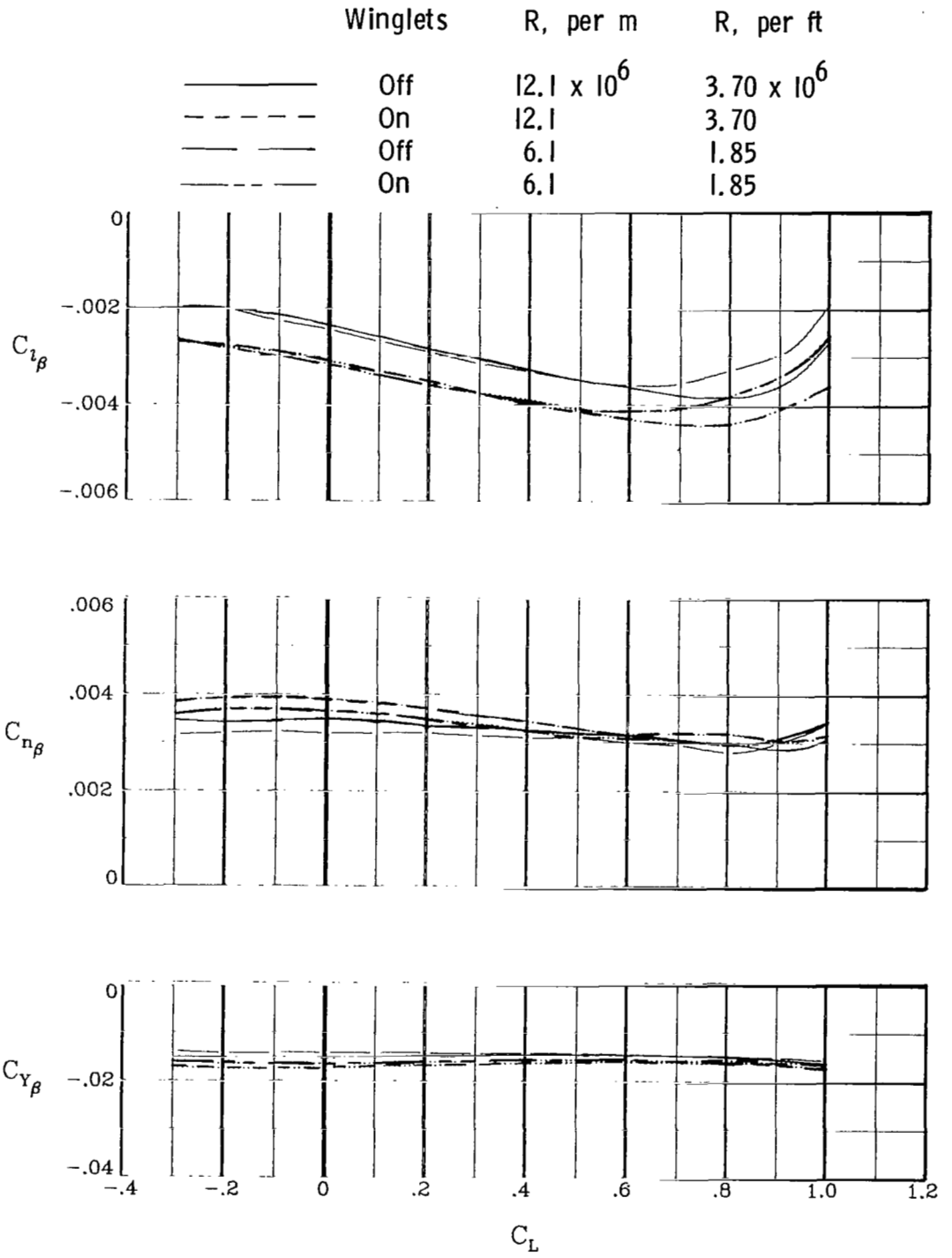

Figure 11.- Lateral-directional stability parameters. $M_\infty = 0.30$; $\delta_h = -10^\circ$.

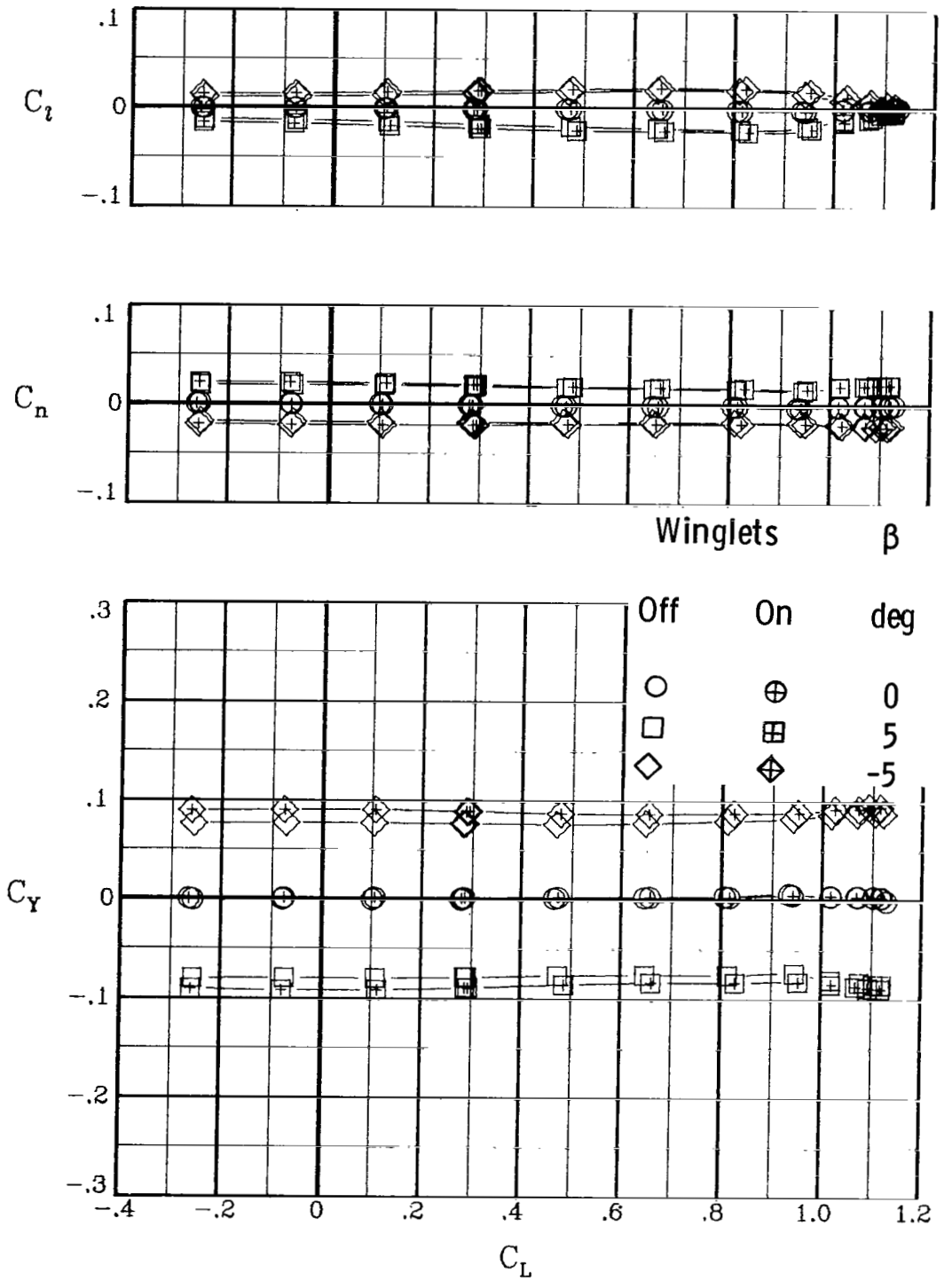

(a) $M_\infty = 0.50$.

Figure 12.- Effect of sideslip on lateral-directional aerodynamic characteristics at high subsonic speeds. $\delta_h = 0^o$.

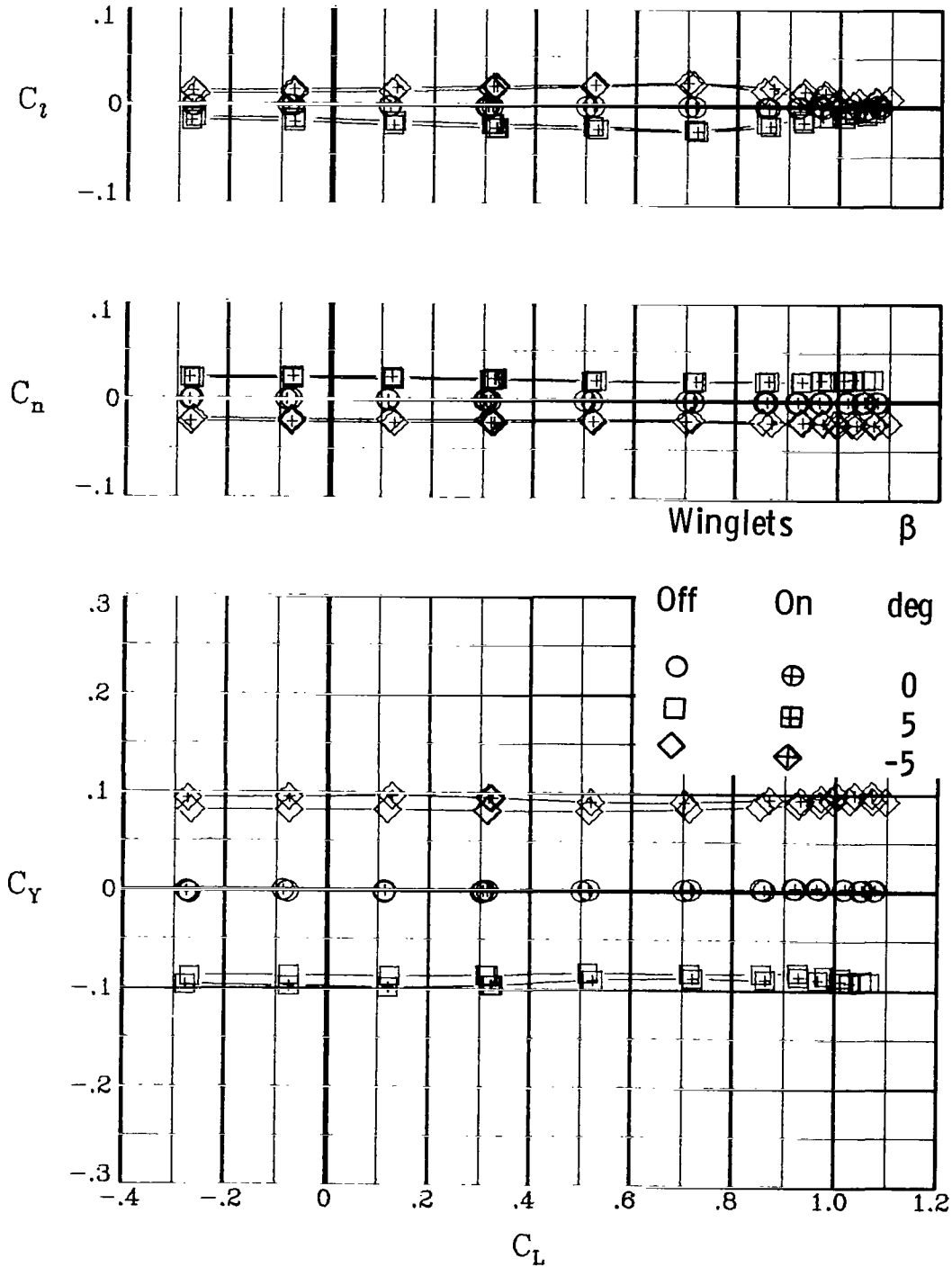

(b) $M_\infty = 0.70$.

Figure 12.- Continued.

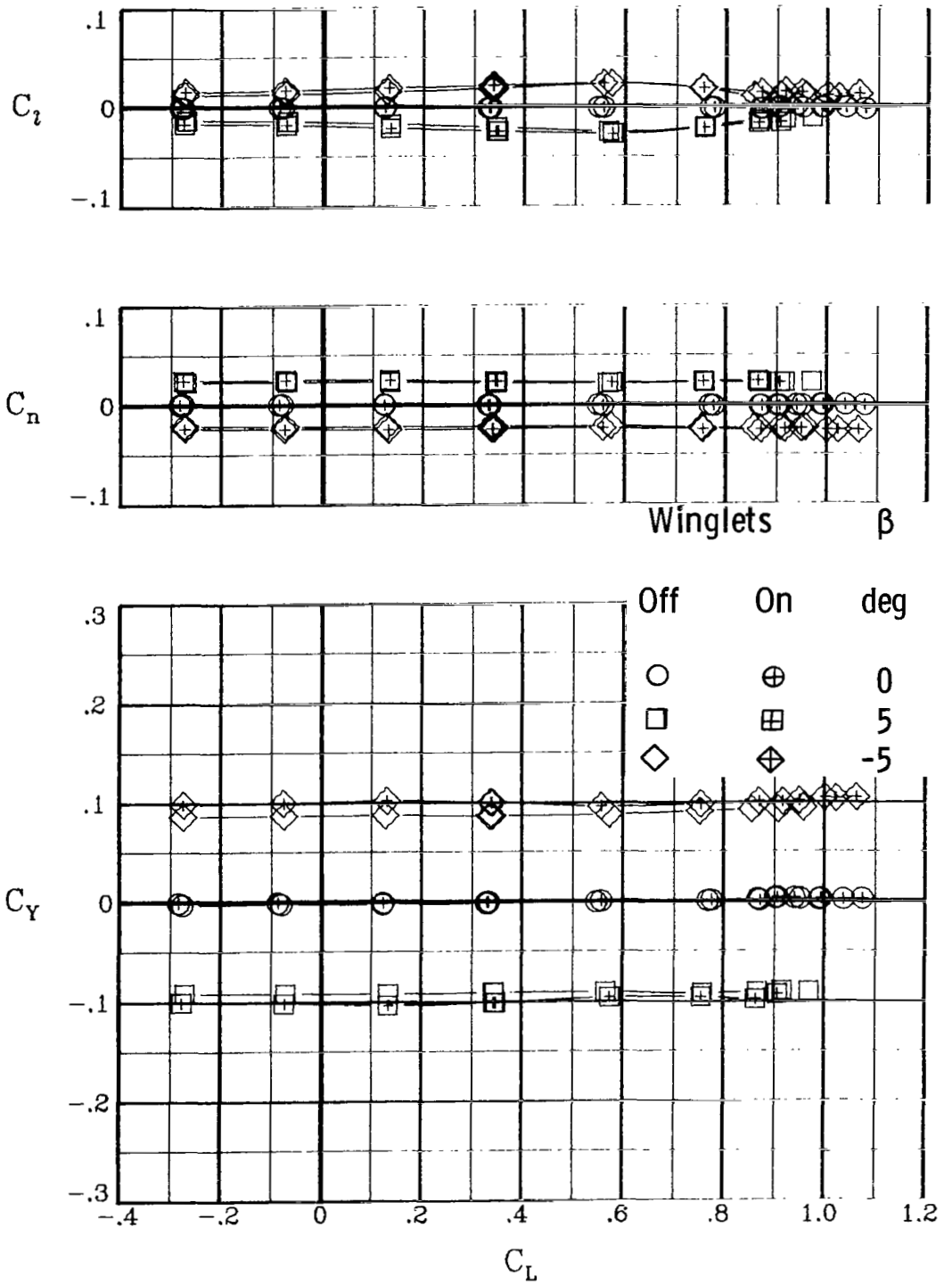

(c) $M_\infty = 0.78$.

Figure 12.- Continued.

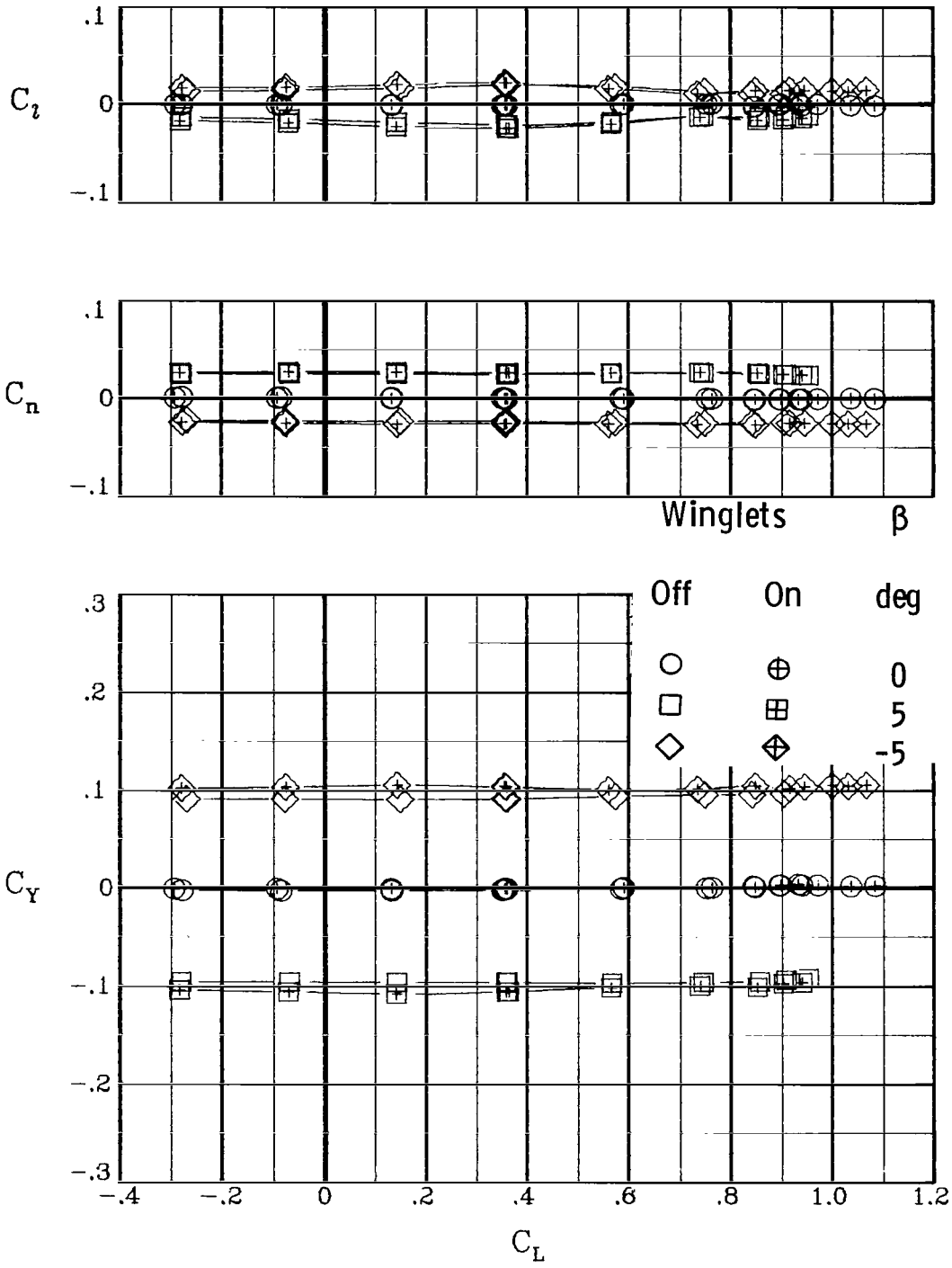

(d) $M_\infty = 0.82$.

Figure 12.- Concluded.

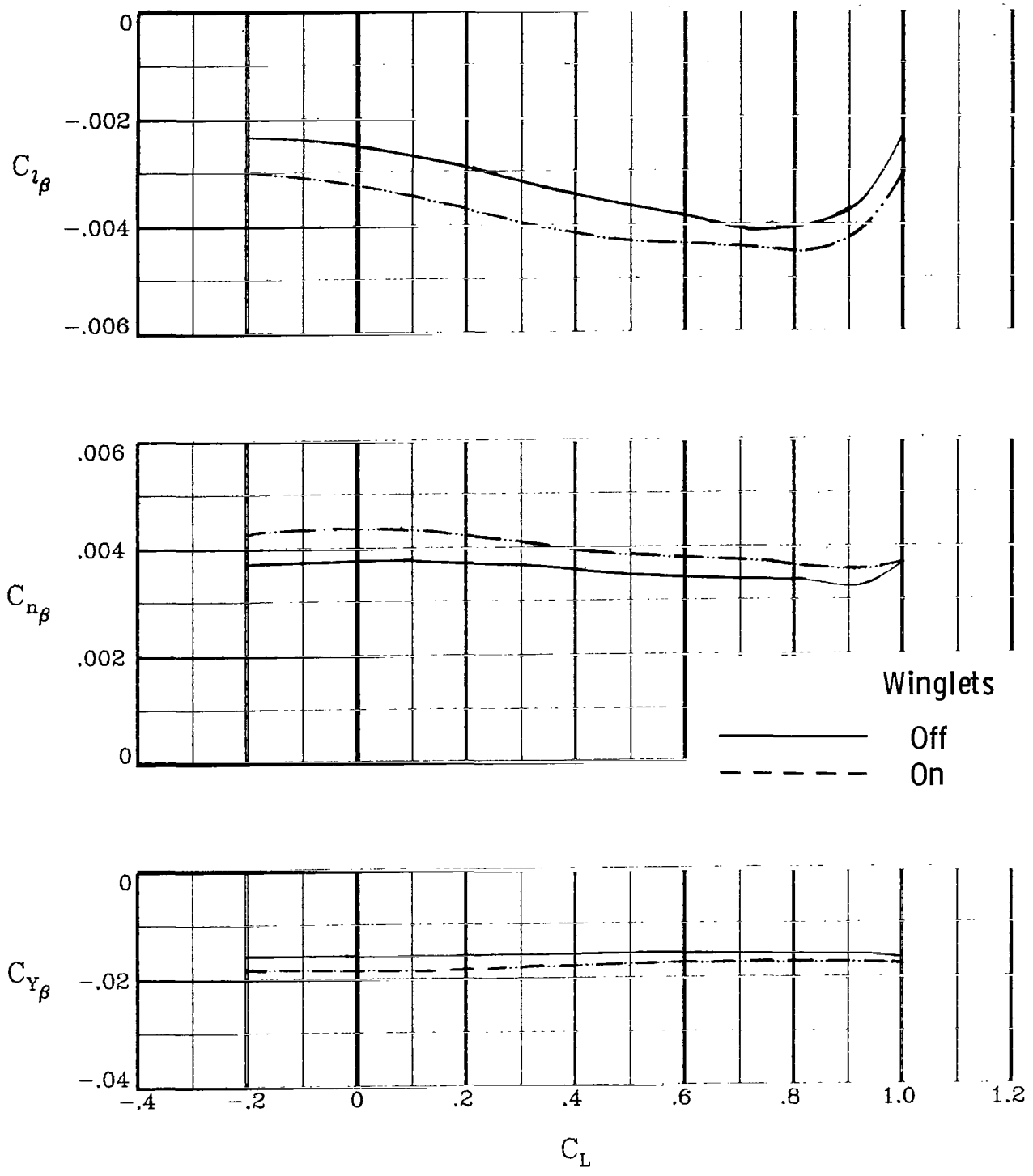

(a) $M_\infty = 0.50$.

Figure 13.- Lateral-directional stability parameters at high subsonic speeds. $\delta_h = 0^o$.

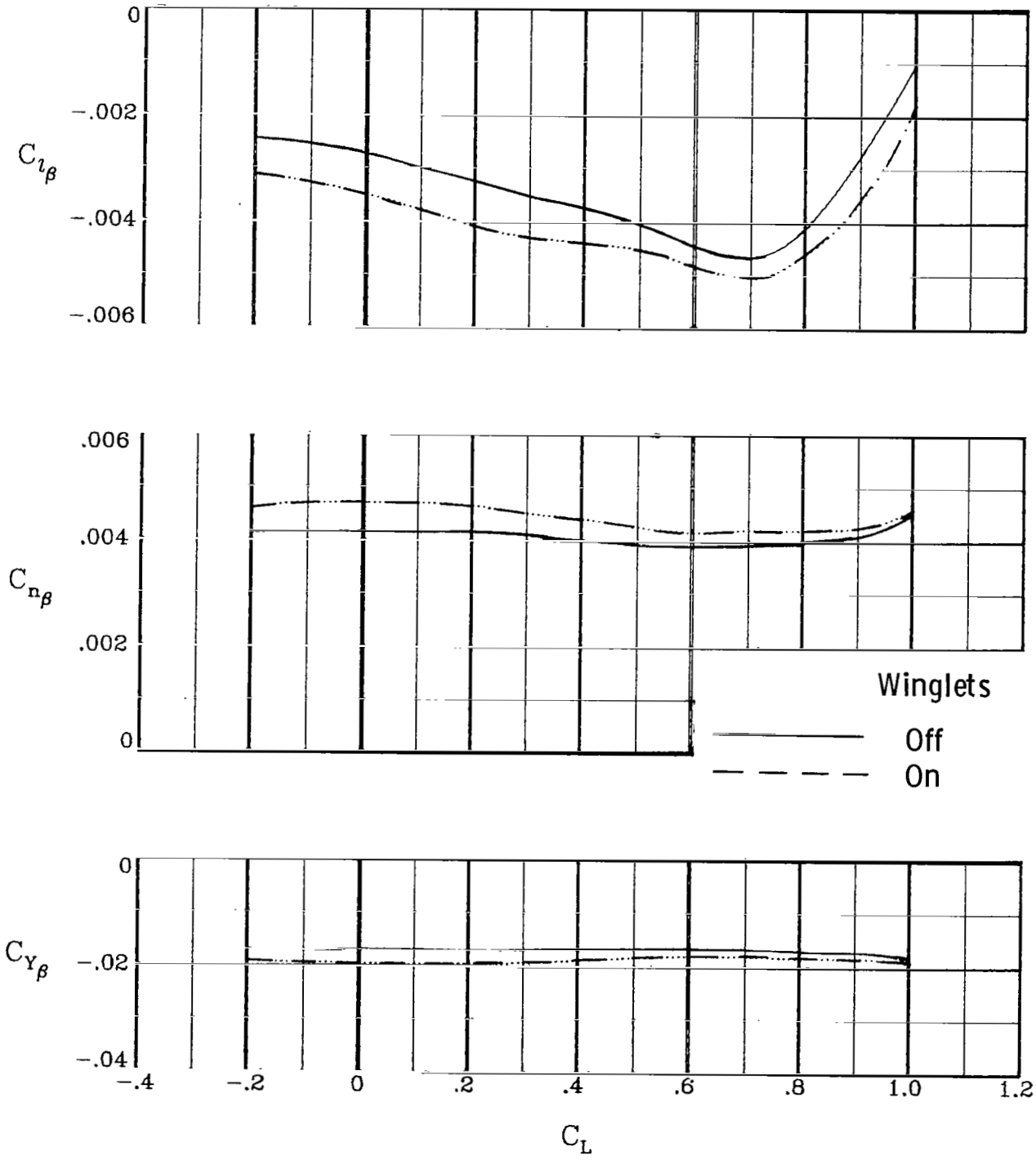

(b) $M_\infty = 0.70$.

Figure 13.- Continued.

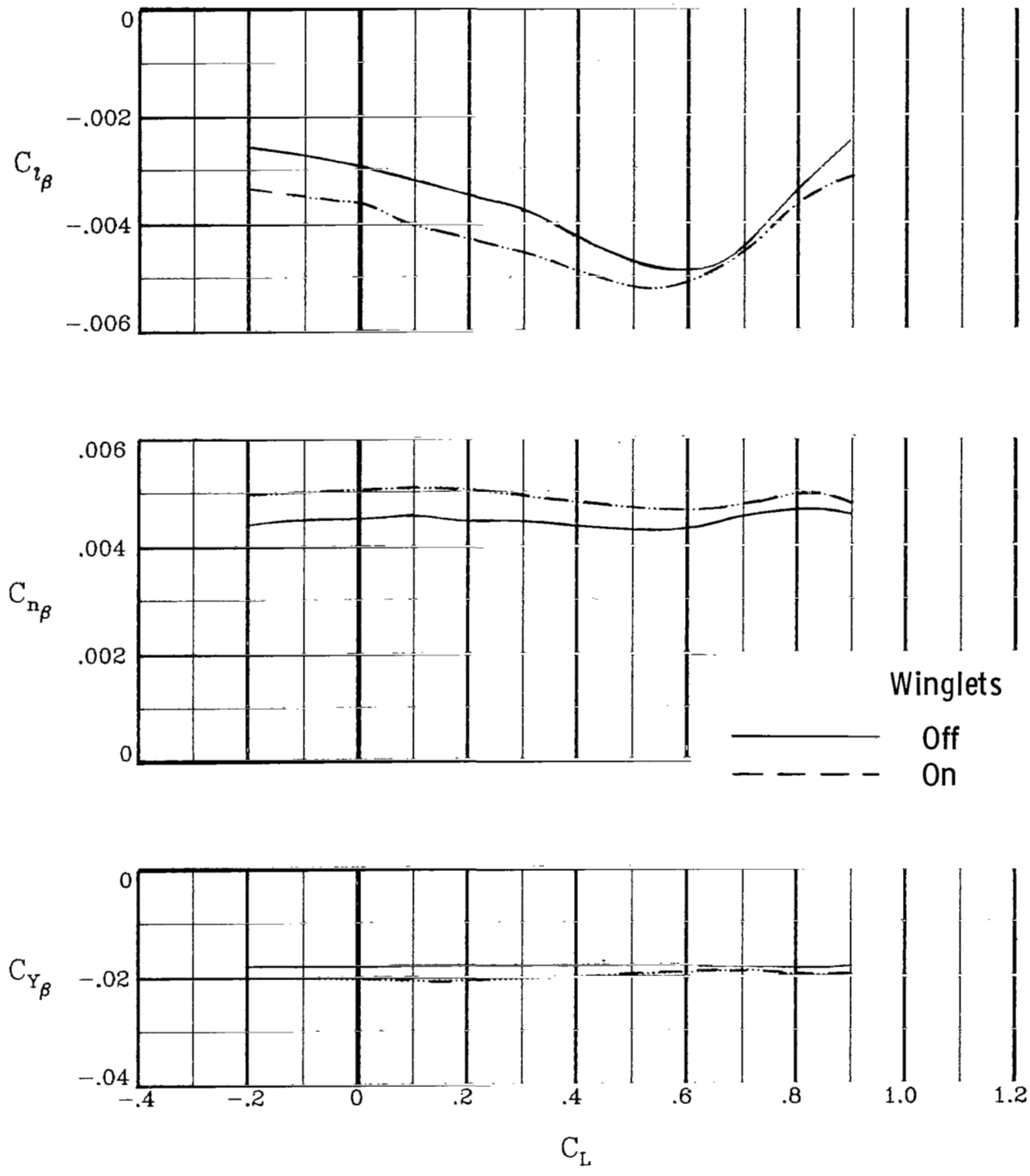

(c) $M_\infty = 0.78$.

Figure 13.- Continued.

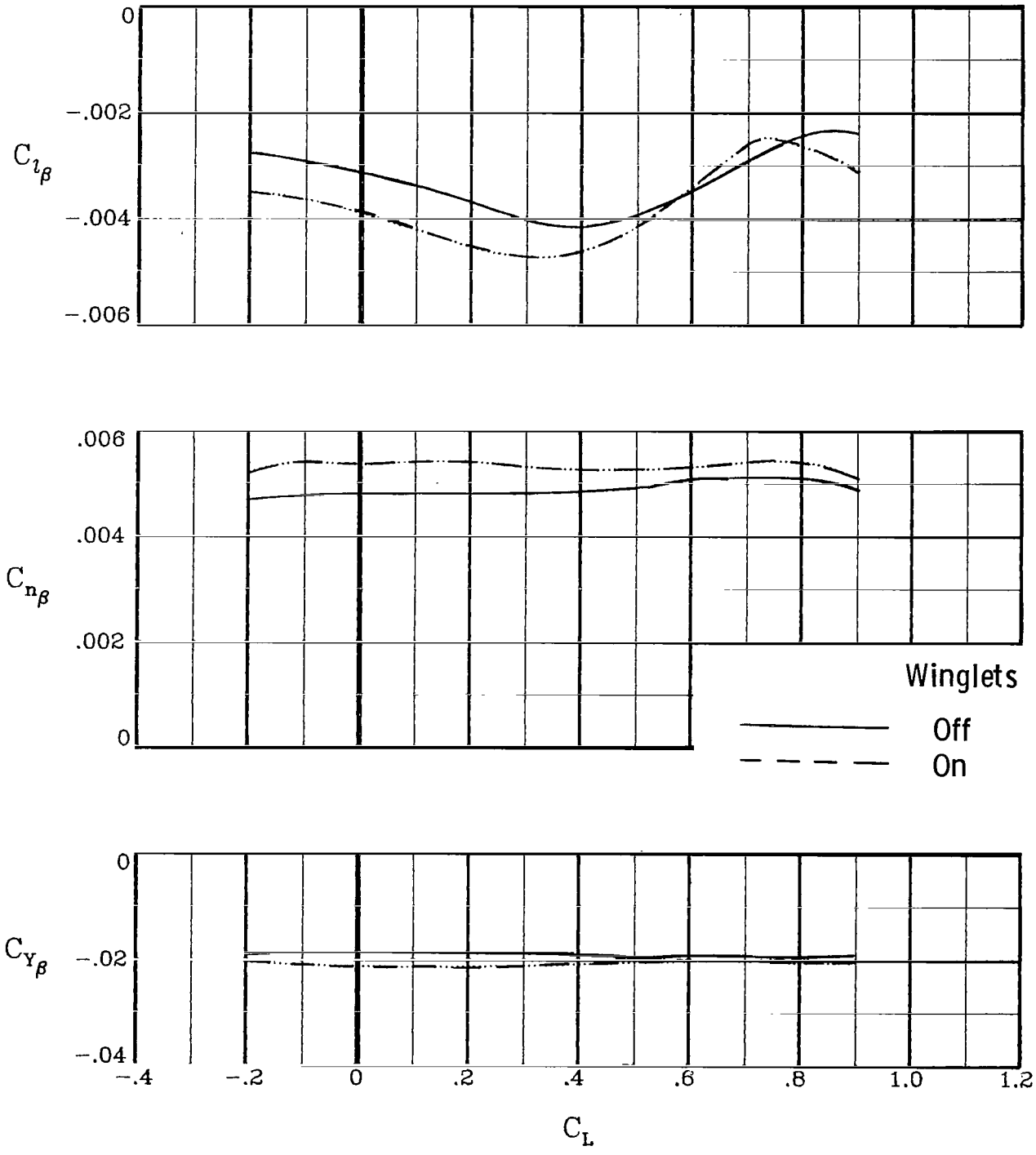

(d) $M_\infty = 0.82$.

Figure 13.- Concluded.

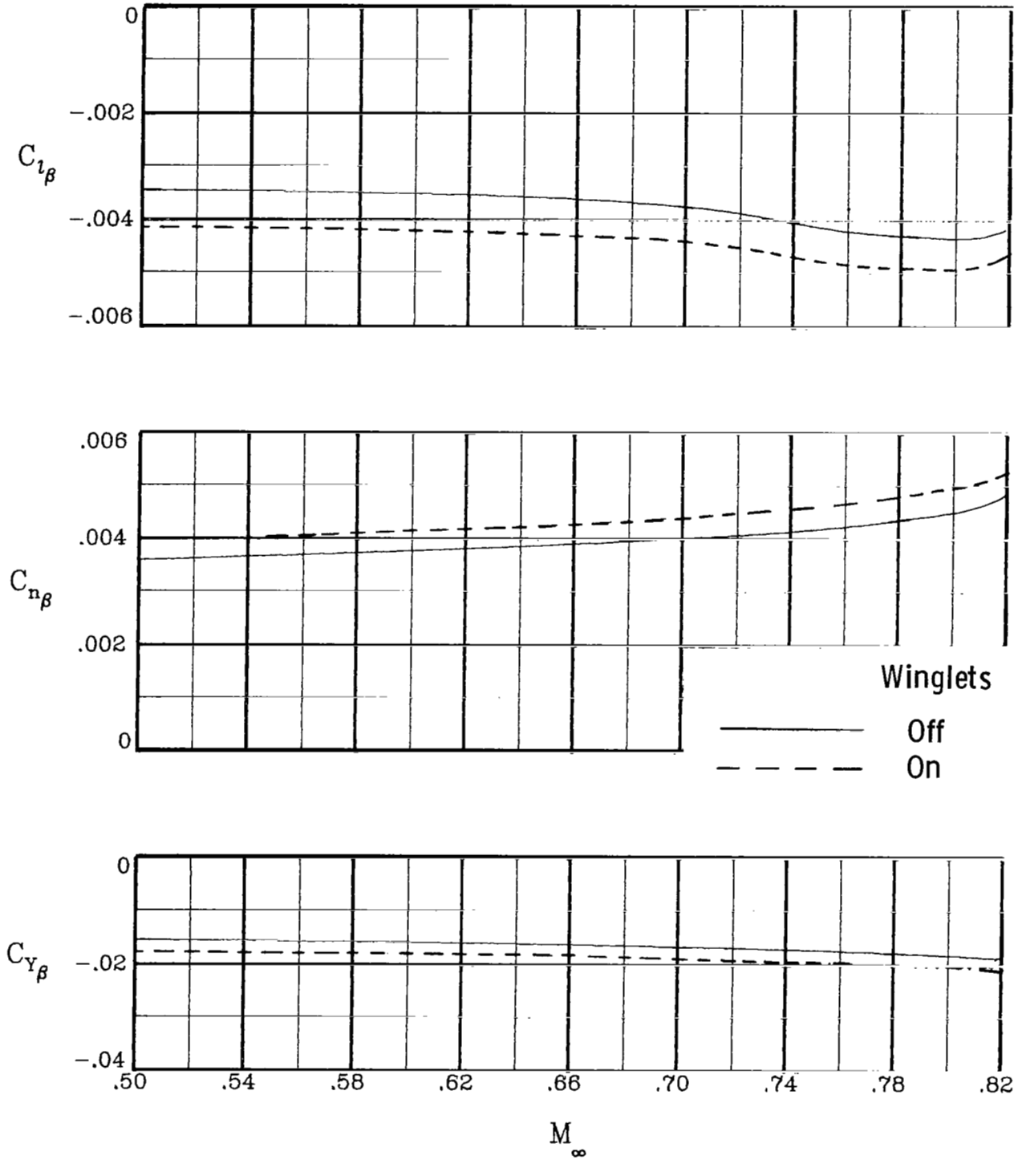

Figure 14.- Summary of lateral-directional aerodynamic characteristics at high subsonic speeds. Derivatives at $C_L = 0.40$; $\delta_h = 0^o$; $\beta = 0^o$.

1. Report No.	2. Government Accession No.	3. Recipient's Catalog No.
NASA TP-1330		

4. Title and Subtitle	5. Report Date
EFFECTS OF WINGLETS ON A FIRST-GENERATION JET TRANSPORT WING. VI - STABILITY CHARACTERISTICS FOR A FULL-SPAN MODEL AT SUBSONIC SPEEDS	October 1979
	6. Performing Organization Code
7. Author(s)	8. Performing Organization Report No.
Stuart G. Flechner	L-12514
	10. Work Unit No.
9. Performing Organization Name and Address	505-11-13-02
NASA Langley Research Center Hampton, VA 23665	11. Contract or Grant No.
	13. Type of Report and Period Covered
12. Sponsoring Agency Name and Address	Technical Paper
National Aeronautics and Space Administration Washington, DC 20546	14. Sponsoring Agency Code

15. Supplementary Notes

16. Abstract

A wind-tunnel investigation was conducted to identify changes in stability and control characteristics of a model of the U.S. Air Force KC-135A due to the addition of winglets. Data were obtained at Mach numbers from 0.30 to 0.82, at angles of attack from approximately -8° to 16°, and at angles of sideslip to approximately $\pm 12^{\circ}$. The data generally indicate that winglets improve stability and control characteristics.

17. Key Words (Suggested by Author(s))	18. Distribution Statement
Winglets KC-135A Stability and control	Unclassified - Unlimited Subject Category 02

19. Security Classif. (of this report)	20. Security Classif. (of this page)	21. No. of Pages	22. Price*
Unclassified	Unclassified	66	$5.25

* For sale by the National Technical Information Service, Springfield, Virginia 22161

NASA-Langley, 1979